DISSERTATIONES PHYSICAE UNIVERSITATIS TARTUENSIS

68

DISSERTATIONES PHYSICAE UNIVERSITATIS TARTUENSIS

68

AARNE KASIKOV

Optical characterization of inhomogeneous thin films

TARTU UNIVERSITY
PRESS

The study was carried out at the Institute of Physics, University of Tartu.

The dissertation was admitted on April 23, 2010 in partial fulfilment of the requirements for the degree of Doctor of Philosophy in Physics (Applied Physics), and allowed for defence by the Council of the Institute of Physics, University of Tartu.

Opponents: Prof. Arne Roos, PhD, Ångström Laboratory,
University of Uppsala, Uppsala, Sweden

Ass. Prof. Arvo Mere, PhD, Institute of Physics,
Tallinn Technical University, Tallinn, Estonia

Defence: July 2, 2010, at the University of Tartu, Tartu, Estonia

ISSN 1406–0647
ISBN 978–9949–19–396–7 (trükis)
ISBN 978–9949–19–397–4 (PDF)

Tartu Ülikooli Kirjastus
www.tyk.ee
Tellimus nr. 290

CONTENTS

LIST OF ORIGINAL PUBLICATIONS

The thesis is based on the following publications referred to in the text by their corresponding Roman numerals.

I. A. Kasikov and A. S. Kuznetsov "Model of inhomogeneity for an evaporated MgF_2 layer on quartz", J. Phys. D: Appl. Phys. **27**, 12 (1994), 2470–2474.

II. A. Kasikov "LaF_3 as a high-index material in VUV", In: *Optical Organic and Inorganic Materials,* S. P. Ašmontas, J. Gradauskas, Eds., Proc. SPIE **4415** (2001), 110–114.

III. J. Aarik, A. Kasikov, M. Kirm, S. Lange, T. Uustare, and H. Mändar "Optical properties of crystalline Al_2O_3 thin films grown by atomic layer deposition", in *Optical Materials and Applications*, ed. by A. Rosental, Proc. SPIE, **5946** (2005), 594601-1-10.

IV. A. Tarre, A. Rosental, T. Uustare, and A. Kasikov "SnO_2 on sapphire", in *Optical Materials and Applications*, ed. by A. Rosental, Proc. SPIE, **5946** (2005), 59460I-1-7.

V. A. Kasikov, J. Aarik, H. Mändar, M. Moppel. M. Pärs and T. Uustare "Refractive index gradients in TiO_2 thin films grown by atomic layer deposition", J. Phys. D: Appl. Phys. **39**, 1 (2006), 54–60.

VI. J. Aarik, A. Kasikov, and A. Niilisk "Spectrophotometric and Raman spectroscopic characterization of ALD grown TiO_2 thin films", in *Advanced Optical Materials, Technologies, and* Devices, S. P. Ašmontas, J. Gradauskas, Eds., Proc. SPIE, **6596**, (2007), 659616–1–6.

VII. A. Kasikov "Optical inhomogeneity model for evaporated Y_2O_3 obtained from physical thickness measurement", Appl. Surf. Sc., **254**, 12 (2008), 3677–3680.

AUTHOR'S CONTRIBUTION TO THE ORIGINAL PUBLICATION

The author of the thesis has performed all the transmission measurements described in the original publications and the analysis of the results, obtained in these measurements. Papers [II, VII] were fully prepared by the author, including the evaporation of the samples. The author performed the main part of the planning and deposition of the samples described in publication [I] and participated in writing of the papers [I, III, V, VI].

LIST OF ABBREVIATIONS AND SYMBOLS

2D	two-dimensional
3D	three-dimensional
AC	alternative current
ALD	atomic layer deposition
CVD	chemical vapour deposition
d	film thickness
DC	direct current
EB	electron beam
EBD	electron beam deposition
EMA	effective medium approximation
k	absorption index, extinction index
n	refractive index
$\overline{n}$	mean refractive index of a film
PVD	physical vapour deposition
R	reflectance
R_b	reflectance from backside
R_f	reflectance from film side
RBS	Rutherford backscattering spectroscopy
RF	radio frequency
SE	spectral ellipsometry
SEM	scanning electron microscopy
T	transmittance
TEM	transmission electron microscopy
UV	ultraviolet
VIS	visible
XRD	X-ray diffraction
XRR	X-ray reflection
λ	wavelength
σ	roughness
ν	wavenumber
α	absorption coefficient, extinction coefficient

1. INTRODUCTION

Thin film coatings are widely used in many different fields such as microelectronics, optical technology, chemistry etc. The selection of the materials varies depending on the application. One of the possibilities to characterize the material properties in thin film structures is to apply optical methods. They enable us to check the proximity of the properties of the thin films to those of a bulk and to control the optical parameters of the layers to adjust the structure of coatings and to achieve the desired results.

The main measurable optical characteristics of the layers used in the multilayer coatings are reflection, transmission, absorption and scattering. The reflection (*R*), transmission (*T*), and absorption (*A*) can be derived from the dielectric constant $\varepsilon = \varepsilon_1 - i\varepsilon_2$ or the complex refractive index $\tilde{n} = n - ik$ whereas

$$\varepsilon = \tilde{n}^2, \qquad \varepsilon_1 = n^2 - k^2, \qquad \varepsilon_2 = 2nk\,.$$

These two characteristic functions are used in parallel and their applicability depends mainly on the convenience of their use in a particular field.

In the field of the optical coatings, the complex index of refraction $\check{n}$ is more often used. It consists of the two components. The first component is the refractive index (index of refraction) *n*, which is the ratio between the phase velocities of light in vacuum and a given material, and the second component is the absorption index (extinction index, index of absorption, extinction coefficient, absorption coefficient,) *k*, characterizing the losses of an electromagnetic field inside a material.

While there is an agreement as to the use of the terms dielectric function $\varepsilon = \varepsilon_1 + \varepsilon_2$, complex refractive index (complex index of refraction) $\tilde{n}$, and refractive index as $n = \mathrm{Re}(\tilde{n})$, there is no consistent rule for naming the imaginary part of the complex refractive index. The term 'extinction coefficient' is used either for $k = \mathrm{Im}(\tilde{n})$ or for $\alpha = \frac{4\pi k}{\lambda}$, also referred to as the absorption coefficient, characterizing the extinction (absorption) losses in a film. In the work [1] the terms real index of refraction and 'extinction index' were introduced for *n* and *k*, the paper [2] differentiated *k* and α as Absorptionsindex and Absorptionskoeffizient. A term главный показатель поглощения (main index of absorption) have also been used for *k* to differentiate it from α in [3]. To resolve the problem, I would advise to use the term 'extinction (absorption) coefficient' for α and 'extinction (absorption) index' for k in a consistent manner. In this case absorption index (coefficient) would be preferable, if the (main) losses are due to the absorption processes in a material, extinction index (coefficient) could be used to indicate that the scattering plays a role in the structure of losses. Throughout this work I shall use the term 'absorption index' to refer to its closeness to the refractive index as the second part of the complex index of refraction.

If an electromagnetic field passes an interface between the two materials, 0 and 1, the ratios of its amplitudes in the two media are presented by Fresnel coefficients

$$r = \frac{n_1 - n_0}{n_1 + n_0}, \qquad t = \frac{2n_1}{n_1 + n_0} \tag{1}$$

and the Poynting vectors for energy transport over this interface will in this case be

$$R = |r|^2 = \frac{(n_1 - n_0)^2}{(n_1 + n_0)^2}, \qquad T = \frac{n_0}{n_1}|t|^2 = \frac{4n_0 n_1}{(n_1 + n_0)^2}.$$

When an electromagnetic field passes through a thin film with refractive index n_1 between two semi-infinite media 0 and 2 (a situation where we can assume the other borders of the media to be infinitely far away from the film) with indices n_0 and n_2 and light falls under the right angle from the medium 2, then the Fresnel coefficients are given by [4, 5]

$$r = \frac{r_2 + r_1 \exp(-2i\delta_1)}{1 + r_2' r_1 \exp(-2i\delta_1)}, \qquad t = \frac{t_1 t_2 \exp(-i\delta_1)}{1 + r_1 r_2' \exp(-2i\delta_1)} \tag{2},$$

where r_2, t_2 are the Fresnel coefficients for the interface $n_{2\text{–}1}$; r_1, t_1 are the coefficients for the interface $n_{1\text{–}0}$; r_2' is the Fresnel reflection coefficient for the interface $n_{1\text{–}2}$, and δ_1 is the phase thickness of the layer $\delta_1 = \frac{2\pi n_1 d_1}{\lambda}$. Here d_1 – thickness of a nonabsorbing layer, λ – wavelength of the light. In the formulae (2) it should be taken into account that the Fresnel coefficients r change the sign if the light approaches the interface in the adverse direction.

For nonabsorbing homogeneous materials and the light falling under the right angle, the transmission spectrum of one thin film between two semi-infinite media will then be

$$T = \frac{n_0}{n_2}|t|^2 = \frac{8n_0 n_1^2 n_2}{\left[(n_0^2 + n_1^2)(n_1^2 + n_2^2) + 4n_0 n_1^2 n_2 + (n_0^2 - n_1^2)(n_1^2 - n_2^2)\cos 2\delta_1\right]} \tag{3}.$$

If the thin film 1 is absorbing, its refractive index n_1 and, hence, the phase thickness δ_1 in (3) will become complex and the formula acquires a more complicated form. The sample spectra of some ideal films are presented in Fig. 1. In practice it is more productive to compute the complex Fresnel coefficients for the whole system and take a module from the results afterwards. For multilayer systems the Vlasov-Kard formulae [6] can be used for this calculation.

For films on transparent substrates one also needs to take into account the reflections inside the substrate. Also, for real materials, both components of the complex refractive index, n and k, are the functions of a wavelength (material dispersion).

Real thin films often do not correspond exactly to the presented theory. Formula (3) clearly shows that in case of $\cos 2\delta_1 = -1$ for the nonabsorbing films the transmission (and also reflection) values of the coated samples must correspond to those of an uncoated substrate. In these extreme points, called the halfwave points, the film optical thickness is $nd = m\lambda/2$, where m is an integer. For $n_1 > n_2$, these points correspond to the maxima of transmission and minima of reflection, and if $n_1 < n_2$, we have a contrary relationship. For real coatings it is not always the case (Fig. 2). The introduction of absorption to a thin film lowers the transmission values, but only slightly affects the reflection values. If the condition $n^2 >> k^2$ does not hold any more, the reflection at half-wave points starts to rise also as the film becomes more conductive. The rigorous formulae for transmission of an absorbing thin film on a nonabsorbing substrate are presented in [4, 7, 8], but usually an analysis is performed using a computer program. If the transmission values at the halfwave points are placed over the transmittance of the substrate, the films are usually called inhomogeneous which means that their optical constants should change moving through a layer [9]. Also, the film properties (optical constants, thickness etc. may change over the surface of a substrate [10], but this problem is not touched upon in this work.

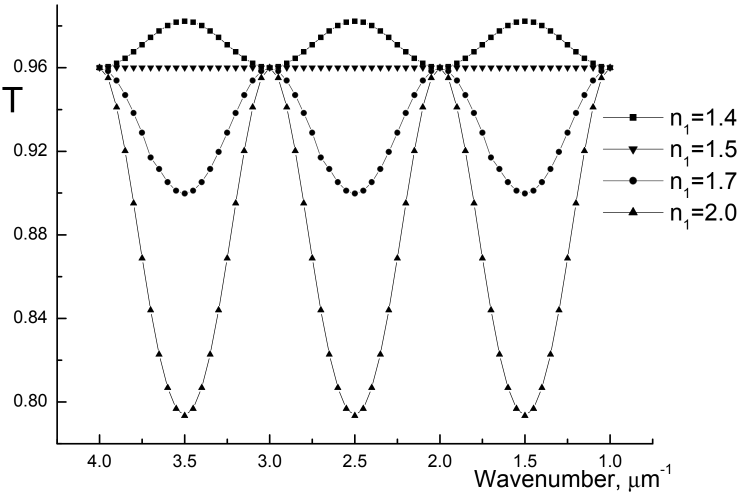

Figure 1. Transmission of some nondispersive nonabsorbing films with different refractive indices n_1 on a semi-infinite substrate $n_0 = 1.5$.

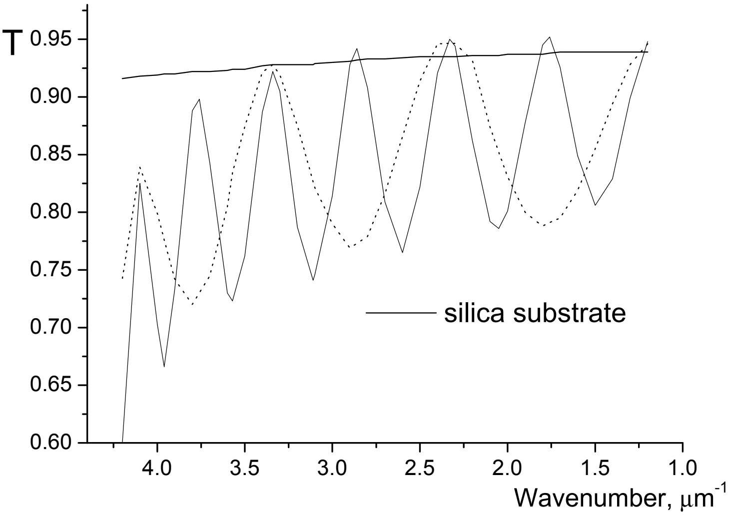

Figure 2. Transmission of the electron gun evaporated inhomogeneous ZrO_2 films on silica.

Up to this point, all the properties of a material have been known and we have been interested in the optical parameters of a system. To characterize a film material one has to solve an inverse problem – to find the optical constants of the film from the measured quantities. In this work I try to perform this for the films, in which the optical spectra are influenced not only by dispersion, but also by the inhomogeneity through a layer.

2. BACKGROUND

2.1. METHODS FOR PREPARATION OF THE THIN FILMS

Thin films can be prepared in different ways. Most frequently the thin films are prepared by chemical (CVD) or physical vapour deposition (PVD) methods. Historically, the first PVD method was a thermal evaporation into a vacuum with a material placed on a wire or boat made of a metal with a high melting temperature and heated by an electrical current. The film material evaporates or sublimates from a hot source and deposits on the walls of a vacuum chamber and on the substrates. In electron beam deposition (EBD), a material is placed in a water-cooled crucible and heated by an electron beam. In this way a possibility to obtain cleaner films is achieved. A common property for both methods is that the atoms, leaving the source through a physical evaporation process, usually have low energies of about 0.2 eV [11]. For the preparation of compound films by vacuum evaporation, additional gas can be led into a chamber to compensate for the faster loss of one component of the source material during the evaporation process (reactive evaporation).

The compactness and quality of the films may be improved if the impinging particles would have more energy to move onto the positions energetically favorable on a surface. This is achieved using higher surface temperatures and/or applying methods of generating particles with a higher energy.

If the nonreactive gases (Ar, Kr) are supplied into the chamber, the additional ions bombarding the surfaces can be generated by a gas discharge or by an ion gun. In the case of ion plating, the film material is evaporated from an electron beam crucible and a discharge is used for accelerating both the evaporated material and the additional rare gas ions. In ion-beam assisted deposition (IBAD), the evaporation proceeds in an ordinary way, but the surface of a growing layer is bombarded by an ion current from an additional ion gun. These methods provide an opportunity to obtain the thin films with better properties, but in nonoptimal conditions, it can also result in lower quality of the films [12]. One must also admit that the bombarded films often display a higher absorption than those deposited by conventional evaporation methods. For AlN films prepared by ion-assisted evaporated from Al, the absorption increased if 500 eV N_2 ions were used [12]. A reason for this is a possibility of introducing ion-induced damage in the film with high acceleration energies of the ions [13].

In magnetron sputtering, the electrons obtained from a discharge are caught by a magnetic field near a cathode made of the material that should be sputtered. These electrons cause an additional ionization, creating the gas ions that are needed for sputtering the source material. The accelerated ions give their impulse to the neutral gas atoms upon collisions causing an additional bombardment of the cathode material and creating the more energetic species leaving the cathode. Depending on the method to excite a discharge, magnetron sputtering can work in an alternative current (AC), direct current (DC) or a radio frequency (RF) mode. If both the dielectric oxide and metal layers are sputtered within a same process, attention should be paid to the prevention of target poisoning for the metal layers. Formation of a NiO interface layer of up to 10 nm has been reported if the presputtering time before the metal layer deposition was not long enough to clean the sputtering target [14].

The ion beam of inert ions may also be directed to a target to sputter a source material (ion beam sputtering) or a coating material itself can be ionised and accelerated towards the substrate by an ion gun (ion beam deposition). A review on the PVD technologies has been presented in [11].

In chemical vapour deposition (CVD), a film is obtained using the chemical reactions on the surface of a substrate or in a reaction chamber resulting in the precipitation of the reaction products.

Atomic layer deposition (ALD) is a specific mode of CVD and PVD methods. It is based on the self-limited adsorption of precursors on the substrate surface in PVD-type ALD processes or on the self-limited surface reactions in the chamber in CVD-type ALD. In both cases, a “digital” layer-by-layer growth of a film is realized, i.e. the film thickness depends on the number of the adsorption or reaction steps performed rather than on the precursor doses that the surface of a substrate is exposed to.

2.2. TRANSMISSION AND REFLECTION SPECTRA OF THIN FILMS

When performing the measurements on the low-absorption substrates, one also has to take into account the effect of a finite thickness of a substrate. The transmission of a nonabsorbing substrate is given as

$$T = \frac{T_0 t_0}{1 - R_0 r_0} = \frac{4nT_0}{(n+1)^2 - R_0(n-1)^2} = \frac{4nT_0}{4n + T_0(n-1)^2} \qquad (4)$$

with T_0, R_0 – the energetic transmission and reflection coefficients of the coated side of a substrate, n – refractive index of a nonabsorbing substrate. Formulae (4) hold if there is no interference of the falling light between the coated and uncoated sides of a substrate. Usually, it is guaranteed by lateral thickness variations of the substrate over a surface and a finite bandwidth of a measurement signal as shown in [15]. For the high-quality substrates interference in a substrate may play a role if a laser beam is used for measurements.

Historically, the first attempts at determining the optical parameters of thin films relied on geometrical methods using the geometrical constructions and the graphs of computed film transmission and reflection values depending on the refractive and adsorption indices, n and k, and the film thickness. An overview of some geometrical methods can be found in [4, 5]. A method for determining the optical parameters of an absorbing film on a bulk material from reflection data together with the tables for constructing the corresponding graphs has been presented in [16].

The approximate methods for determining the film thickness and optical parameters on the basis of the measured transmission extrema have been presented in [17, 18]. In these works, absorption and the influence of the backside of a substrate have not been taken account in their exact form. Using an infinite substrate approximation, [17] suggested to begin a film analysis by computing the absorption values over a transmission spectrum from the transmission maxima values and to use them as the first iteration to obtain the refractive index and film thickness.

A simpler way has been introduced in the works [15, 19] showing that the optical constants of the film can be computed using the envelopes built through the maxima and minima of the transmission spectrum of the film on the nonabsorbing substrate. [19] proposed to consider the values of the transmission extrema T_{min} and T_{max} as the continuous functions of wavelength (the envelopes) and presented the formulae for finding the values of refractive and absorption indices based on the adjacent values of the extrema. In this work, only a border of the two transparent media with a film having a complex refractive index between them was considered, without taking into account the backside of the substrate.

In [15] it has been shown a reason for not taking into account the interference effects in a substrate even in the case of the ideally parallel surfaces is a fact that a bandwidth of the spectrophotometer is wider than a period of interference. The formulae for calculation of the transmittance of a transparent substrate with a weakly absorbing film on it were given taking into account the backside reflections and a method for finding the parameters of a film using an iterative method and the precalculated nomograms presented. It was stated that a criterion for having a nonexistent absorption in a film is a coincidence of the transmittance extrema with the transmission of a substrate at the halfwave optical thickness points and that the existence of an inhomogeneity in a film makes it impossible to connect the transmission spectrum extrema using a smooth curve. Swanepoel [8] developed further the envelope method of [19] and presented the straightforward formulae for calculating the refractive index and absorption from the transmission spectrum alone using the envelope methods and taking into account the finite thickness of a transparent substrate. It was shown that a standard formula for film thickness is sensitive to errors and a better way of finding the optical constants of a film is to determine the thickness values by taking the exact integer values for the maximum order numbers m and to calculate the film parameters using the obtained thickness values as $2nd = (m + \frac{1}{2})\lambda$, where n – index of refraction, λ – wavelength. Also, the formulae for correcting the spectrophotometer slit width effects on a spectrum were presented. The effects of the finite bandwidth of a spectrophotometer were discussed for a case of the thick films and the correction formulae for calculating the refractive index were presented.

A work [20] used a transmission modelling developed in [8] together with an envelopes parametrization introducing a dispersion formula for the film thicknesses exceeding 1000 nm.

An extension of the envelope method [8] using an iterative algorithm to avoid the errors in drawing the transmission envelopes was given by [21]. Iteration at the film transmission spectrum turning points with the polynomial Cauchy or Sellmeier dispersion functions was used in [22]. Also, the iterative algebraic methods using the values of film-substrate system transmission and the two reflection values R_f and R_b from film front and back sides [23, 24] have been elaborated. These methods suffer from a need to use the reflectance values being inherently obtained with bigger measurement errors.

Another set of the formulae for obtaining the optical constants of a film, taking into account a finite thickness of a transparent substrate has been presented by Konovalova and Shaganov [25]. The influence of the film inhomogeneity over surface (a situation where there is a difference in the film thickness inside a recorded measurement beam) on the envelopes was taken into account in the works of Swanepoel [9] and in [10]. In [9] it has been shown that one can overcome some of the discrepancies in establishing an order of the spectral extrema arising from the interaction of the dispersion and inhomogeneity effects using the wavelength of the reddest transmission maximum in the transmission region. In fact, the same approach can also be used for a film of a constant thickness with dispersion. The Valeev turning point method was extended to an inhomogeneous case also in [26]. All these methods yield the optical constants for a film in the selected points determined by the spectral extrema only. The values between them are obtained by interpolation.

To obtain a full spectral characterization of a thin film on a known substrate over N measurement points one needs at least $2N+1$ independent parameters (N for refractive indices, N for absorption indices and 1 for film thickness). A spectrophotometric transmission measurement gives us N parameters or, if the measurement of reflection would be added, $2N$ parameters. As for the information amount gained, it is more beneficial to use spectroscopic ellipsometry (SE) where $2N$ parameters Ψ, Δ can be obtained from the same measurement

$$\frac{R_p}{R_s} = \tan\Psi \exp(i\Delta), \qquad \Delta = \delta_p - \delta_s,$$

where R_p, R_s – reflected light amplitudes for p- and s-type polarized light, Δ – a phase difference between the reflected light components with δ_p and δ_s in p- and s-polarization states. Subsequently, the optical constants of a material can be calculated from Ψ and Δ.

So, neither of the methods provides us with a unique presentation of a film. The spectroscopic ellipsometry presents more data, but involves a problem in the determination of an order of a spectral extrema and, hence, the thickness of a layer. Using a spectrophotometry there are less difficulties in obtaining the spectral order (for the films with a thickness of less than 0.5 μm, it can usually be made just by counting), but one has to make more additional assumptions. For SE, the measurements are often made under different angles for the same sample, but for a spectrophotometry it adds an additional complexity as the polarization state of light leaving the monochromator of a spectrophotometer may not be fully characterized. Also, a shift of the light beam on the receiver occurs if a sample is inserted to the optical path at an angle.

Dobrowolski et al. [27] presented a method of inverse synthesis for determination of the film optical constants using multiparameter fitting of the measured transmittance or reflectance and a predefined dispersion equation. The optical functions of an absorbing thin film material were presented not by $2N$ independent n and k values at N wavelengths, but a predefined optical dispersion formula with one or more Lorentz dispersion bands for a given spectral region was used. Additional information was obtained by measuring both the transmission and reflection spectra of the films. A predefined dispersion formula with $m < N$ parameters allowed calculating the optical constants over a full range, being defined from measurements at much smaller number of points and maintaining the others to solve an optimization task on a computer minimizing a merit function. The universal merit function was defined as $M = \left[\frac{1}{m}\sum_{i=1}^{m}\left(\frac{C_i - E_i}{\varepsilon_i}\right)^2\right]^{1/2}$, where m – the number of measurement points, E_i – the experimentally measured values, C_i – the values calculated with the given film parameters, ε_i – the accuracies of the given photometric quantity. A merit function can also be weighted, if, for example, some parts of a measured spectrum are valued less. As an example, a function $M = \sum_i \left(T_{i,computed} - T_{i,measured}\right)^2$ (5) or a sum of both the squared differences for the transmission and reflection spectra may be used with the sum taken over the measured spectrum points. Then, using the dispersion parameters and the quantities defining an inhomogeneous structure of a film as the free parameters, a merit function can be minimized, using a Nelder-Mead [28], often also called Levenberg-Marquart, or any other optimization procedure. The method has been used for dielectric, metal and semiconducting films [27], yielding the average deviation of the calculated data from the experimental values by about 2.5% for ZnS films and less than that for MgO and MgF_2. Inhomogeneity was not taken into account, but a possible usefulness of a method for such films was marked if one would approximate the film by a two- or three-component coating model. After defining the dispersion formula, the optical constants of a film for the points of interest were calculated, and based on them, the optical spectra of a film computed. The theoretical spectrum obtained this way could then be compared to the measured one. Subsequently, a merit function based on the differences between the two spectra was used to optimize the dispersion parameters.

Some possible dispersion formulae [27, 29, 30, 31] are presented below.

$$n(\lambda) = A + \frac{B}{\lambda^2} + \frac{C}{\lambda^4} \qquad \text{(Cauchy),}$$

$$n^2(E) = 1 + \frac{E_m E_d}{E_m^2 - E^2} \qquad \text{(Wemple-Didomenico),}$$

$$n^2(\lambda) = A + k^2(\lambda) + \frac{B\lambda^2(\lambda^2 - C^2)}{(\lambda^2 - C^2)^2 + D^2\lambda^2}$$

$$k(\lambda) = \frac{1}{2n(\lambda)} \cdot \frac{BD\lambda^3}{(\lambda^2 - C^2)^2 + D^2\lambda^2} \qquad \text{(Lorentz),}$$

$$n^2(\lambda) = A + k^2(\lambda) + \frac{B\lambda^2}{\left(1 + C^2\lambda^2\right)}$$

$$k(\lambda) = \frac{BC\lambda^3}{2n(\lambda)\left(1 + C^2\lambda^2\right)} \qquad \text{(Drude),}$$

$$n^2(\lambda) = 1 + \frac{A}{1 + \left(\frac{B}{\lambda}\right)^2}$$

$$k(\lambda) = \frac{C}{n(\lambda)D\lambda + \frac{E}{\lambda} + \frac{1}{\lambda^3}} \qquad \text{(Sellmeier),}$$

$$n(E) = n(\infty) + \frac{B_0 E + C_0}{E^2 - BE + C}\ , \qquad \text{where}$$

$$B_0 = \frac{2A \cdot \left[-\frac{B^2}{2} + E_g B - E_g^2 + C \right]}{(4C - B^2)^{1/2}} \text{ and } C_0 = \frac{2A \cdot \left[(E_g^2 + C)\frac{B}{2} - 2E_g C \right]}{(4C - B^2)^{1/2}},$$

$$k(E) = \frac{A \cdot (E - E_g)^2}{E^2 - BE + C} \qquad \text{(Forouhi-Bloomer).}$$

Here, a Lorentz dispersion formula can be derived from the one-oscillator model $\varepsilon = \varepsilon'_\infty + \frac{\left(\varepsilon_s - \varepsilon'_\infty\right)\omega_t^2}{\omega_t^2 - \omega^2 + i\Gamma_0\varpi}$, [32] describing a dielectric lattice with a damped single oscillator without the free carriers (Appendix II). The constants A, B, C, D, etc. do not have the same meaning in the different formulae. A Drude model describes the optical constants of a material, in which the free carriers bear the main responsibility for its properties. A dispersion model for amorphous semiconductors and dielectrics was proposed by [29] assuming the transitions taking place between the parabolic valence and conduction bands. In this model, E_g denotes the position of an absorption edge. However, it implies a parabolic rise of the absorption for the photon energies that are lower than a bandgap value. To overcome this discrepancy, [33] changed Forouhi-Bloomer dispersion function to $k(E)=\frac{A\cdot(E-E_g)^2}{E^2-BE+C}$, $E\geq E_g$; $k(E)=0$, $E\leq E_g$. [34] introduced a combination from the Tauc density of the states above the band edge [35] and quantum mechanical calculation of a collection of non-interacting atoms as an imaginary part of the dielectric function $\varepsilon_2(E)=2nk=\frac{AE_0C(E-Eg)^2}{(E^2-E_0{}^2)^2+C^2E^2}\cdot\frac{1}{E}$, $E>E_{g,}$; $\varepsilon_2(E) = 2nk = 0$, $E<=E_g$, a real part of a dielectric function would be obtained by the Kramers-Kronig integration then. The same approach was followed in [36]. For absorbing materials, more than one term in the dispersion equation has been used [27, 37].

A method for calculating the optical constants of a film from the transmission spectrum using only a computer program with defined linear constraints between the values of parameters over a wavelength region and an optimisation according to the merit function has been presented in [38]. The equations system still demanded solving it at the different given possible film thicknesses and choosing a solution giving a minimum value of the merit function. Unfortunately, no comparison between the measured and computed data was given. It was noted that the method does not yield the results for inhomogeneous films. A method suggested by [39] also needed a double minimization process for retrieving a data. By using a dispersion formula as a reciprocal power function and the iterations it is also possible to obtain the refractive index and thickness of a nonabsorbing film from the exact positions of transmission extrema at two different angles of light incidence [40]. The different transmittance analysis methods were compared for AlN in a paper [41].

The sputtered amorphous TiO_2 films on crystalline Si were compared against different dispersion models (Sellmeier, Forouhi-Bloomer, corrected Forouhi-Bloomer with k = 0 below bandgap, Jellison-Modine and combined Sellmeier-Forouhi-Bloomer) using ellipsometry data and a structural model with a SiO_2 interface layer and surface roughness layer in [42]. The best results for the region of 5.0 –1.5 eV were achieved with the Jellison-Modine dispersion model that is also consistent with Kramers-Kronig relation. The material bandgap values as the parameters of the dispersion equations deviated considerably from each other while the Tauc gaps obtained in a linear region near the bandgap as $(\varepsilon_2 E)^{1/2}$ gave similar results. Also, the Jellison-Modine model yielded the smallest difference between them.

In [43] the thin SnO_2 films grown from $SnCl_4$ using a CVD method were analyzed using the transmittance spectra and Forouhi-Bloomer dispersion model in a homogeneous approach. The results were quite good (mean difference between the measured and computed transmission values of about 0.4%) for the films deposited at substrate temperatures 350–420°C, but not so good (about 0.9%) for the films deposited at 450–520°C. Here, also the formulae for transmission and reflection coefficient calculation, generalized from [8] for an absorbing substrate were presented. Another approach to the problem of a weakly absorbing substrate has been presented in [31].

A work [44] has shown that the photoacoustic onset of laser damage for oxides is determined by the defect states in the band gap and is exponentially dependent on the material bandgap. This result points to the circumstance that it may be helpful to include the Urbach tail type exponential dependence of absorption in the dispersion formula, but at the moment no such formula is known to me. An exponential dependence of the absorption coefficient on energy was found also for the range of up to 4 eV below the energy gap E_g of magnesium fluoride in [45]. A possible link between such behaviour and the material dispersion relationships remains open at the moment.

2.3. EXPRESSION OF AN INHOMOGENEITY IN THE OPTICAL SPECTRA

As noted in Part 1, the transmittance and reflectance values determined for the homogeneous nonadsorbing films at halfwave points must correspond to those of a low-adsorbing substrate. If the films are absorbing, the transmission for the halfwave points is lower than for a substrate. In spectral ellipsometry with low adsorption levels not influencing a phase balance, a condition for film homogeneity is $\tan\Psi(HW) = \tan\Psi_s$, where $\tan\Psi(HW)$ – the amplitude reflectance ratio of a system at a halfwave point, $\tan\Psi_s$ – the reflectance ratio for an uncoated substrate [46].

Another factor influencing the behavior of the optical spectra is scattering of light. A theory for computing the diffuse transmission and reflection spectra (light scattered forwards and backwards) on the thin film boundaries based on modification of the Fresnel coefficients for the case with uncorrelated roughness on boundaries is presented in [47]. Scattering can occur on the boundaries between the different media if they possess a roughness or because of the refractive index inhomogeneities inside a film. The roughness is partially due to the surface profile of a substrate and is amplified by a nonuniform growth of a film due to randomness during the transport of a material to a sample [48] and/or a possible crystallization during a film growth giving a rise to local planes of preferred growth. At a lower values scattering manifestates itself as a transmission loss, i.e. like absorption. If the scattering loss rises, it inflicts a decrease in the values of both the transmission and reflection spectra. At strong scattering levels, the interference pattern changes and the increasing absorption index no longer allows for a good presentation of the system behaviour [49, 50].

The diffuse reflectance and transmittance (scattered light) spectra were calculated for a thin film on a transparent substrate in the approach of reduced Fresnel coefficients in [47]. A diffuse component is equal to the reduction of the specular component when the surface roughness σ is introduced [51] as

$R_D = \lfloor 1 - \exp\lfloor -(4\pi n\sigma/\lambda)^2 \rfloor\rfloor R_T$, R_T – the total reflectance for an ideal interface (σ = 0). For totally uncorrelated interfaces the maxima and minima of the diffuse reflectance spectra are oppositely phased to the maxima and minima of specular reflectance. On a same time, the diffuse transmittance extrema are in phase with the extrema of specular transmittance. It has been shown that a rough front surface of a film gives a larger diffuse reflectance than a film-substrate interface, and the difference is higher for a case with higher refractive index film on a low-index substrate. A reason for this is the larger difference in the refractive indices between a rough film and incident medium, giving a higher reflective power on this interface. The variations in the spectra of diffuse light were analyzed depending on film and substrate properties. The diffuse reflectance and transmittance oscillations were in phase and the diffuse transmittance was higher than the diffuse reflectance for a case with a rough front surface. It was shown that the values of an interface roughness in the region of 5 to 25 nm can be obtained from the measured spectra of diffuse transmittance and reflectance [52].

A simulation of scattering for a TiO_2 layer in [53] showed that the scattering losses are in phase with the transmission values for uncorrelated surface roughness and in phase with the reflection values for correlated surfaces.

It has been demonstrated [54] that for a number of ion-assisted-deposited and ion plated dielectric films, a perfect replication takes place. At the same time, the overcoating of a Cu substrate with an 0.2–0.5 μm Cu film results in a reduction of the surface roughness caused by the high spatial density structures [55].

It has to be noted that the approach using the Fresnel coefficients takes into account only scattering from the interfaces between the media (surface scattering). In addition to this, scattering may originate from the local refractive index inhomogeneities inside a film (bulk or volume scattering). It has been shown that for TiO_2 and ZrO_2 thin films, the scattering losses originate mainly from bulk but not from the surface [56]. The main part of scattering also came from bulk for sputtered and annealed TiO_2:Nb films [57]. For ZnS, volume scattering rises at the deposition rates over 4 nm/s [58].

All these processes influence the spectra of thin film coatings. Both the absorption and scattering lower the positions of the half-wave maxima in the transmission spectra while in the reflection spectra they work in the opposite directions – halfwave points are rising in the case of absorption and falling in the case of scattering. Both of them also reduce the amplitude of the interference fringes, but neither can give a rise of half-wave extrema over the transmission of a pure substrate as observed in a number of PVD materials [I, II, VII].

So, the thin films displaying the transmission maxima lower than the transmission value of the substrate (or the transmission minima higher than that of an uncoated substrate, if $n_1 < n_2$) may be characterized by absorption (or scattering). The films with $n_1 > n_2$ and the transmission maxima higher than that of a substrate require the involvement of yet another factor. A solution can be achieved by introducing transversal inhomogeneity – a hypothesis that the refractive index of a material changes in the growth direction of the layer.

An inhomogeneity in a film means that the refractive indices of a thin film are different on its two borders with adjacent media. As a consequence, the Fresnel coefficients (reflection amplitudes) on these interfaces are also different from those of a homogeneous film, affecting the transmission and reflection spectra of a full system. Abelés [7] has presented a review of interferometric and spectrophotometric methods to evaluate the optical constants of thin films including a case for inhomogeneous films if a refractive index is a slowly varying function of thickness in which $(\frac{dn}{dz}\cdot\frac{1}{n})^2 \langle\langle (\frac{2\pi n}{\lambda})^2$. In fact, a possible influence of the inner part of the film on the reflectance and transmittance is not taken into account in this approach and the system is characterized by the reflections from the interfaces between the materials having different local indices of refraction.

A simplest form of an inhomogeneity is a linear one where a refractive index is claimed to change linearly from the value n_a on the border with a substrate to n_b on the border with an adjacent medium (e.g. air) (Fig.3). In this case it is proposed that no reflection takes place inside a film, justified if the change of the refractive index inside a film is slow [7]. If the reflection of a light from the interior of the film can be ignored, the reflection coefficients on the interfaces substrate/film and film/ambient are determined by the material refractive indices n_1'' and n_1' accordingly. The components of the reflected and transmitted light are summed like in the case of a homogeneous film. If absorption is negligible, we obtain $R_Q = \left(\frac{n_2 - n_1' n_1''}{n_2 + n_1' n_1''}\right)^2$ for quarterwave points and $R_H = \left(\frac{n_1'' - n_2 n_1'}{n_1'' + n_2 n_1'}\right)^2$ for halfwave points of the film. Here, n_2 – the refractive index of a substrate, the index for ambient is taken as $n = 1$. Then, if a dispersion is approximately introduced using the envelopes of the spectra, the refractive indices are obtained as $(n_1')^2 = \frac{(1+\sqrt{R_Q})(1+\sqrt{R_H})}{(1-\sqrt{R_Q})(1-\sqrt{R_H})}$,

$$(n_1'')^2 = n_2^2 \frac{(1+\sqrt{R_Q})(1-\sqrt{R_H})}{(1-\sqrt{R_Q})(1+\sqrt{R_H})}$$

A theory for such films [3, 7, 59] and the exact results for some other inhomogeneity profiles [60, 61, 62] have been presented in several papers. A work [60] has given an approximate method for finding the spectra of the inhomogeneous films if at a light entrance, the refraction index of a film equals to that of the surrounding medium. A method for finding the reflection spectrum of an arbitrary refractive index profile using its quadratic approximation was presented in [62].

In [63] the determination of the optical constants of a film from *in situ* measured spectra of transmission vs time has been demonstrated giving a possibility to find the refractive indices on both the innermost and outermost border of a layer. The refractive and absorption indices were measured during the deposition of TiO_2 at 678 nm using an automatic scanning monochromator [64].

A method for calculating the optical profiles through the films was presented by [65], also based on the data gained during a coating process and assuming a slow monotonic variation of the refractive index as a function of thickness. Here, the film thickness increment between the successive spectral orders like in [66] and the transmission envelope values at spectral extrema were used. For TiO_2 and ZrO_2 films deposited by reactive electron beam evaporation, a negative refractive index profile (the profile with the lower refraction index value at the interface with ambient and a higher value at the substrate – film interface) was obtained. Still, for ZrO_2 films, the main difference in the refractive index occurred in the first 80 nm of the film. Also, a possibility of a growth of an unstable film with the properties changing during deposition was demonstrated for titania deposited by electron beam evaporation from Ti_2O_3 at the conditions of oxygen deficiency.

The model assuming a linear index profile is not reasonable, however. As it is seen in Fig.3, the refractive indices defined on the two interfaces define its values through all the film. It means that the index values at the same depth inside a film will become a function of the film thickness [I]. If the film thickness changes while the refractive index n_b stays constant, the slope of the index profile must be different from that existing up to that moment and the value of the refractive index at every particular point inside the film has to change during the film growth. Sometimes, it may happen [63], but it is not a usual case. This problem can be overcome assuming that there is not a structure with a linear transition between the two values, but a structure consisting of two sublayers with refractive index values n_a and n_b is used instead. This adds another refractive index step causing an additional reflection from inside a film together with its effect to the spectra. At the same time, the refractive index profile inside a film no longer depends on the overall film thickness. This approximation corresponds to the situation where the change of an index takes place in a restricted region of thickness, above (and below) of which it stays constant.

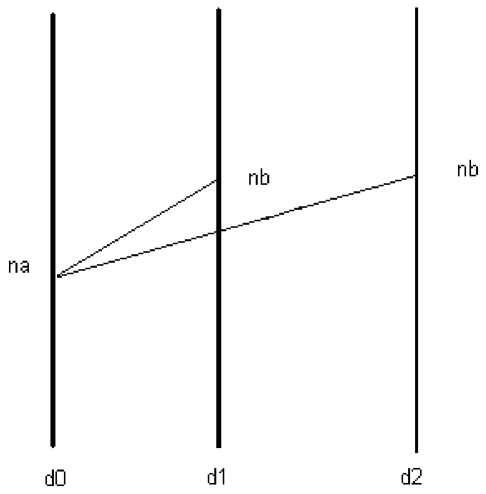

Figure 3. A linear inhomogeneity of refractive index changing from n_a to n_b in a film with the thickness d_1. The same thickness gradient can not be reproduced in an another layer with the thickness d_2.

The reflectance of a thin dielectric film around the Brewster angle has been analyzed by [67]. It was demonstrated that the differences in the spectral behavior exist between the inhomogeneous (with the refractive index changing continuously and slowly) and double-layer films. In the case of thick films, a beating can occur in a spectrum if both sublayers have a thickness of more than a quarterwave for the given wavelength [68, I] (Fig.4).

An analysis of the slightly inhomogeneous films in linear inhomogeneity approximation has been performed in [59]. It was shown for numeral calculations that there is virtually no difference between the results obtained by summing the internal reflections from two interfaces between the media with different refractive indices and the results from a stack of sublayers with a linearly changing index if the number of sublayers is 10 or higher. It was demonstrated that the reflectance maxima (corresponding to the quarterwave optical thickness points) for high-index layers (with the refractive index higher than that of a substrate) are insensitive to the coefficient of inhomogeneity $\Delta n/\bar{n}$ enabling determination of the mean index $\bar{n}$. For halfwave points (optical thickness multiple of halfwave of a given wavelength) the reflectance was a function of only its relative variation through a material in the case of linear variation of the refractive index. A program based on the reflectance data measured from the external and internal sides of a coating and on the transmittance has been developed and Y_2O_3, TiO_2, MgF_2, HfO_2, and SiO_2 layers have been analyzed. The results of the analysis in homogeneous and inhomogeneous approximation have demonstrated that all the materials had a negative inhomogeneity except MgF_2, which, in this approach, yielded a change from negative to positive inhomogeneity moving from the blue to the red part of the visible spectrum. Unfortunately, no measured spectra for magnesium fluoride were given. For SE, the model spectra of the inhomogeneous thin films with a linear gradient have been presented in [46, 69].

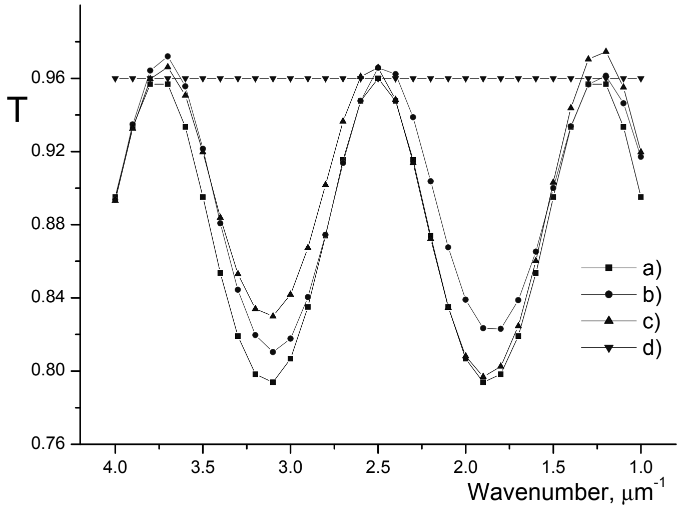

Figure 4. A transmission spectrum of a two-layer film system on a semi-infinite substrate a) n = 2.0, optical thickness λ/2 for 800 nm; b) n = 2.0–1.9 λ/20–9λ/20; c) n = 2.0–1.9 4λ/10–6λ/10; d) substrate n_0 = 1.5. A beating is seen for c) in the blue region, where the optical thickness of a thin sublayer exceeds a quarter of wavelength.

A method for solving an inverse problem with regard to establishing a slightly inhomogeneous structure of a nonabsorbing film from spectroscopic ellipsometry data was presented in [70]. The Chebyshev polynomials were used to characterize a deviation from a homogeneous profile with the Cauchy dispersion model and a standard merit function based on Ψ and Δ was used to estimate the quality of approximation. It was shown that the Ψ values at the quarterwave points might be taken independent of the inhomogeneity only if the inhomogeneity profile was antisymmetric in respect to the centre of the film, however, this condition did not hold for convex profiles. Using an ellipsometry, the results can also be obtained for the structures with more complicated inhomogeneous profiles like porous silicon [71]. For two-layer approximation the model spectra have been presented by [67]. The similar pictures emerge in the cases when a thinner sublayer is situated between a substrate and the main film and when it lies between the main film and the ambient. In case a thinner sublayer has a thickness of less than a quarterwave, no beating is seen, so one can describe a spectrum of such inhomogeneity also by a linear inhomogeneity model. This claim holds if we look at a measured spectrum of only one film at a time or if a change in the optical parameters of the material has terminated at the end of the deposition process. If it is not the case, an inhomogeneity can still reveal itself in the change of the optical parameters for films of a different thickness deposited in identical conditions [IV, V]. An inhomogeneous structure consisting of a double-layer structure has been found for vacuum-evaporated cryolith on the basis of the reflection measurements by [68]. The inhomogeneous films were of both, positive and negative, type of inhomogeneity, but they were alike to each other for every process. It was interpreted introducing an upper sublayer with a thickness of $\lambda/8$ to $\lambda/4$ for visible light and a possible change of the ratio of NaF and AlF_3 components during the evaporation.

An analysis of the optical properties for films with linear inhomogeneity can be performed by an envelope method [72], but a two-layer inhomogeneity cannot be depicted in a simple analytical form. For this case, the method of inverse synthesis presented by Dobrowolski et al. [27] may be used with the dispersion curves for a film predefined.

Besides a transversal inhomogeneity through a film, an inhomogeneity over a film surface where a light beam used for measurement encounters the regions with different film thicknesses at a same time is also possible. Each film region has its own thickness value different from that of the other regions. So, the measured transmission and reflection values are the integrals over a beam cross-section. This situation has been analyzed by [9, 10], but is not touched upon in this work. Swanepoel [9] has demonstrated that a transmission spectrum can be strongly influenced if the film properties vary over the surface area illuminated during the measurement (linear change or periodic irregularities of film thickness or refractive index and the finite bandwidth of the spectrophotometer were taken into account) and the equations presented for calculating the mean thickness and optical constants over this area. The validity of this approach requires the fulfillment of the condition $0 < \Delta d < \lambda/4n$, where Δd is the difference of the film thickness over a beam area.

In the case of thickness inhomogeneity, the measured spectra are smoothed, the amplitudes of the interference fringes diminish and the spectra seem to have a higher absorption with a lower refraction index. In [10] a method for analysis of thin films was presented for the case where the refractive index, thickness variations and surface roughness have not linear but Gaussian profiles.

A paper [73] proposed a method where an inhomogeneous layer is divided into sublayers and a random search is performed in a narrow wavelength range, in which the refractive index does not depend on the wavelength. Then the results for the mean refractive index and its variation ${}^{\Delta n}\!/_{n}$ would be fitted to a dispersion formula according to the measured T and R curves. The method was used for the layers artificially created as inhomogeneous varying the deposition conditions. In this way an arbitrary inhomogeneity profile could be described using a Sellmeier dispersion model.

The transmittance spectrum of a film of amorphous Si:H on glass deposited by the plasma-enhanced chemical vapor depositionhas been analyzed in [74]. It was shown that a measured spectrum can be modeled either with thickness variation over a light beam $\Delta d = 20$ nm or with an inhomogeneous structure possessing a positive inhomogeneity and two thin transition layers at film boundaries with refractive index difference $\Delta n = 1.6$. Still, as a strong positive inhomogeneity had to be introduced to explain the measured lower transmission, the same structure in a spectrum can be reproduced with a two-layer structure, Δn only about 0.2, if a little amount of absorption $k = 0.006$ were added into the model.

Montecchi et al. [75] have presented the model calculations for a slightly inhomogeneous thin film with rough and unparallel interfaces using a perturbative approach. It was demonstrated that at the film-substrate interface, the roughness results in a shift of the specular reflectance and transmittance maxima to smaller values and a shift of the minima, by a smaller degree, to larger values. In the case of a rough film-ambient interface the spectral maxima of the reflectance and transmittance decrease while the minima of transmittance are left unchanged and for the minima of reflectance there is only a small decrease in the reflectance. These results were compared to those obtained by an effective-medium approximation (EMA) theory where the roughness is presented by 50:50% mix of the two contacting media. It was concluded that the EMA model is quite accurate provided that the reflectance spectrum is investigated like it usually is in ellipsometry, but it fails to present the transmittance spectra of the rough films. In fact, for film-ambient interface, a transmission spectrum moves to higher values due to the introduction of a layer with a lower refractive index in contact with air in the EMA approach while it should move to lower values if the scattering losses are introduced. The results for modeling the measured spectra of a thick (2.9 μm) thermally evaporated LiF film demonstrating a positive inhomogeneity in reflectance were also presented [75].

2.4. INHOMOGENEITY IN THE PVD COATED THIN FILMS

To analyze the inhomogeneity in the physical vapor deposited optical thin films, spectroscopic ellipsometry [76, 77, 78, 79, 80 etc.] has frequently been used. Here, a preferred model has been a system consisting of a main material, a porous material on the top of a film characterized in a Bruggeman effective medium approximation [46], and, possibly, some additional sublayers to achieve a better merit function. Another possibility, as already stated, is to introduce a change of the refractive index through a film. Below an overview of the results obtained analysing the optically inhomogeneous PVD films is presented.

In epitaxial silicon grown on a sapphire substrate, a layer with a thickness of about 20 nm and different optical properties is formed between an Al_2O_3 substrate and Si bulk layer [81]. In [82] the existence of a near stoichiometric MgO phase with a thickness of less than 5 nm thickness has been detected on different substrates while an oxygen-rich phase grew over this layer in reactive ion beam sputter deposition process performed in excess O_2 containing atmosphere. A SiO_2-type interfacial layer of 3–4 nm between a Si substrate and DC magnetron sputtered ZrO_2 has been seen when using SE in [80]. When the RF magnetron sputtering was used to deposit the films, a thickness of the interface layer between Si and ZrO_2 increased from 4 to 10 nm with a rise of O_2 content in the process chamber [83].

A possible reason for negative inhomogeneity (lower refractive index, i.e. lower density) may be the higher void fraction in the upper part of a film as was demonstrated by [78]. A two-layer film of thermally UHV evaporated Ti consisted of a pure titanium layer of 15 nm in thickness and a void-containing metal layer of 27 nm if evaporation was stopped at 15 nm and continued later. The physical mechanism of this process remains open.

It has been demonstrated in [84] that reactive magnetron sputtered Nb_2O_5-TiO_2 films are positively inhomogeneous (i.e. have a rising refractive index towards the layer growth) due to the rise of the substrate temperature from 50°C to 200°C during deposition. The authors presented a method of comparing the transmission spectra of a single-layer and a two-step films (consisting of two identical single layers) using an envelope method and showed that the two-step method gave a lower extinction coefficient compared to the traditional envelope method, and the film inhomogeneity increased markedly in the blue visible region.

The existence of columnar structure in films has been shown for MgF_2 and ZnS films evaporated at room temperature, for TiO_2 evaporated at 350°C [85], and also for RF sputtered TiO_2 [86]. For both molecular-beam deposited and PVD MgF_2 and NdF_3, the cone-like columns have been reported [87]. In PLD TiO_2, the nanocolumns were seen in [88] and for EB TiO_2 on floated glass in [89]. Yttria-stabilized zirconia showed a fibrous structure when deposited on glass at 600°C for both ion-beam-assisted and electron beam deposited without IBAD methods [90]. For highly oriented RF sputtered ZnO films on Pt electrodes a columnar structure has been seen by SEM in [91].

A columnar structure in a film has been demonstrated to form in PbF_2 [48], in BaF_2 and LaF_3 films according to SEM and TEM [92] and ion plated TiN and Mo layers [93], while CaF_2 exhibited a granular structure.

In the work [94] the optical structure of TiO_2 films prepared by ion-assisted electron beam with an ion gun current fixed at the value at which the refractive index was maximal has been analyzed. A best fit using spectroscopic ellipsometry was obtained for a non-linear refractive index structure with ca 170 nm of lower-index material on a substrate. For reactive electron-beam evaporation of titania from different Ti oxide materials, the films had a slight positive inhomogeneity on unheated substrates while both positive and negative inhomogeneities were observed on heated substrates [95]. In a paper [66] the evaporated titanium oxide layers have been analyzed. The authors used the transmittance values from measurements in the vacuum chamber to record the mean refractive index between the consecutive transmission extrema. It was found that the mean inhomogeneity of the films $\Delta n/n$ can vary from 0 to –12%

(negative inhomogeneity) depending on the evaporation conditions, with oxygen partial pressure and the cleaning conditions having a greater influence on inhomogeneity than the temperature. At evaporation with a constant deposition rate, a linear dependence of the refractive index *n(z)* was obtained for the films with a thickness of up to 320 nm.

A nearly linear negative inhomogeneity of the refractive index measured *in situ* during the deposition of EBD TiO_2 has been recorded in [96]. However, this result was obtained in a linear approximation and a structure with a two-layer negative inhomogeneity having a thin sublayer with a higher index and material with a lower index upwards would give the same decrease in the mean refractive index, if that approximation were used. In this work, also a decrease of the refractive index for a material deposited on a multilayer film compared to a monolayer on glass was measured *in situ*.

The Ti oxide films produced by reactive DC magnetron sputtering have been analysed in [33] using the Forouhi-Bloomer model. The results for extinction were good for a region with k higher than 0.005. The method worked for amorphous films, but not so well for the crystalline ones exhibiting an inhomogeneous nature and the diffuse components of transmittance and reflectance due to roughness. Also, an extraneous maximum in the refractive index vs wavelength curve has been obtained in the region of high losses, remaining unexplained. For TiO_2 and TiO_2-SiO_2 coevaporated films no inhomogeneity has been seen in [97].

E-beam TiO_2 anatase films deposited on float glass resulted in positive inhomogeneity if the substrate temperature was 150ºC and in negative inhomogeneity at 250ºC according to the SE analysis [88]. For ion-assisted e-gun deposition [98], the transmission electron microscopy images of TiO_2 detected an amorphous-like thin sublayer with a thickness of about 20 nm at the film-substrate interface depending on the coating conditions though this inhomogeneity could not always be revealed by the SE analysis. A phase structure of the films switched from amorphous to anatase and then to rutile with the rise of the ion energy. A fall of the extinction with a rise in the film thickness for TiO_2 was reported in [99]. However, the presented data were not self-consistent, needing a negative extinction for the upward part of a layer. As the rise of the refractive index with the thickness reported for the same layers would mean a lower transmittance not reflected by the data, there were probably some changes in the evaporation conditions in this work.

Sol-gel produced TiO_2 films have been analysed in [32] using a single oscillator dielectric function for spectroscopic ellipsometry and a structure consisting of an inhomogeneous film and a rough surface layer. The inhomogeneity was characterized by the Bruggeman effective-medium theory according to the formula $(1-f_v)\frac{\varepsilon_m-\varepsilon}{\varepsilon_m+2\varepsilon}+f_v\frac{1-\varepsilon}{1+2\varepsilon}=0$, where f_v – the volume fraction of the voids, ε_m – the dielectric function of the material with the highest refractive index in the film. The inhomogeneity was claimed to be of linear profile and a good agreement was achieved in a wavelength region without absorption. Here, a possible reason for the inhomogeneity was supposed to be the heat treatment between the successive dip-coating processes.

Koppelmann et al. [68] have described the cryolite films using a thin sublayer in contact with ambient as described above. A double-layer structure for the refractive index of cryolite has also been used in [100]. This structure had a higher index at the first 30 nm of the electron gun evaporated layer in vacuum conditions. The refractive index of the same material could be fitted using a homogeneous model after adsorption of water by the coating in normal air conditions. Using Brewster angle measurements and a double-layer model with a boundary layer in contact with a substrate [101], a rising refractive index profile for ZnS, CdS and HgS, and a falling index profile for MgF_2, CaF_2 and cryolite have been obtained. Here, a low-index boundary layer was interpreted as a result of decomposition of the evaporated material and formation of the corresponding oxides on a substrate.

A fall of the refractive index through a film has also been reported in [102] for a reactive RF sputtered SnO_2 films.

Electron microscopy studies have shown that electron gun evaporated CdS, ZnS and ZrO_2 had rough surfaces with a roughness in the order of 20 nm. The surface roughness caused a need to take into account a double-layer structure in the analysis of the R and T spectra in this experiment [103]. A refractive index structure with sublayers of a lower index in contact with a substrate as well as with air has been reported in for inhomogeneous ZnS and ZnSe layers [104]. This result was based on the He-Ne laser ellipsometry measurements during the evaporation. ZnS film grown by atomic layer epitaxy showed a structure with a lower and rising density within the first 50–100 nm followed by a 300 nm thick layer with about constant density and then, in the next 1000 nm of the film, the density fell again nonlinearly in a way yielding a nearly linear dependence for the refractive index [105].

HfO_2 evaporated by electron gun in an oxygen reactive atmosphere possesses a low negative inhomogeneity with a larger inhomogeneity value obtained at a lower evaporation rate [106]. The same effect was seen in [107] with a scattering, i.e. loss, exponentially rising with the increasing film thickness. A negative inhomogeneity of electron beam gun deposited hafnium oxide can also be seen from the spectra published in [108] (not taken into account in the paper). A work [109] has analysed the transmission spectra of the electron-beam evaporated HfO_2 films. A linear refractive index dependence model was used and an index change explained by the formation of truncated cone-shaped grains during the film growth. It was noted that the exponential and combined profiles in which the refractive index changes linearly near the contact with air and remains constant downwards in the film also provide acceptable dispersion curves while the measurements are insufficient to yield an exact profile.

The inhomogeneous ZrO_2 films electron beam evaporated on single-crystal silicon were studied using near-normal spectroscopic reflectometry and variable-angle spectroscopic ellipsometry [79, 110, 111] and the results combined using a least squares fitting. It was shown that at using Cauchy dispersion and not taking into account the absorption in the films they can be modelled with a structure having two regions with a negative gradient of the refractive index – a wider one between a silicon wafer and the main material and a narrower one at the contact with air. The authors also found a 4-parameter function to characterize the refractive index structure for both ZrO_2 and HfO_2 films and showed that one of these parameters characterizing the refractive index dependence at the border with air can possibly be related to the roughness parameter σ determined from the atomic force microscopy measurements. In this case the refractive index variation in this sublayer would represent the microroughness related to the columnar structure of the films.

Electron-beam evaporated zirconia films have been analyzed in [112] using the data of the transmission measurements, fitted point-by-point to the different inhomogeneity models, and a Rutherford backscattering spectrometry. An exponential variation of the refractive index was preferred with a faster rise into the depth of the film at the border with air. Fitting of RBS spectrum was made and the two best solutions for refractive index structure resulted in a thickness of the outermost, least dense sublayer of about 20–30 nm. The inhomogeneity was also explained by the changing diameter of a hexagonal array of the cilindrical columns. Still, modeling together with absorbance results in an even better merit function for two-layer inhomogeneity compared to the exponential one. A negative inhomogeneity can also be seen in the ZrO_2 films RF magnetron sputtered at lower temperatures in [113].

Using reflectance and X-ray diffraction measurements, Klinger and Carniglia [114] have demonstrated that a high-index sublayer in an inhomogeneous ZrO_2 e-beam evaporated at 300°C consisted of a cubic material with a thickness of less than 70 nm on which a lower-index material grows. This result was obtained by measuring the films with different thicknesses having a reflectance minimum at the same wavelength. A material in the film above the first 100 nm was mainly of monoclinic phase with a lower refractive index and less dense.

Duparré et al. [115] have analysed the losses and structure of a ZrO_2 film with multiple halfwave optical thickness deposited on BK-7 glass and on high-reflecting multilayer system to suppress the losses at interfaces by using the thus obtained structure of the electric field distribution. For polycrystalline films, an approximated double-layered structure with a higher-index sublayer with the refractive index of 2.0–2.1 for the inner and with the refractive index of 1.8–1.9 for the outer region was obtained using the multilayer fitting of transmittance and ellipsometry data. For the amorphous films deposited at room temperature and the polycrystalline ones deposited at a substrate temperature of 200–250°C the transmission electron microscopy (TEM) of the film cross-sections showed the existence of a fibrous structure with a pronounced thin sublayer in contact with the substrate. The reflection electron diffraction revealed a preferential localization of the monoclinic phase near the substrate in a layer of 30–40 nm in thickness while cubic crystallites with increased grain sizes and higher amount of voids dominated in bulk. The refractive indices of the two phases were reported being similar and the inhomogeneity results explained by the condensation of a more fine-grained phase mixture in the near-substrate region and less dense structure in the other part of a layer. A secondary neutral mass spectrometry showed also a drastic reduction of the contaminants in the high refractive index region. The absolute amount of absorption was seen to be proportional to the thickness of a ZrO_2 film and it was concluded that the contaminants were a main source of absorption in film material. As baking of the ZrO_2 films resulted in a decrease of the OH and N-CH_2 signals it was emphasized that for a reduced absorption one needs to avoid carbon and hydrocarbon contamination during deposition.

In electron beam evaporated zirconia, the thickness of a high-density film in the near-substrate region decreased from 80 to 40 nm with the increase of the substrate temperature from room temperature to 500 K [91]. A layer formed in the initial stage of deposition was cited as cubic like in [114] while monocline phase started to grow when a film obtained a certain thickness. It occurred possible to stabilize a high-refracting cubic film by using small amounts of other oxides in the material. The same results (tetragonal zirconia as the bottom and monoclinic as the upper sublayer in a double layer structure) have been obtained for ZrO_2 evaporated by an electron beam gun from metallic Zr in [116] at oxygen pressures exceeding 10^{-3} mbar. It was claimed that the tetragonal and cubic forms of zirconia might be stabilized in films in the presence of the oxygen vacancies.

Adding SiO_2 to the evaporated ZrO_2 film by coevaporation of these materials has helped to extend the bottom high-refractive-index region and stabilize it as an optically homogeneous film [97]. It was claimed that mixing the different materials during coevaporation might suppress crystallization of the film material and help achieve the amorphous homogeneous layers. It has been shown [91] that the mobility of the adsorbed species parallel to a substrate surface has a strong influence on the packing density and morphology of the films.

Using an ac reactive magnetron sputtering [117] obtained mainly monoclinic growth of ZrO_2 on Si, supported with a rise of a tetragonal content starting from 125 nm thickness. This effect was attributed to the rise of the substrate temperature during a deposition.

Evaporation of Sc_2O_3 and Y_2O_3 films from boats on unheated substrates resulted in films without obvious inhomogeneities [118]. Still, even for evaporation in oxygen atmosphere, there was a clear absorption in an yttria film at 310 nm wavelength, leaving a possibility that an absorption existing in the visible region hides an inhomogeneity. The Sc_2O_3 films electron beam evaporated at 150°C were shown to be negatively inhomogeneous with the degree of inhomogeneity rising with decreasing wavelength [26].

2.5 INHOMOGENEITY IN THE ALD THIN FILMS

In the films grown by atomic layer deposition processes, the multilayer profiles have been seen using the phase analysis methods. As the self-limited growth of the thin films in the ALD processes proceeds through the surface reactions, it is more strongly influenced by the state of the already grown material. A change in the crystalline phase has been seen for the ZrO_2 thin films atomic layer deposited from $ZrCl_4$ and H_2O or H_2O_2 [119]. According to reflection high-energy electron diffraction, the film growth began with formation of the amorphous phase up to the thickness of 50 nm at 180°C. The thickness of this sublayer decreases, however, to about 1 nm at 600°C. From this thickness on, the preferentially cubic (180–210°C) or tetragonal (230–600°C) phases grow in the 10–50 nm layer while the thicker films also contained also a monoclinic phase. For the ALD ZrO_2 films grown in the same way it has been shown by Raman scattering, that the films grow in a tetragonal phase in the first stage and switch over to a monoclinic growth afterwards [120]. A switchover for the films grown at 500–600ºC took place at a film thickness of about 50 nm [121]. For ALD HfO_2, a metastable phase has also been seen at the first stage of ALD growth [121].

The HfO_2 films grown at 300ºC to a thickness 25–30 nm contained only amorphous phase while monoclinic crystallites started to form in the thicker films. In the films deposited at 400ºC the thickness of the amorphous material diminished to 8–10 nm [122]. The reflections of a high-pressure orthorhombic polymorph were reported in the films grown at 400–600ºC while at 880–940ºC a cubic phase with its thickness not dependent on the overall thickness of the film was formed on the surface according to RHEED [123].

In the films, obtained from $TiCl_4$ and H_2O at 210°C, a structure containing less than 10 nm of amorphous phase followed by a layer of an unoriented poly-crystalline anatase TiO_2 with a thickness of 15 to 55 nm and oriented anatase as the main component in thicker films could be deduced from the data of RHEED studies [124]. In the films deposited on silicon (111) substrates at 425°C a high-density crystal phase of TiO_2-II has been observed at film thicknesses of up to 200 nm if sufficient $TiCl_4$ doses and purge after H_2O pulses were guaranteed. Depending on the process conditions, a rutile phase started to grow on this layer with a switchover to a growth of pure rutile with increasing film thickness [125].

2.6. OBJECTIVES OF THE RESEARCH

The research, the main results of which are presented in this dissertation, began as an attempt to improve the reflective properties of dielectric mirrors produced at the Institute of Physics, Academy of Sciences of the ESSR. The evaporated oxide and fluoride films displayed the transmission maxima demonstrating negative absorption values making it impossible to characterise individual films and find the optimal process conditions resulting in the lowest absorption losses.

As it is not physically reasonable to have a material with negative absorption, the films under discussion had to be taken as possessing an inhomogeneous structure. So, a need arose for a better understanding the optical structure and finding possibilities to obtain reliable information about the evaporated films. A multiparameter fitting of a transmission spectrum occurred to be a suitable method in our conditions. In this way, the vacuum evaporated (PVD) films both the homogeneous and inhomogeneous (only results on the inhomogeneous films have been published), and atomic layer deposited (ALD) films, being absorbtive according to transmission measurements, became the objects of the research. Understanding and finding the limitations of such procedure was another objective of the studies performed.

3. RESEARCH METHODS

Our physical vapour deposited films were obtained using a vacuum evaporation plant BALZERS BAK-600 having two electron gun sources, one thermal boat evaporator and a planetary mechanism for rotating the substrates during evaporation. The analysed films were deposited at different times using optical material from different sources (AG BALZERS, Liechtenstein, and NMT, Odessa, Ukraine). MgF_2 was evaporated from a thermal boat, LaF_3, Y_2O_3, Al_2O_3, ZrO_2, Ta_2O_5 and TiO_2 from a water-cooled e-gun crucible. All the evaporated coatings were produced at a substrate temperature of about 280°C at a base pressure of about 10^{-5} mbar. MgF_2, LaF_3, Y_2O_3 and ZrO_2 were evaporated without any additional gas in a chamber, the other oxides reactively at different oxygen pressures. All the named materials except Al_2O_3 were consistently seen to be transversally inhomogeneous and were analysed.

The atomic layer deposited films were grown in a home-built system using a sequential dosing of reaction materials with purging of a reactor using pure (5.0 grade) nitrogen between the reactant pulses. A reactor structure has been described in earlier publications [122].

For the measurements of the the transmission and reflection spectra we used a two-beam spectrophotometer “SPECORD M40” (“Carl Zeiss Jena”) with a measurement range 190–900 nm, deuterium lamp and double monochromator for UV region, halogen lamp and a grating-filter monochromator for VIS region, theoretical precision of transmission measurements of 0.5% and theoretical repeatability of 0.2%. In order to measure the reflection spectra, the device was used together with a W-type appendix from “Beckman” having an Al reference mirror and adjustable angle of incidence.

The transmission and reflection spectra of thin films were measured, but only the transmission spectra of the films on transparent substrates were analyzed. The substrates were considered as transparent in a spectral region where the absorption did not exceed 0.5% compared to the transmission values computed as $T = \frac{2n_0}{(n_0+1)^2}$ (6)) .

Here n_0 – the substrate refractive index from literature data for fused silica, A reason for this limitation was that only for transmission we could obtain the data with an error of less than 0.5% and so be sure that the information obtained from modelling concerns inhomogeneity and that the data from different specimen could be compared. Of course, this limits us not only to transparent substrates, but also to films with low values of absorption. In reality, the transmission measurements of pure fused silica substrates on our device initially gave higher transmission values than it was expected from the calculations based on the table values of the refractive index. Thus, to achieve a better uniformity of a light beam over the surface of a photomultiplier receiver a homemade integrating sphere with an $MgSO_4$ coating was added to the spectrophotometer between a specimen and the receiver.

By using a sphere it was possible to get the transmission values of an uncoated high quality silica substrate coinciding with the value of formula (6), where n_0 is the tabulated refractive index of fused silica, with a difference between them within 0.1%. The substrates to be analysed were checked before using to ensure a maximal transmittance without the traces of absorption in the wavelength region of 240–800 nm (4.2 – 1.25 μm^{-1} at a wavenumber scale). At every measurement, a 100% transmission line, the transmission of another prechecked pure substrate, the transmission of a coated substrate and a new 100% line were recorded and the measurements repeated if the transmission values of the empty spectrophotometer before and after the measurement did not coincide. The substrate and film transmission values were smoothened and corrected against a 100% transmission line before data fitting. Such a procedure enabled us to keep the transmission result for pure silica substrates within an error limit of 0.5% errors the measurements.

A possible column formation in the films was suppressed using the planetary mechanism of a plant causing the falling angle of the film material to change continuously during evaporation. The main gas residue in the chamber according to the mass-spectrometric measurements was H_2O. In the experiments, the thickness differences over an area where the specimen were held were usually less than 1.5% for PVD coated thin films and there was no need to account for film inhomogeneity over a surface. For the ALD deposited films, the diaphragms were used to guarantee that only the part of a film with visually the same color would be illuminated by light beam as much as possible.

To compute the model data for the film transmission we have used a home-written program icap11t written in Pascal by L.Sossi and coworkers. A program for the analysis of recorded data was written in FORTRAN 77 according to the approach of [27]. At the first stage, using a simplex method [28] a dispersion equation for (3) was computed as $n_0 = 1.44 + 5.24 \cdot 10^{-3} \nu^2$, with ν – the wavenumber in μm^{-1}, based on the measured transmission line of a pure substrate [I]. In the later work with other materials, instead of using an equation, the refractive index values were calculated right from the pure substrate transmittance, measured alongside with a specimen as $n_0 = \dfrac{1+\sqrt{\dfrac{1-T_0}{1+T_0}}}{1-\sqrt{\dfrac{1-T_0}{1+T_0}}}$, where T_0 – the measured transmission value for given wavenumber. So it became possible again to present the transmission of the substrate with a film as a function of the film dispersion parameters and thickness taking the substrate refractive index as a predefined constant for each wavenumber. An interference spectrum of a thin film depends on the quantity $2\pi nd/\lambda$ (Eq. 2) that is inversely proportional to the wavelength, thus, the data was taken with a wavenumber step of 0.1 μm^{-1} as a single film spectrum is more or less periodic as a function of the wavenumber and the features of a measured structure are more equispaced there. The films were modelled using the Lorentz dispersion formula as it uses the same four parameters to obtain the refractive and absorption indices. A procedure was built on the predefined initial parameters and their changing rates usually yielding a result with the found parameters and merit function M (5) in less than 300 computing cycles. If 300 cycles were not enough to converge, the program was terminated. As the optimization procedure can result in a local, not a global minimum, several optimizations with different initial values were performed and the parameters obtained with the best merit function chosen. The dispersion parameters of the best result were taken as the new initial parameters then and varied again as long as the fit result continued to diminish. Special attention was paid to the initial value of the layer thickness that had to be obtained beforehands by counting the spectral extrema (in the wavenumber scale, the value 0 μm^{-1} corresponds to the zeroth transmission maximum). A reason for this is that the optimization procedure tends to end in any of the secondary minima if the predefined film thickness is too far from that for the global minimum of the merit function. If a computed spectrum changes during the optimization, part of the spectral values must move from one spectral minimum to another overcoming the maximum where a part of the merit function originated from this part of the spectrum significantly worsens, so the procedure involves problems of changing a spectral order dealing with task of this kind. The value of the resulting merit function is a measure of the applicability of the particular dispersion and film inhomogeneity models and, based on its magnitude, we can compare the different models. If the used spectral regions differ, a better parameter for comparison is the mean difference between the measured and computed values over a spectrum obtainable from the merit function.

4. RESULTS AND DISCUSSION

4.1. PVD THIN FILMS

Here, the results of analysis for vacuum evaporated inhomogeneous films grown in our laboratory as described in Part 4 are presented.

4.1.1. MAGNESIUM FLUORIDE

As showed in Section 2.3 (Fig. 3), the approach that assumes linear inhomogeneity [3, 7, 59] and does not take into account the reflections inside a film may give a good representation of one particular film, but must fail when the films of the same material, but with various thicknesses, are analysed together. For MgF_2, we computed the theoretical transmission spectra for different inhomogeneity profiles and compared the parameters obtained for the linear inhomogeneity model with the initial ones. The agreement was good for the cases with a slow change of the refractive index through a layer (linear and square function changes) and poor when there were abrupt changes of the index (square root and the functions having a part with a sharp slope). We could not use the unknown differences of the refractive indices on the film interfaces for such structures; so, the first approximation had to be an inhomogeneity model having two sublayers with different indices.

As it is seen on the presented transmission spectra of the real coatings (Figs. 2, 6), we have a restriction that the differences between the transmittances of the coated specimen at half-wave points and those of an uncoated substrate should stay approximately constant. To look at the possible structures, we computed the transmittances of some model structures presented in Figs. 4 and 5. We made a conclusion that to obtain a spectrum like we have for MgF_2 (Fig. 6), we need to choose a model with a thin sublayer with a higher refraction index in contact with the substrate and a main material with a lower index on the top of that sublayer. In order to analyze an inhomogeneity of the evaporated MgF_2 film [I] the four parameters of Lorentz dispersion and the film thickness were taken as the free parameters, a transmission spectrum of a pure fused silica specimen was used to obtain the refractive index of a substrate and a transmission spectrum of a full system including the backside of a substrate was computed over a spectral region of 4.2 to 1.2 μm^{-1} with a step of 0.1 μm^{-1}. A theoretical spectrum was compared to a measured one and optimised to minimize the merit function $\sum_i (T_{i,computed} - T_{i,measured})^2$ (5), so the best solution for a homogeneous coating with the given optical dispersion was found. The minimization of the merit function was done using the Nelder-Mead simplex method [28].

It occurred practical to make a fit for a homogeneous film at first and use these results as the initial parameters for a system of two sublayers, having two fit parameters for the thicknesses of the two sublayers and an additional parameter for the difference of the refractive indices between them. Next, a more detailed analysis was performed to specify the character of the refractive index change inside a film. So, the different transition profiles were checked with the additional parameters using another full optimisation process. A thinner sublayer was divided into 5 even thinner layers of equal thicknesses and the refractive index step presented as a parametric function of the sublayer number. The best results were obtained with a transition according to the power law. So, it was possible to characterize the structure of the transition between a substrate and the main material of the film (using two sublayers with the thinner layer being placed in a contact with a fused silica substrate). The results are presented in Table 1 and Fig.7.

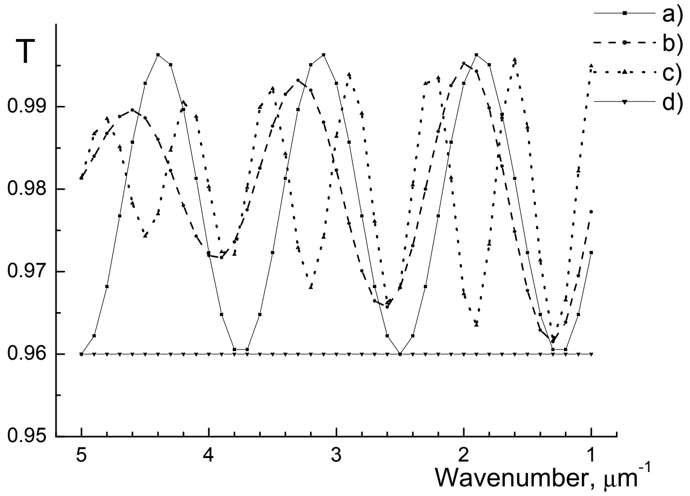

Fig. 5. Transmission structure of a two-layer system n = 1.4 – 1.3 on a semi-infinite substrate n_0 = 1.5. a) film n =1.3, nd = λ/2 at 800 nm; b) structure 1.4 – 1.3 λ/20 – 9λ/20 at the same wavelength; c) structure λ/20 – 19λ/20. d) uncoated substrate;

Table 1. MgF$_2$ film fitting results depending on a defined refractive index structure at the first stage of growth.

No	Δn(j)	Merit function (·10^{-5})	Main layer thickness d$_1$(µm)	Sublayer thickness d$_2$(µm)
1	$0.067j^{0.40}$	4.4	0.619	0.020
2	$0.070(j-1)^{0.393}$	4.4	0.597	0.023
3	$0.063(j-1)^{0.383}\lambda^{-0.165}$	3.76	0.596	0.023
4	$0.0039j^{0.922}+0.075$	7.7	0.625	0.013

Here, *j* – index of a particular sublayer d_2, *j-1* means a structure with 4 sublayers d_2, $\Delta n(j)$ – refractive index difference for a sublayer *j*, λ – a wavelength value in µm.

For vacuum evaporated MgF_2, the best fit to the experimental results yielded the structures with a 90–100 nm sublayer of a higher refractive index in contact with fused silica substrate and a homogeneous material of the main film above it. The mean difference between the measured and calculated transmission points was 0.12%. A structure maintaining an index step between the two parts of a film material yielded a thinner transition layer and worse fit (Table 1, row 4). Adding the dependence of the transition layer refractive index against wavelength lowered the merit function still, but not enough to obtain a quantitative difference in a structure.

To check the results, another layer with different thickness was evaporated from a different batch of MgF_2 under the same conditions. A full analysis in a two-layer approach was carried out together with a fit using the dispersion parameters obtained for the first film with the film thickness as the single free parameter (Fig. 8). A difference in the film thickness between the two approaches was 1 nm, the transmission spectrum calculated with the dispersion parameters of the first film being placed higher. It means that the films had different absorptances with the indices of absorption being $2.8 \cdot 10^{-4}$ for the first and $3.7 \cdot 10^{-4}$ for the second film, respectively, at the blue end of the analysed spectrum at 4.2 µm^{-1}. A good coincidence of the refractive index values of the two films in contact with the fused silica substrate is probably accidental as the difference between the main material indices is clearly bigger.

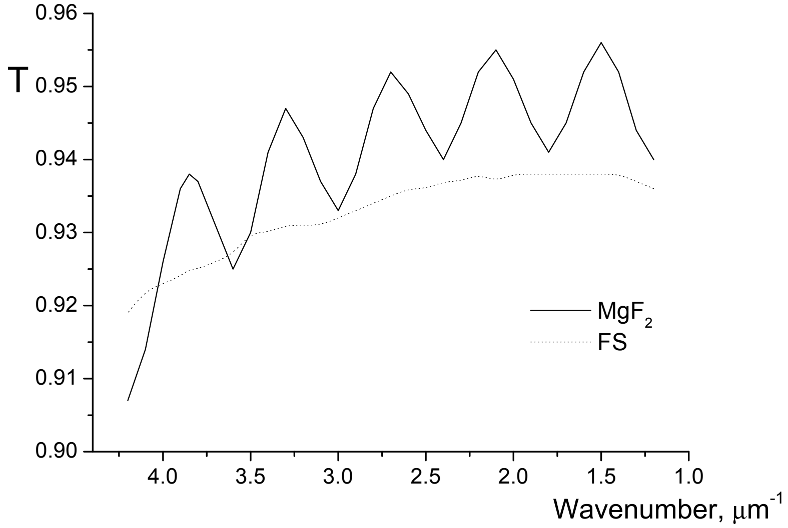

Figure 6. Transmission spectrum of the MgF_2 film on fused silica substrate.

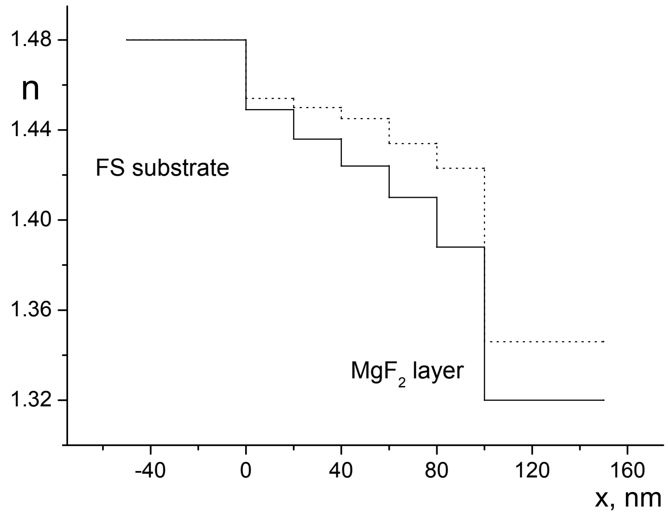

Figure 7. Fitted structure of the first stage of MgF_2 layer growth on fused silica according to profile 1, Table 1. Lower line – structure for the first film, upper line – structure for a control film.

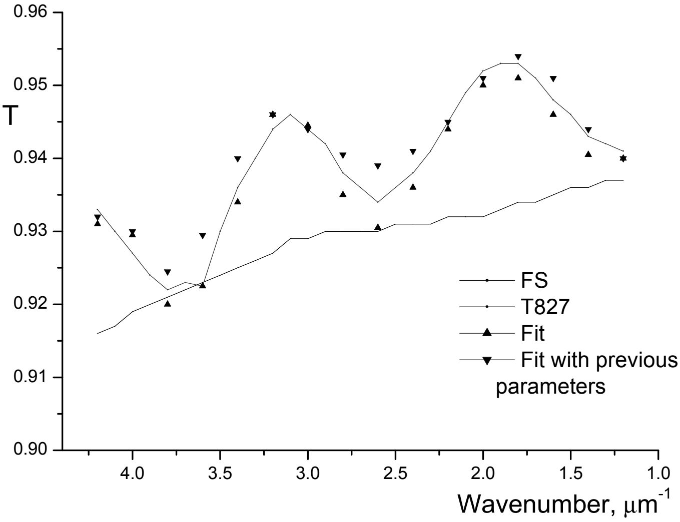

Figure 8. Fitting of the transmission of the second MgF_2 film with the parameters obtained from the first one.

The model used here does not take into account the possible existence of the Urbach absorption tail with its exponential dependence of absorption coefficient on energy (wavenumber). Luckily, for the materials we have analysed, it can influence only some points at the blue edge of the used spectral region ($\alpha < 10^4$ cm^{-1} corresponds to $k < 0.03$ for 400 nm or $k < 0.075$ at 1000 nm).

The refractive index for MgF_2 $n = 1.39$–1.40 has already been reported for evaporation at substrate temperatures of about 300°C in [126]. The MgF_2 refractive index values higher than the table values for crystalline material were also obtained in [127] from Abelès-Brewster angle measurements for thermally evaporated material. There, a positive inhomogeneity recorded was connected to a possible rise of crystalline content in films with thicknesses over 230 nm. A refractive index $n = 1.40$ for MgF_2 evaporated at a substrate temperature of 340°C was reported in [128] together with a decrease of the index with an increasing film thickness. This decrease was explained by irregularities in crystal growth and surface roughness. In this work, the packing density also fell slightly when the film thicknesses exceeded 600 nm. The index of refraction higher than that for massive material was also obtained by [27].

4.1.2. LANTHANUM FLUORIDE

When a need arouse to coat the mirrors for the 157 nm F_2-lasers, we could not use the oxide materials as a high index material due to the absorption in them For this reason, LaF_3 was chosen instead. The films of LaF_3, electron beam evaporated at about 0.8 nm/s, were analysed in preparation for mirror production to find the material optical parameters [II].

In a work [129] the refractive index values for electron beam evaporated LaF_3 were reported as $n = 1.61$ and $n = 1.60$ at 266 and 355 nm wavelength, respectively. LaF_3 films on vitreous silica have been measured by spectroscopic ellipsometry in [76]. A good fit was obtained assuming a contribution of a rough layer with a thickness of 9 nm according to the Bruggeman effective layer theory. A series of fluoride films has been characterized using spectral ellipsometry and a multilayer approach for an analysis of their spectra in [130]. The presented results showed the different structures, either with a negative or positive inhomogeneity. The transmission spectrum of LaF_3 computed from the data given by [130] is clearly different from those measured by us, so the structures of these films are supposed to differ as well. Possibly, a two-layer structure can also be seen in SEM images in [131] for the RF magnetron sputtered LaF_3 films obtained using a pre-fluorination of a LaF_3 target with SF_6 gas.

Information about the optical properties of a film at a laser wavelength of 157 nm was obtained from the transmission and reflection spectra of the 23-layer quarterwave layer LaF_3 – MgF_2 mirror stack. The absolute reflection and transmission spectra of the mirrors were measured in a vacuum ultraviolet region using a vacuum monochromator BMP-2 with a flow-through hydrogen lamp. As the transmission minima values of a quarterwave stack are not sensitive to the small absorption losses, the reflection index of one film can be estimated using a multilayer coatings analysis program if a reflective index of the other material is known. For MgF_2 with its low dispersion we choose to use a value of n = 1.44 that is slightly smaller than the tabulated value for crystalline MgF_2. So it became possible to estimate an absorption index value at a wavelength of the maximum reflectance of the mirrors having a transmittance close to zero at this wavelength. Here, it was assumed that the MgF_2 layers are nonabsorbing and homogeneous and that all the absorption is represented by a higher refractive index and lower absorption edge energy material, LaF_3.

Two batches of LaF_3 material were used and the transmission spectra of the films were analysed separately in the same way as described above [I] with fused silica and MgF_2 used as the substrates. The results for the batches in Fig. 9 are presented in Figs. 10–12 together with the data from LaF_3 films transmission fitting. Although the absorption in lanthanum fluoride material obtained for 157 nm should be overestimated, the accord between the results at working wavelength and those obtained from the dispersion calculations was still good enough (Fig. 11). The resulting absorption indices obtained from the measurements at a maximum reflectance of a mirror fell into a range of 0.001–0.007 for the first series and 0.008–0.015 for the second series. As it can be seen, there is still a chance that due to the difference in real dispersion compared to that, used in fitting the refractive index on the blue edge of the spectra was in turn overestimated at the expense of absorption. So, it may compensate for the error in the absorption index due to not taking into account the MgF_2 absorption. Also, the scattering losses were not introduced, but they should be minor as the absolute reflectance of the produced LaF_3 – MgF_2 mirrors measured on a BMP-2 vacuum monochromator was close to 99%. For LaF_3 prepared by magnetron sputtering using a pre-fluorination of a target before the sputtering step, n = 1.85 – 0.0085i was obtained for 157 nm [131]. The high value of a refractive index is evidently due to a higher density of a material.

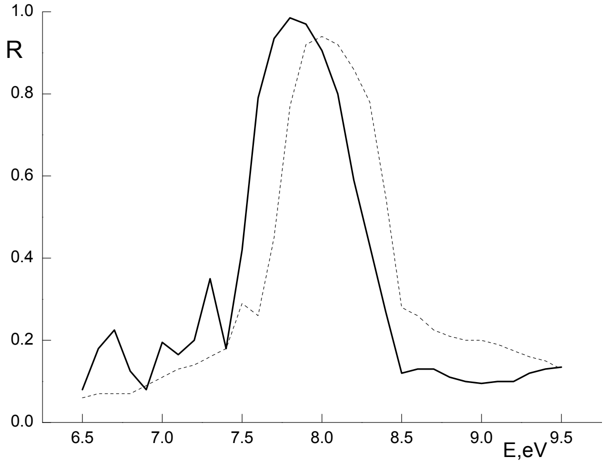

Figure 9. Reflection of the different batches of LaF_3-MgF_2 mirrors for 157 nm. The sample with lower reflectivity was deposited later.

It can be seen that the films are negatively inhomogeneous (the film transmission maxima exceed the transmission values of the bare substrate), so they were fitted using a homogeneous index model and a two-layer model with a higher refractive index for a sublayer in contact with a substrate. The fit results in one- and two-layer approximations (Specimen) for two LaF_3 films on fused silica and MgF_2 substrates are presented below.

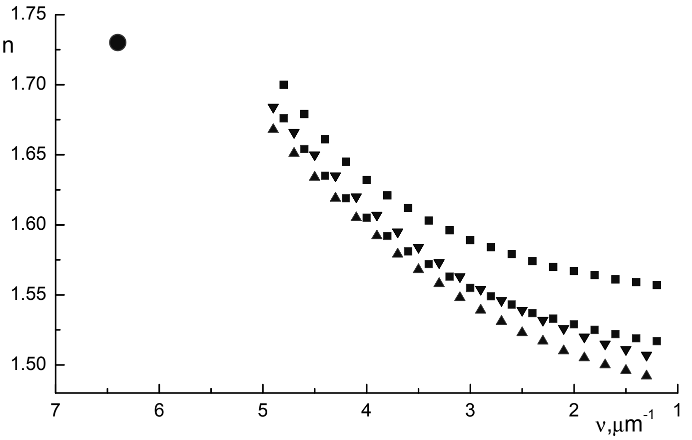

Figure 10. Refractive index dispersion for a LaF_3 material used for mirrors represented in Fig.9. Data for a mirror with higher reflectivity is marked by squares, for the mirror with lower reflectivity by triangles. The upper curves show the result for the homogeneous model, the lower curves for main material in a two-layer approach. Big dot – estimate from a mirror transmission spectrum.

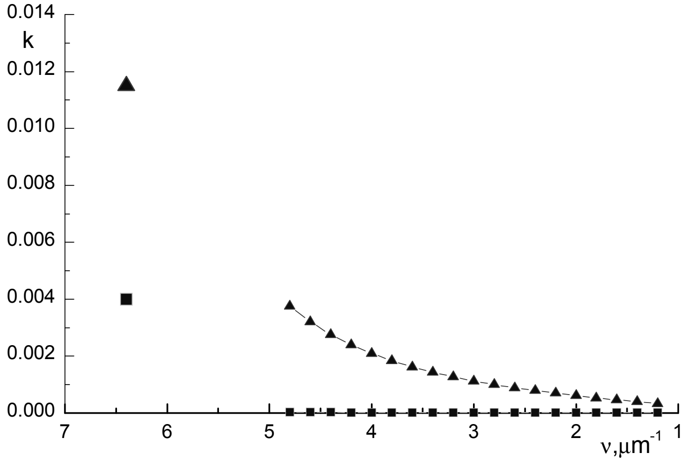

Figure 11. Absorption index dispersion for the LaF_3 material used for mirrors in Fig. 9. Data for a mirror with higher reflectivity is marked by squares, for the mirror with lower reflectivity by triangles. Big dots – estimates from mirror reflection measurements.

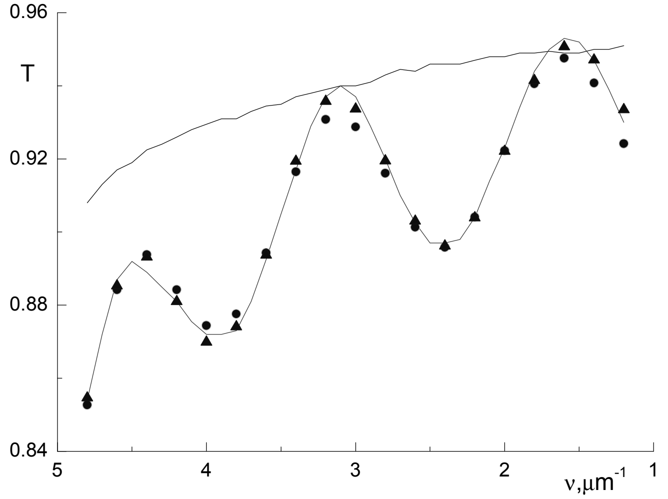

Figure 12. Transmission spectrum of a LaF_3 film on a MgF_2 substrate. Dots – a homogeneous approximation, triangles – a two-layer model.

Table 2. The merit functions for the transmission fitting of the evaporated LaF_3 films in different approximations. 1 – homogeneous approach, 2 – inhomogeneous model.

Specimen	Substrate	Number of data points	Merit function	Mean difference ΔT
192–1	MgF_2	31	$1.2\cdot10^{-3}$	$5.7\cdot10^{-3}$
192–2	MgF_2	31	$8.53\cdot10^{-4}$	$4.8\cdot10^{-3}$
360–1	FS	31	$1.84\cdot10^{-4}$	$2.4\cdot10^{-3}$
360–2	FS	31	$7.45\cdot10^{-5}$	$1.6\cdot10^{-3}$
360–1	MgF_2	37	$5.7\cdot10^{-4}$	$3.9\cdot10^{-3}$
360–2	MgF_2	37	$1.18\cdot10^{-4}$	$1.8\cdot10^{-3}$

A change from 1- to 2-layer approximation (5 and 7 fitting parameters accordingly) reduced the merit function from 1.5 to 4 times. A difference between the refractive indices of the two sublayers fell into the region Δn = 0.015–0.04. For most of the coatings, the sublayer of a higher refractive index had a thickness of 50 to 70 nm. The clear differences in absorption between the different LaF_3 films evaporated from the same batch with a time lag between them is probably a result of material oxidation as it is known that the LaF_3 material tends to turn into a more absorbing oxyfluoride LaOF with time.

4.1.3. YTTRIA

The same picture of an inhomogeneity, which can be described by two layers with a constant shift of a refractive index, has been obtained for some other materials (Y_2O_3, ZrO_2, Ta_2O_5, TiO_2) as well. Still, as a later analysis demonstrated, an optimization of such kind gives two different solutions with different inhomogeneous structures – a thin transition layer can be either in contact with a substrate or on the interface between a film and air. The merit functions for these two cases are identical, and to differentiate between them one needs the exact measurements of the films physical thickness. The two-layer inhomogeneity models with a constant step in the refractive indices and with a thin sublayer either in contact with the substrate or in contact with the adjacent medium have the same optical thickness determined by the positions of the spectral extremes and their amplitudes. However, their physical thicknesses will be different as for a situation with negative inhomogeneity a thin sublayer belongs either to a film material with a higher (the first case) or to a material with a lower (the second case) refractive index (Fig. 13). So, a physical thickness of the film measured e.g. by a profilometer gives a possibility to differentiate between the inhomogeneity models.

Earlier, an electron-beam evaporated Y_2O_3 has been studied by [72, 132]. Ying et al. [72] discussed the transmission results for co-evaporated yttria-silica films where the maxima of pure Y_2O_3 film transmittance were slightly higher than the theoretical curve for a nonabsorbing film. The Cauchy and Sellmeier formulae for refractive indices and exponential dispersion law for absorption α were used and a linear homogeneity model introduced for multiparameter least-squares-fitting of the transmission spectra. This resolved the problem of negative absorption while giving higher α value for the inhomogeneous model. Using a linear inhomogeneity profile for pure yttria resulted in $\Delta n = 0.11$ between the two boundaries. At a wavelength of 500 nm the analysis yielded $n = 1.86$ for the films deposited at 300°C [72] and $n = 1.80$ to 1.84 for the films deposited at different temperatures using an oxygen background of $6.5 \cdot 10^{-4}$ mbar [132]. In [132] the Swanepoel envelope method was used with no inhomogeneity. The value of $n = 1.94$ for cubic crystalline Y_2O_3 at 550 nm and $n = 1.87$ for evaporated films was presented in [133].

In our studies [VII], an attempt was made to compare the different inhomogeneity models for e-beam Y_2O_3 films evaporated on fused silica at 280°C at a rate of about 0.6 nm/s. The transmission spectra were measured and fitted like described before using the Lorentz dispersion model in a homogeneous approach and with the 3 inhomogeneity models: linear change of a refractive index through the layer, two-layer model with a thinner sublayer in contact with a substrate (Step1) and a model with a thinner sublayer in contact with air (Step2). One film was later deposited under the same conditions having an oxygen background of $2 \cdot 10^{-4}$ mbar in a chamber. A linear approximation was taken using a system of 10 sublayers with an equal thickness and refractive index steps as it has been demonstrated [59] that using more than 10 sublayers for describing homogeneous inhomogeneity does not add accuracy to the computed spectra.

Some spectra of the analysed films are presented in Fig. 14. It can be seen that the transmission of a thinner film in visible region exceeds the value of that for an uncoated substrate. This implies that a negative inhomogeneity (lower refractive index in the upper sublayer, in contact with ambient) should be expected. Accordingly, no fits using a positive inhomogeneity model presented an improvement in the merit function compared to the homogeneous case. For the negative inhomogeneity, all the three models for inhomogeneity gave better merit functions than the homogeneous approach did. The differences in the merit functions were not big enough to prefer one solution to another, except for the thinnest film where a linear model was clearly inferior. For this film, the absorption index values obtained using a linear approach were also clearly larger than those for the two-layer models and much bigger than those obtained from a homogeneous model. In Fig. 15, a transmission spectrum of an Y_2O_3 film evaporated with oxygen background is shown together with the fit values. Table 3 presents the inhomogeneity results for the homogeneous, linear and Step1 inhomogeneity models. Table 4 shows the mean differences between the transmission values for the measurement and fitting results in different approximations. The Step2 model always yielded a bigger thickness for the thinner sublayer. For a linear inhomogeneity model, the refractive index difference between the transition boundaries was always higher than that for the two-layer models.

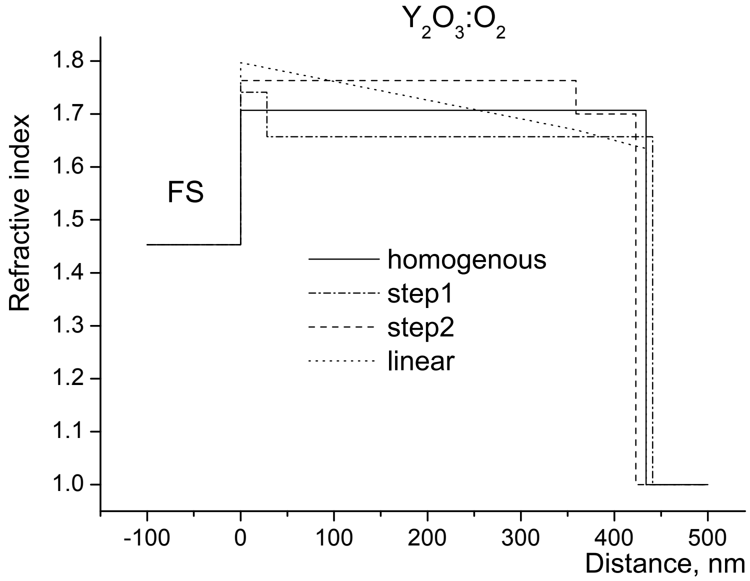

Figure 13. Different possible inhomogeneity structures for Y_2O_3 film evaporated with an oxygen background (fitting results).

Table 3. An inhomogeneity structure of an Y_2O_3 layer using different models.

Film thickness, nm, homogeneous	Thickness, nm, Step1	Refractive index difference, Step1	Refractive index difference, linear
700	31+681	0.05	0.105
484	31+457	0.035	0.09
124	49+76	0.05	0.105
434 (with O_2)	28+413	0.085	0.16

Table 4. Characterization of a fit quality for different inhomogeneity models.

Film thickness, nm,	Mean computed point transmission difference		
homogeneous	homogeneous	step	linear
700	0.009	0.006	0.008
484	0.0045	0.0025	0.003
124	0.004	0.001	0.002
434 (with O_2)	0.008	0.0035	0.0035

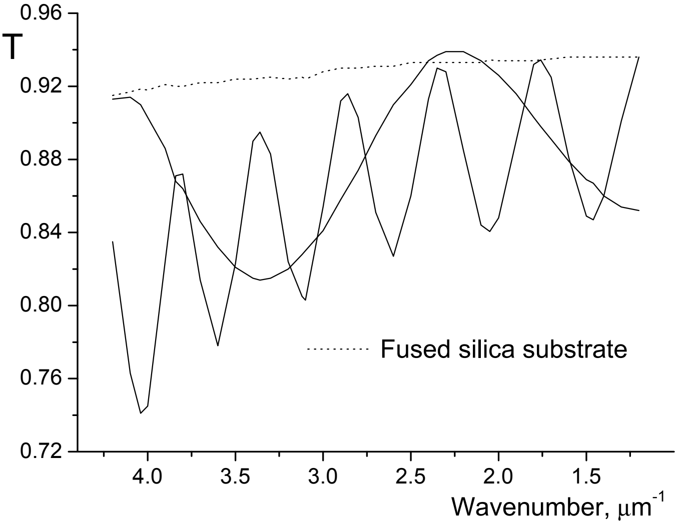

Figure 14. Transmission spectra of some electron beam evaporated Y_2O_3 films with different thicknesses.

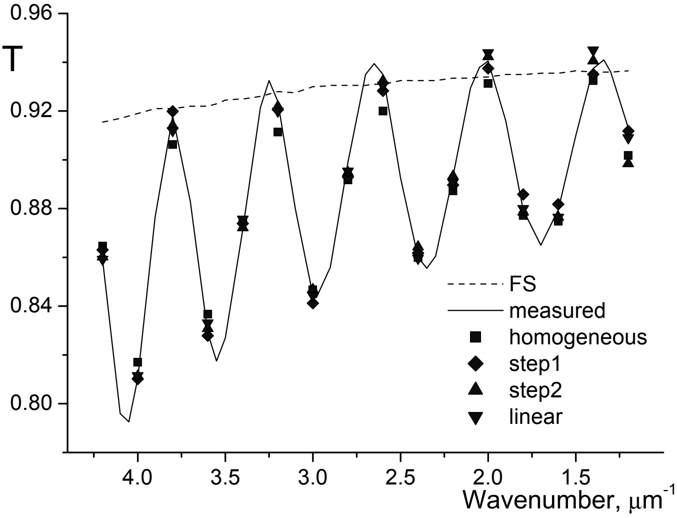

Figure 15. The transmission fitting results for an Y_2O_3 film with a homogeneous thickness of 484 nm in different inhomogeneity approximations.

For an oxygen-doped Y_2O_3 film, the physical thickness measured at Veeco Europe GmbH laboratory in Mannheim equaled to 441 nm using a “Dektak” mechanical profiler and 437 nm using the “Wyko” optical profiler. Fitting gave the film physical thickness values of 434 nm for the homogeneous and linear models, and 441 and 423 nm for the two-layer models. Both profilometry results yielded higher values than these obtained for the homogeneous, linear and Step2 (thinner sublayer in contact with air) approximation with the Step2 structure being the least suitable. The refractive index profiles through a layer obtained for the different inhomogeneous structures were presented in Fig. 13.

One can see that the fit merit function does not allow us to make an unambiguous conclusion about an inhomogeneity structure for an Y_2O_3:O_2 film. The addition of the physical thickness measurement makes it possible to choose one of these – a model with a thin transition layer in contact with a fused silica substrate. A reason for this is the fact that the interference properties of the coating are determined by the optical thickness of the film while the same optical thickness may be achieved by different physical thicknesses of the sublayer. To have the same optical thickness, Step1 model with a thinner sublayer of a higher index material and the main material of a lower index must possess a bigger physical thickness than Step2 model possessing a higher index main material and only a small part of a lower index material. The closeness of optical parameters of the Y_2O_3:O_2 film to those of the pure Y_2O_3 film allows us to maintain that the obtained structure is justified for the pure material also. A similar result was obtained for evaporated ZrO_2 by [114] using the reflection and X-ray diffraction measurements of films with a different thickness.

Our results confirm information of [72] that the linear inhomogeneity model yields higher absorption than the homogeneous one does. This is understandable for envelope methods in case where the transmission of coated objects exceeds that of an uncoated substrate, resulting in a negative absorption index for a film. However, as the same situation is seen in fitting also for thicker films with the transmission maxima lower than the transmittance of a pure substrate, it has to be taken as a peculiarity of a defined structure. Quite to the contrary, if the absorption index k exceeds 0.0005, the two-layer models show less absorption than the homogeneous model does. Like in [V] we see the absorption rising with the layer thickness, probably due to the increase of the structure defect concentration with thickness.

Strictly said, such a model of inhomogeneity with the two sublayers and a sharp transition between them has problems with both the Kramers-Kronig relations and the dispersion formulae that were used in optimization. But, in the same manner as [27], I claim that a model can be used in a limited wavelength range to characterize the structure of a coated layer. Due to the same reason, the parameters in the formulae for optical constants, which have a physical meaning, must not be taken as such when describing the particular analyzed films. Very close merit function minima can sometimes be obtained with the very different sets of dispersion parameters. Even for a homogeneous approximation, the obtained dispersion constants do not have to necessarily correspond to their physical arguments. Possibly, a better approach is to introduce a dispersion inhomogeneity through a void factor as suggested in [46].

4.2. ALD COATED THIN FILMS

In the previous section, the results for negatively inhomogeneous evaporated films with transmission maxima exceeding the values of a pure substrate were presented. Another situation can be observed in some atomic layer deposited materials. In these materials, a transmission spectrum does not cross the transmission line of a pure substrate and a homogeneous approximation of a standard analysis would take them as absorbing (Fig. 16). However, if the analysis procedure is applied as described above (Section 4.1.1) using a two-layer inhomogeneity model, an improvement of fitting results can often be achieved with a positive inhomogeneity introduced (a sublayer in contact with air having a higher index of refraction compared to that in contact with a substrate). It is manifested in a considerable improvement of the merit function and in a thin transition layer near the substrate. It means that these films have a different optical structure, probably caused by the mechanism of its growth – in an atomic layer deposition the growth is due to the chemical surface reactions, not to a sticking of the evaporated species onto the substrate. We have seen this structure in the ALD TiO_2, Al_2O_3 and ZrO_2 films.

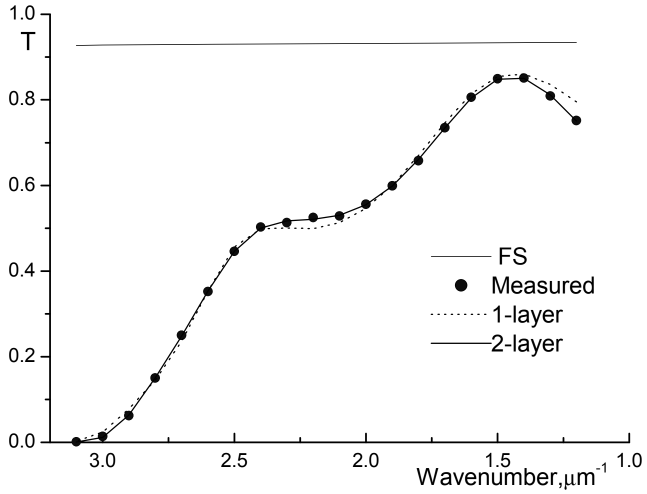

Figure 16. Transmission of the positively inhomogeneous ALD TiO_2 film with fit results in homogeneous and two-layer approximations.

4.2.1. ALUMINA, TIN OXIDE

A method of inverse synthesis was used to characterize the optical parameters of the atomic layer deposited Al_2O_3 films [III]. The films deposited at different temperatures were too thin to use the envelope methods (Fig. 17), but parametric modelling made it possible to obtain the refractive and absorption indices and thickness for each of them.

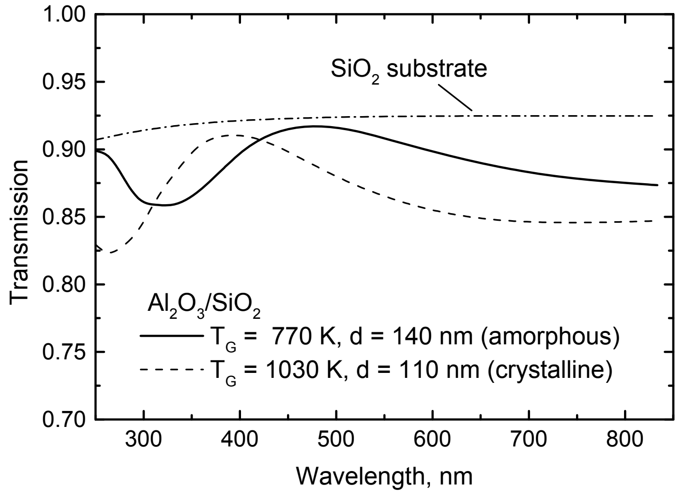

Figure 17. Transmission spectra of the ALD Al_2O_3 films grown at 770 and 1030 K.

The films of ALD grown Al_2O_3 with a thickness of 170 to 270 nm were analysed using the Lorentz dispersion and obtained dispersion data compared to XRD and RHEED measurements giving information about their crystallinity. Some differences in film properties are possible as the objects for optical analysis were deposited on SiO_2 substrates while those for XRD were deposited on silicon. Nevertheless, such approach is justifiable as the results clearly correlated. The amorphous films deposited at the substrate temperatures below 870 K were amorphous, had lower refractive indices and extinction as well as higher dispersion than the films made at higher temperatures did (Fig. 18). Lower dispersion in a crystalline material deposited at temperatures above 870 K indicates to a bigger distance between the measured wavelength region and the onset of interband excitation (i.e. higher bandgap) in them.

Although the spectra of Al_2O_3 films did not display the features like seen before in the PVD films, an attempt was made to characterize them with a two-layer model similar to that used in the case of PVD films. No improvement of the merit function was obtained as the fits converged to the same value as for the homogeneous approach. However, an improvement was achieved with a two-layer model if the sublayer in contact with a substrate was taken having a lower refractive index (Fig. 19). Dependent on the substrate temperature, the thickness of this sublayer was 60–80 nm with a maximum difference of 0.06 in the refractive indices. An exception was the fit for nearly homogeneous films deposited at 470 and 870 K for which there was almost no improvement with the inhomogeneous models used. The value of the refractive index step obtained for the two-layer model did not depend on the wavelength as such dependence was not included in the model.

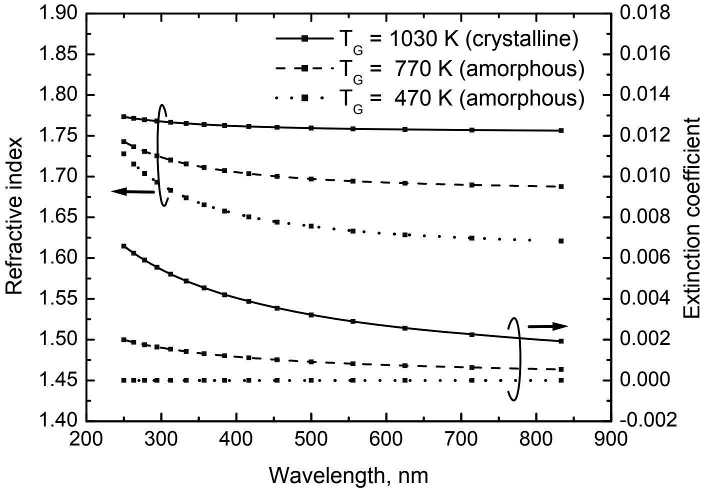

Figure 18. Dispersion curves of the refractive and absorption indices (extinction coefficients) of ALD Al_2O_3 films grown at 470, 770 and 1030 K.

A correlation with roughness was seen, in which the Al_2O_3 samples with a better optical homogeneity correspond to the cases with a minimal relative roughness. At the same time, an increase of the material refractive index with temperature was not accompanied by a well-defined dependence of the inhomogeneity on temperature. It was proposed that a reason for the inhomogeneity was the rise in the crystallinity rate through a layer with a rising film thickness though the type of crystallinity could not be revealed by XRD. The samples with lower roughness have a structure in which the small crystallites do not grow into the bigger ones causing the smaller observed roughness.

SnO_2 ALD films grown on α-Al_2O_3 (r-plane sapphire) were analysed in a homogeneous approach [IV] using an envelope method of [8, 25] to obtain data about the film quality and growth rate dependence on process conditions. The highest thickness increment per process cycle as well as the highest refractive index $n = 2.0$ was obtained for the SnI_4-H_2O_2 process at 150°C and for the SnI_4-O_2 process at 600°C. According to the RHEED measurements, a mosaic epitaxial growth observed at higher temperatures began in a 3-dimensional mode, it was substituted by an extremely flat 2D around the thickness region of 40 nm and it changed back to 3D at higher thickness. The dependence of the refractive index on the thickness was not analysed, but the dependence of the absorption on the film thickness is seen in the results of 600°C SnI_4-O_2 film where the absorption index determined at 400 nm wavelength was almost nonexistent at 90 nm thickness, rose to k = 0.0002 at 210 nm and k = 0.0030 at 415 nm thickness (Fig. 20).

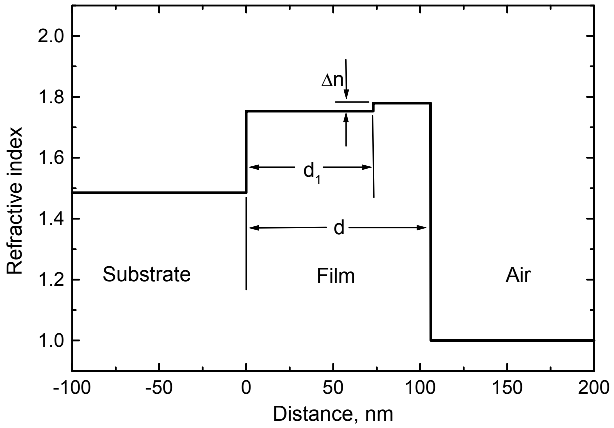

Figure 19. Two-layer model for ALD Al_2O_3 film showing refractive index as a function of the distance from the substrate-film interface for a film grown at 1030 K.

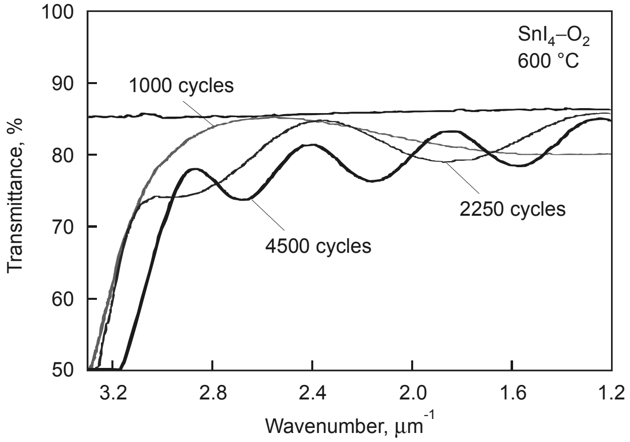

Figure 20. Transmittance of the ALD SnO_2 films of different thickness grown from SnI_4-O_2 precursor pair at 600°C.

4.2.2. TITANIA

Atomic layer deposited titanium dioxide films were investigated in [V, VI]. ALD TiO_2 demonstrates the different crystallographic phases (anatase, rutile, brookite, orthorhombic TiO_2-II) dependent on the growth parameters. The TiO_2 layers were grown from $TiCl_4$ and H_2O at 425°C with the different N_2 carrier gas and $TiCl_4$ pressure values in a reaction chamber. The films of the first group were deposited at a nitrogen flow of 20 μmol/s and titanium chloride pressure of 7 Pa, for the second group the values were 50 μmol/s and 3 Pa, respectively. A continuous flow of nitrogen both carried the precursors to the reactor and purged reaction zone between the precursor pulses. The different $TiCl_4$ pulse durations did not seem to influence the obtained film structure, so the difference in the growth modes should lie in the sequence of intermediate reactions on the film surface. The films deposited at a lower carrier gas rate had anatase as the main phase at lower thicknesses and rutile in the thicker films (the films deposited using a larger number of process cycles) according to XRD and Raman spectroscopy. In addition to these, RHEED detected a low amount of TiO_2-II high-pressure phase in the thicker films of this group. In the films deposited at a higher carrier gas flow rate, XRD did not detect any crystallinity, but Raman spectroscopy demonstrated a dominating anatase phase with the addition of rutile in the thickest sample. So, the films of both groups should have an anatase-rich layer near a fused silica substrate and a rutile phase at the outermost surface of the thicker films. A TiO_2-II phase formed only, if soda lime glass samples were in the reactor together with silica and silicon substrates, so a little amount (undetected, however, by Auger electron spectroscopy) of sodium impurities could play a role in the creation of this phase.

The transmission spectra of the samples were fitted using the Lorentz dispersion within the homogeneous one-layer and inhomogeneous two-layer models. Every film was fitted independently, at first in the homogeneous and then in the inhomomogeneous approach. In Fig.16, a transmission spectrum of one of the thicker films of the first group is shown together with the fit results. The films of the first, low carrier gas rate group, turned out to be similar to those of ALD Al_2O_3, yielding a merit function improvement if the upper sublayer was taken with a higher refractive index. The films grown at a higher N_2 flow were similar to the PVD films demonstrating negative inhomogeneity according to the multiparameter fits. The analysed samples had a thickness of 60 to 160 nm not showing a standard spectral structure with multiple transmission extrema (Figs. 16, 21), so a comparison with the envelope methods was not possible. The Figs. 22–25 present the dispersion data for both groups of films. For the first group, we can see that the refractive index curves for a two-layer model are more similar to each other than those for the homogeneous model. Probably, the curves for one-layer model are influenced by the different ratios of the thicknesses of the two sublayers for various films, displaying a reflectance component from an interface inside a film as dispersion information. The decrease of the refractive index at the blue edge of the spectrum for two films in Fig. 22 demonstrates the limits of our dispersion model as in the region $\lambda < C$, the one-oscillator model [27] is no longer applicable. The data on fit results for the films under discussion is presented in Table 5. The improvement of the merit function moving from the homogeneous to inhomogeneous two-layer model was 0.5 to 2 orders of magnitude.

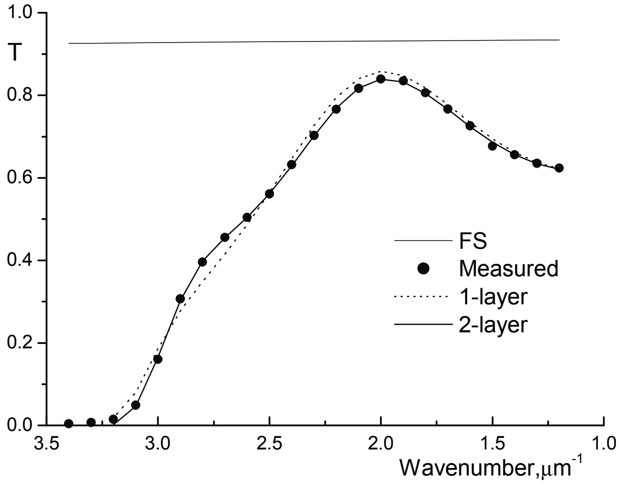

Figure 21. Transmission together with the fits in homogeneous and two-layer approximations for a 125 nm thick ALD TiO_2 film on fused silica containing anatase, rutile and TiO_2-II phases.

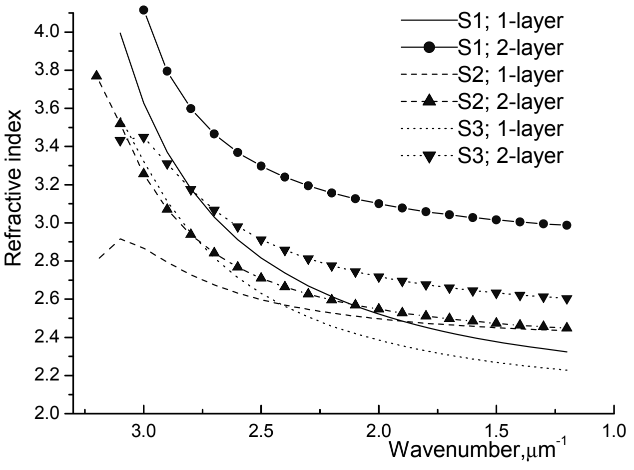

Figure 22. Refractive index dispersion of the TiO_2 films grown by ALD at a lower carrier gas flow. S1 to S3 – films with rising thickness from 61 to 157 nm in homogeneous approximation, 2-layer curves present results for upper, higher-index sublayer.

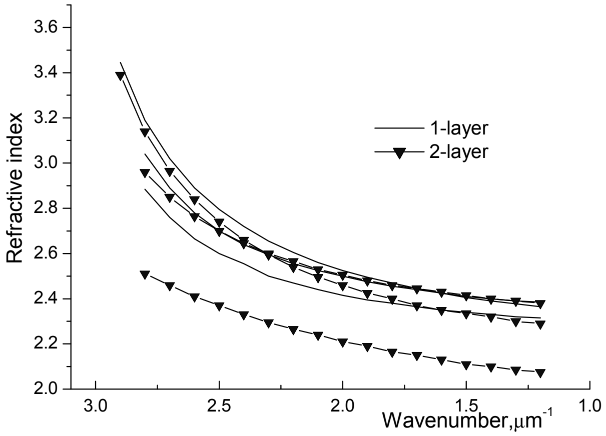

Figure 23. Refractive index dispersion of the different TiO_2 films grown by ALD at a higher carrier gas flow (S4 – S6). 2-layer curves present the results for upper, lower-index sublayer.

In Figs. 24 and 25 we see that the absorption index vs. wavenumber dependencies determined for a low carrier rate deposited films using a two-layer approach are steeper than those obtained using a homogeneous model. It means that a simple model could not present the absorption dispersion well enough. A rise of *k* with the material thickness indicates to a higher defect concentration and/or lower homogeneity of thicker films. An increasing amount of rutile can also explain the increase of absorption with the film thickness, most significant for the films grown at a lower flow rate of carrier gas containing larger amounts of rutile. A low value of the absorption index for the thinnest film deposited at a lower gas flow can at least partially result also from a difference in the ratio of the upper and lower sublayer thickness, if we assume that most of the absorbance occurs in the upper sublayer. During a transmission fitting procedure, the structure of absorption is not revealed and the resulting absorption is obtained as a mean value over the film thickness.

Table 5. Internal structure of the TiO_2 films and the results of transmission modelling.

Sample	Thickness of a lower layer, nm	Thickness of an upper layer, nm	Merit function $\Sigma\ (\Delta T_i)^2$ for 1-layer model	for 2-layer model	Mean ΔT for 2 layers
S1	39	22	$1.1\cdot10^{-3}$	$2.2\cdot10^{-5}$	$1.0\cdot10^{-3}$
S2	35	92	$1.0\cdot10^{-3}$	$3.8\cdot10^{-4}$	$4.3\cdot10^{-3}$
S3	35	118	$5.0\cdot10^{-3}$	$8.1\cdot10^{-5}$	$2.0\cdot10^{-3}$
S4	10	42	$1.3\cdot10^{-4}$	$1\cdot10^{-4}$	$2.3\cdot10^{-3}$
S5	97	48	$3.45\cdot10^{-3}$	$1.05\cdot10^{-3}$	$7.9\cdot10^{-3}$
S6	75	84	$3.75\cdot10^{-3}$	$6.1\cdot10^{-4}$	$6.0\cdot10^{-3}$

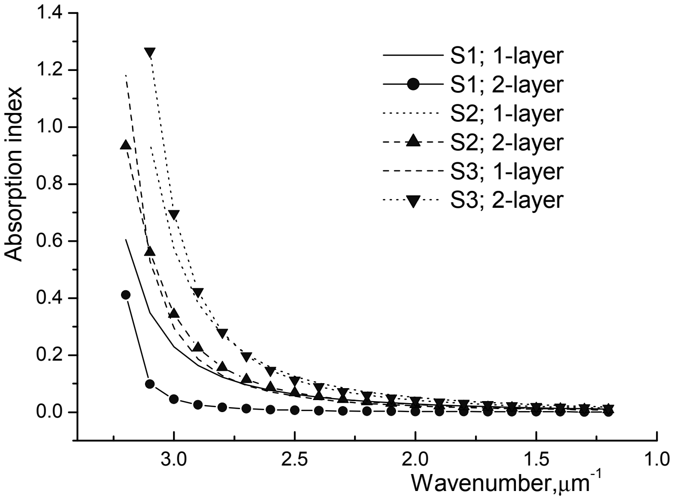

Figure 24. Absorption index dispersion of the ALD TiO$_2$ films deposited at a lower carrier gas flow with the different thickness (S1 to S3). 1-layer means homogeneous approximation, 2-layer – an inhomogeneous model.

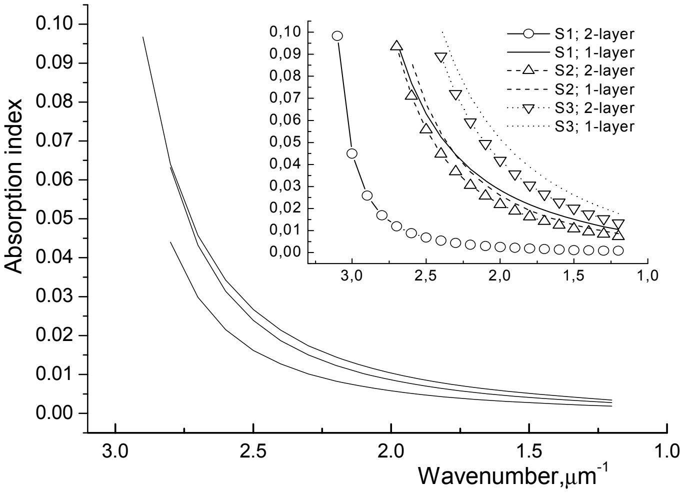

Figure 25. Absorption index dispersion of the ALD TiO$_2$ films deposited at a higher carrier gas flow. Insert – data for the first group presented on the same scale.

Fig. 26 shows the refractive index structure at wavelength λ = 500 nm perpendicular to the TiO$_2$ films if deposited at low carrier gas flow. The independent fits for three films demonstrate the same lower index material sublayer with a thickness of about 35 nm in contact with a fused silica substrate and higher index material with an index of refraction of about 2.65 growing above it. The refractive index for this sublayer for the thinnest low carrier gas rate TiO_2 film (61 nm) seems to be physically unsound demonstrating a limit of our approach of not taking into account a difference in the sublayer dispersions and using a simplified film structure. Another factor influencing the results is a structure of losses on reflection for this type of film inhomogeneity. The components of the reflected light are set by the Fresnel coefficients (1) on the borders between the media with different refractive indices. The main component of reflection comes from an interface film – air, the reflection from an interface inside a film has a lower index difference and accordingly less influence on the measured spectrum. This can account for the big scatter of the refractive index values for the inner sublayer.

In [VI], the composition and structure of the ALD TiO_2 films grown on amorphous SiO_2 with a higher N_2 carrier gas flow (90 µmol/s) and shorter $TiCl_4$ pulses than in [V] were analysed dependent on the growth temperature. Using the same approach as described above, the dependencies on the temperature of the optical parameters, growth rate and film crystal structure based on Raman spectroscopy were obtained. The TiO_2 films grown at 100 to 175°C were homogeneous with a mean transmission difference between the measured and calculated points of 0.6%. For films in which inhomogeneity was obvious, i.e. the merit function decreased at least twice for the two-layer inhomogeneity model compared to the homogeneous one, the mean difference over a series fell from 1.3% to 0.5% moving from an one-layer to a two-layer approximation.

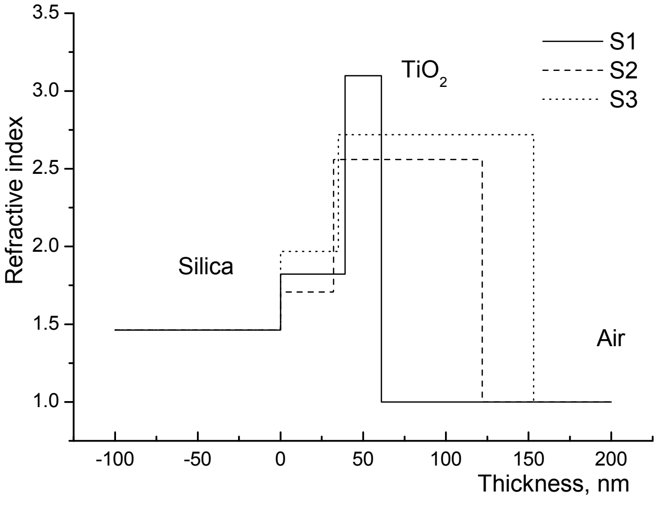

Figure 26. Refractive index structure of the inhomogeneous TiO_2 films deposited at a lower carrier gas flow in [V]. Data is given for a wavelength of 500 nm.

With the $TiCl_4$ pulses with a length of 0.2 s, the films grown at 200 to 500°C were positively inhomogeneous, i.e. the refractive index *n* was higher at the outermost surface than in contact with the substrate. For 0.5 s pulses, the film had positively inhomogeneous refractive index profile in a deposition temperature range from 225 to 425°C. The TiO_2 films deposited using either of the growth modes at 600°C and using the 0.5 s $TiCl_4$ pulses at 500°C were negatively inhomogeneous while the films deposited at 680°C displayed a positive inhomogeneity again. Some spectra of the measured films on fused silica together with the fitting results are presented in Figs. 27 and 28. Fig. 29 shows the Raman spectra of the TiO_2 films grown at different temperatures. The first traces of anatase were seen in the films deposited at 175°C while the amount of anatase increased with deposition temperature. At the growth temperature of 600°C, the films consisted of rutile and anatase while at 680°C rutile was seen only in a film grown using longer, 0.5 s $TiCl_4$ pulses.

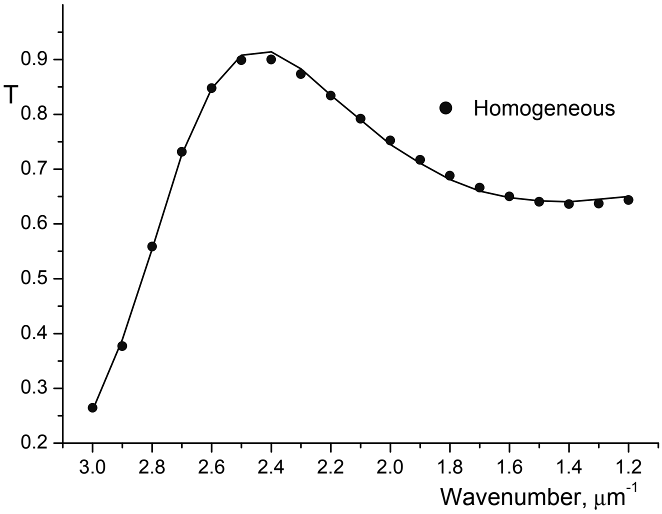

Figure 27. Transmission of an ALD TiO_2 layer deposited at 150 °C using 0.2 s $TiCl_4$ pulses.

A positive inhomogeneity in the films grown above 200°C is probably related to the growth of the crystalline phase during deposition. The works discussing the structure of the ALD TiO_2 films [124, 134] according to XRD results have shown that at lower temperatures the deposition starts with the growth of the amorphous phase and continues with anatase forming. With increasing thickness, the anatase phase formed causes an increase of the refractive index. At the temperatures over 425°C, the crystallization starts from the beginning of the film growth with no well-developed preferential orientation, so the effects of porosity rise during the growth and surface roughness may not be compensated by a phase change. The refractive index fit results for the structure of some analysed films are shown in Fig. 30. The other possible reasons for positive optical inhomogeneity may include the growth of conical crystalline grains from an amorphous interfacial layer like seen for HfO_2 ALD grown on Si(100) at 226°C for films with a thickness of up to 100 nm [135].

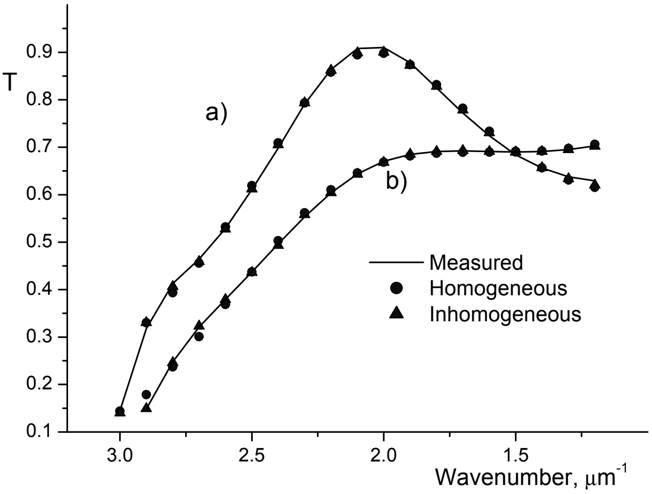

Figure 28. Transmission of the ALD TiO_2 films deposited at 500 °C using 0.5 s (a) and at 680 °C using 0.2 s (b) $TiCl_4$ pulses.

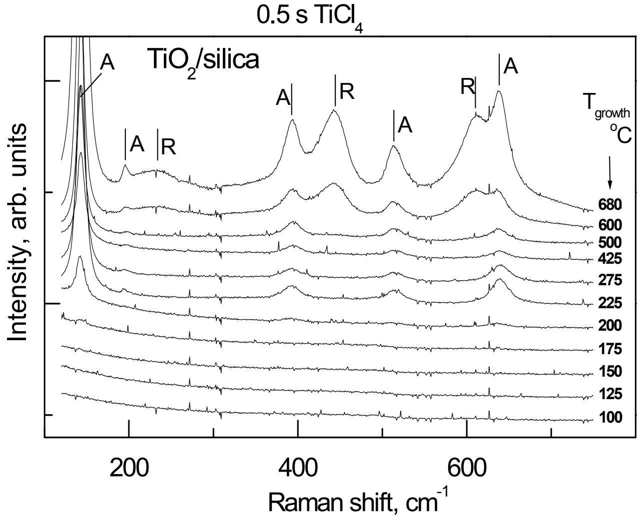

Figure 29. The Raman spectra of the ALD TiO_2 films deposited using the 0.5 s $TiCl_4$ pulses. A – anatase peaks, R – rutile peaks.

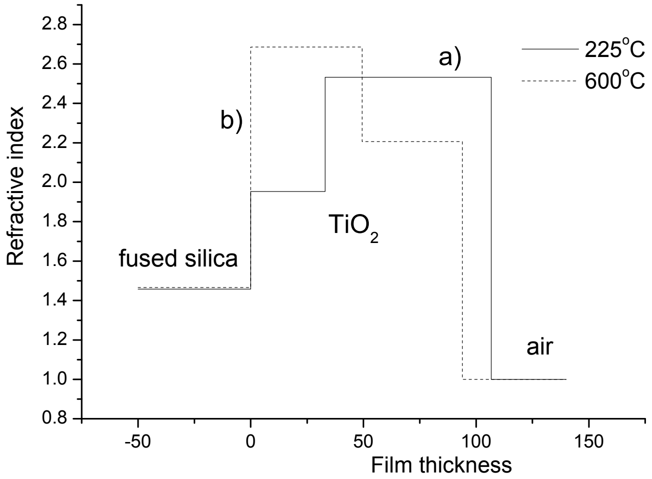

Figure 30. Structure of the ALD TiO_2 films grown using the 0.5 s $TiCl_4$ pulses at (a) 225°C and (b) 600°C at $\lambda = 500$ nm in a two-layer refractive index approximation.

A mean refractive index of the ALD TiO_2 films increased from 2.4 to 2.6–2.7 with the increase of the growth temperature from 100 to 600°C, with the extinction index slightly increasing. With the increase of the growth temperature to 680°C, the refractive index decreased and extinction index rose sharply. For growth temperatures over 600°C, [77] has shown that the TiO_2 films grown at silicon substrates contain silicon oxide, so it can be speculated that for the films deposited at the highest temperatures, the growth starts with an interface layer containing titanium silicates possessing lower refractive index values than TiO_2. Figs. 31, 32 present the dependencies of the refractive and extinction indices on the TiO_2 growth temperature in a homogeneous approximation. We see a refractive index minimum and extinction index maximum at 250°C, in the region where the anatase phase starts to dominate in the films. In an earlier study [124], formation of the biggest crystallites in this transition region has been observed whereas also a significant increase of material growth rate compared to lower temperatures has been registered. The large crystallites may induce a higher surface roughness causing rising scattering losses. The films under discussion grown on different substrates have also been investigated using XRR [136]. For the films deposited at 250°C, the surface roughness value for the films rose up to 6 nm. This gives us an estimate of surface roughness at which a procedure of parametric dispersion fitting of the transmission fails and one needs to introduce the scattering losses into a model.

Fig. 20 (SnO_2) and Fig. 24 (TiO_2) present us also a possibility to analyse the dependence of the absorption index on the film thickness for atomic layer deposited films [IV, V]. We see that an absorption in a range spectrally far from the region of fundamental absorption (being mainly due to the defects in coating) rises not only at moving towards the shorter wavelengths according to the dispersion law but also transversally through a deposited layer in these cases (for constant absorption, the absorption index should remain independent of film thickness). A change in the amount of crystallinity, related material inhomogeneity and increasing concentration of defects with a rising thickness can be a reason for this in TiO_2 but more probably it is caused by the defects in the material. The same picture was seen in vacuum evaporated Y_2O_3 [VII] (Fig. 33). Data on absorption in all these films is presented at 500 nm wavelength.

In all these cases, the absorption index is rising through a film during its growth. These results contradict the results of [137] showing a linear rise of the absolute absorption value against thickness in EBD and ion-plated TiO_2 films studied using photothermal deformation method.

Another possible explanation for this may lie in not taking into account the scattering processes in analysis. The maximum effect of scattering in these films may be estimated if we address all the losses in the coating as a scattering. Then, using only the first term of backward scattering from [47] and relating the proportionality constants in this formula and in the formula for absorption losses of a nonabsorbing film to its reflection values, we obtain an estimated value for roughness $\delta = \frac{\sqrt{A}}{n} \cdot \sqrt{\frac{kd\lambda}{4\pi}}$. Here, n and k are the film optical constants at the wavelength λ, d - film thickness, and A depends on the interference in the film. As the optical constants were obtained on different film optical thicknesses, I use the mean reflectivity values to get the first approximation for A as $A = \frac{(2-R-r)(R-r)}{2(R+r)^2}$, where R and r are the reflection values from the coated and uncoated sides of a substrate, respectively. In this case the obtained

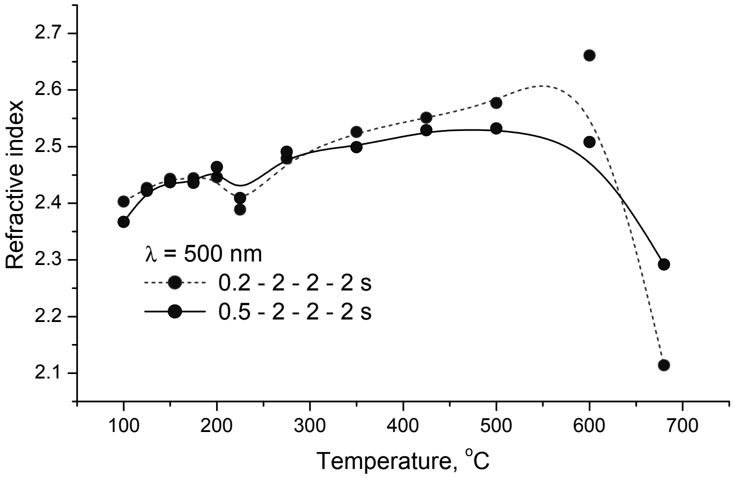

Figure 31. Dependence of the refractive index of ALD TiO_2 films on growth temperature (homogeneous approximation). Wavelength λ = 500 nm.

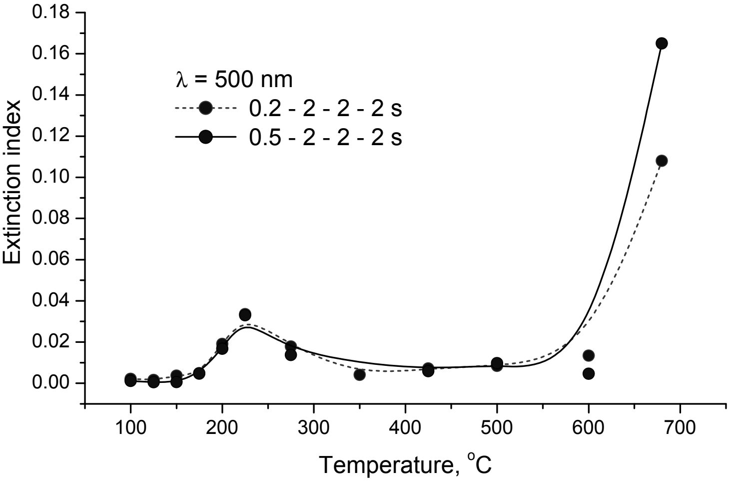

Figure 32. Influence of the growth temperature on the extinction index of the ALD TiO_2 films determined for λ = 500 nm in a homogeneous approximation.

roughness value rises from 0.8 to 4 nm with thickness for Y_2O_3 films represented in Fig.33 and from 4 to 8.5 nm for TiO_2 films represented in Figs. 24 and 26. These are the maximum values for possibly nonabsorbing films, better results would need taking into account both inhomogeneity and roughness in the film presentation. The values of the constant *A* used for Y_2O_3 and TiO_2 were 2.8 and 1.45, respectively.

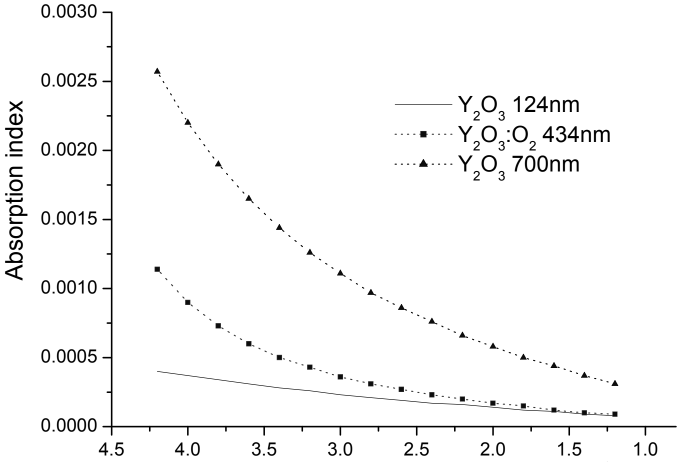

Figure 33. Dependence of the absorption index on the thickness for EBD Y_2O_3 thin films.

4.2.3. ZIRCONIA

For a comparison of the different methods to analyze the thin film optical properties, the inhomogeneous ZrO_2 films (e-beam evaporated and ALD coated) were studied using both the envelope and multiparameter optimization methods. Figs.34 and 35 show the optical function results computed with different analysis methods [8, 9, 25, 27] for one ALD film with a transmission spectrum depicted in Fig. 36. The first three methods are the envelope methods based on modelling of the values of the spectral extrema and [27] is used together with the Lorentz dispersion as described above. The envelope methods use the procedures in which the film thickness and optical constants are found independently for each spectral extreme [8, 25] or the film thickness is computed for the reddest extreme in the region without absorption (the one with supposedly minimal dispersion) and this value is used afterwards to obtain the optical constants over a full measured region [9]. The latter approach was proposed to diminish the effects of a thickness inhomogeneity in the measured spectrum, but in practice it occurs to be useful also for the films with a high dispersion of the refractive index. Almost lacking dispersion in the results of [8, 25] points to a better representation of real coatings peculiarities by the other [9, 27] methods. The absorption index dispersion occurred not to be influenced much.

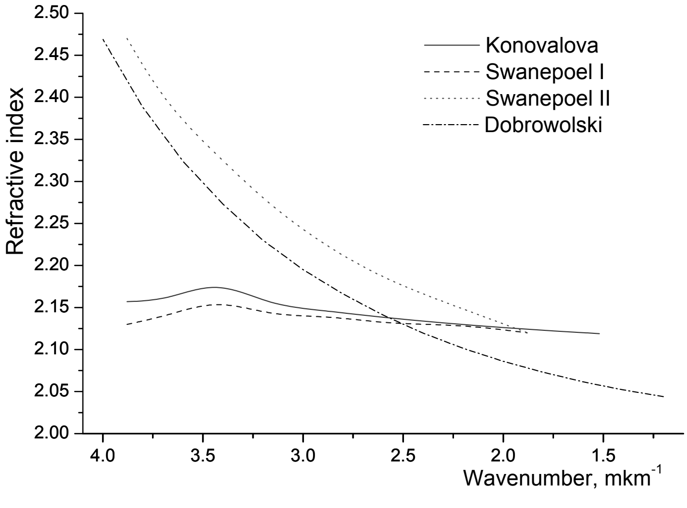

Figure 34. Refractive index dispersion dependencies using different analysis methods for the same ALD ZrO_2 film. SwanepoelI – [8], SwanepoelII – [9].

Figs. 37 and 38 present the results for the same coating if the spectral optimisation is realized using the Lorentz or Forouhi-Bloomer dispersion law. It demonstrates a better (physically more reasonable, and also having the better merit functions values) representation of atomic layer deposited ZrO_2 film transmission spectrum with the Lorentz than with the Forouhi-Bloomer dispersion model. Also, all the attempts to optimise the transmission of a film using two sublayers and Forouhi-Bloomer dispersion failed. So, it may be stated that the Lorentz dispersion is preferable for the oxide materials. The merit functions for an ALD ZrO_2 film computed according to Eq. (6) are presented in Table 6. The success of using the Forouhi-Bloomer model in [30] remains questionable, as the extinction minimum around 0.5–0.65 μm from a power series fit can not be seen in the transmission result obtained using the Forouhi-Bloomer dispersion parameters.

Table 6. A quality of modelling an ALD grown inhomogeneous ZrO_2 film using multi-layer fitting with different dispersion models.

Dispersion formula	Merit function
Lorentz homogeneous	$4.7\cdot10^{-3}$
Lorentz inhomogeneous	$1.1\cdot10^{-3}$
Forouhi-Bloomer	$2.4\cdot10^{-2}$

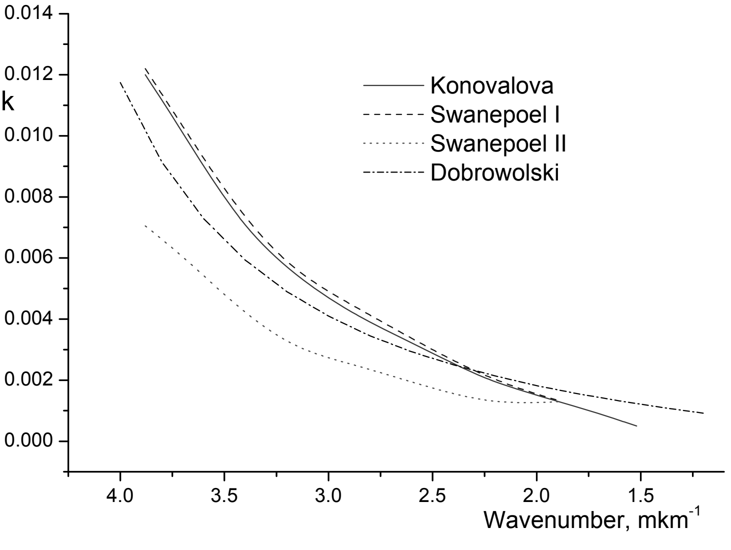

Figure 35. The absorption index dispersion dependencies obtained using different analysis methods for the same ALD ZrO_2 film.

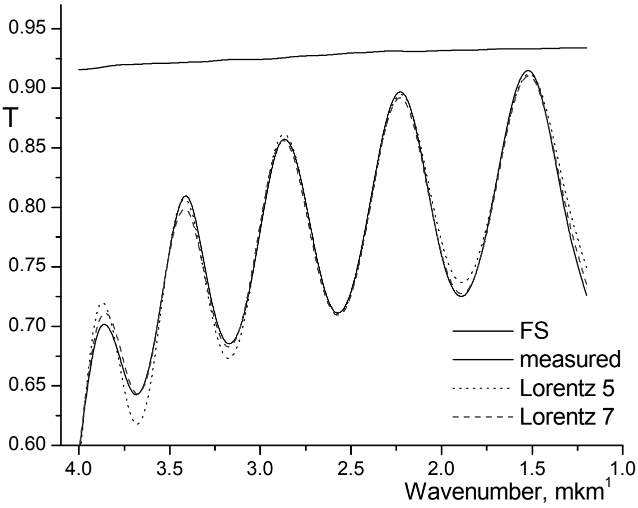

Figure 36. Fitting of the ALD ZrO_2 film transmission spectrum using the Lorentz dispersion in homogeneous (4 parameters and thickness) or two-layer (6 parameters and thickness) approximation.

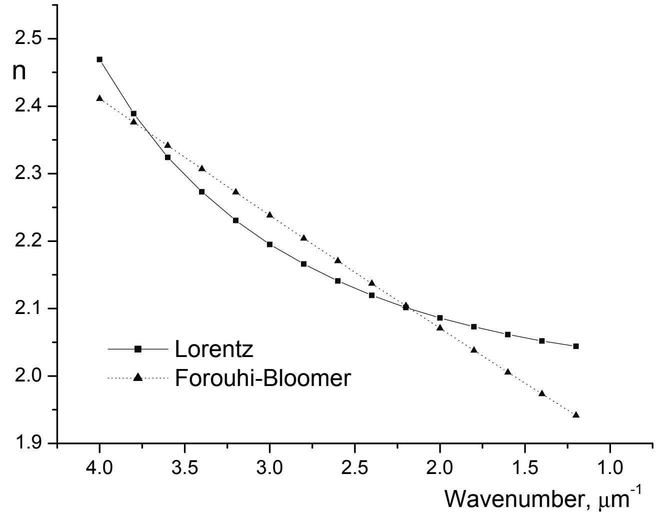

Figure 37. Refractive index dispersion for ALD ZrO_2 film from fits according to Lorentz and Forouhi-Bloomer dispersion models.

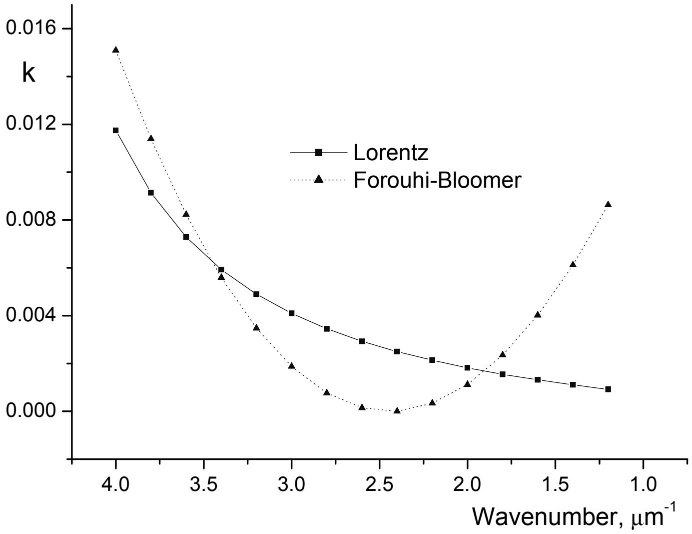

Figure 38. Absorption index dispersion for ALD ZrO_2 film from fits according to Lorentz and Forouhi-Bloomer dispersion models.

5. CONCLUSIONS

This work deals with the possibilities and limitations of the determination of the optical constants of the inhomogeneous thin films. The results obtained show that it is possible to model the structure of a weakly absorbing film on a non-absorbing substrate using only the transmission spectra of a system film-substrate and of an uncoated substrate, applying the Lorentz dispersion and a structure consisting of two sublayers with a constant refractive index difference between them. For modelling, a multiparameter optimisation according to the Nelder-Mead algorithm is used as proposed in [27] and this approach extended to a system consisting of multiple sublayers. It is demonstrated that a structure obtained from optimisation is reproducible if evaporation proceeds under the same conditions. Better results can be achieved, if a smooth transition between the sublayers is introduced, but in this case we need more free parameters and it is not clear whether the improvement is due to a better fit of the model to a real optical structure or is due to a better representation of noisy measurement data. A merit function for fitting defined as a sum of the squares of differences between measured and computed data diminishes 2–7 times if an inhomogeneity consisting of two sublayers is introduced into the model for the materials that demonstrate inhomogeneous behaviour. A modelling practice indicates that a refinement of the merit function less than 1.5 times may be not sufficient to make the sound conclusions about the film structure.

For vacuum evaporated films (MgF_2, LaF_3, Y_2O_3, but also for other oxides), a multiparameter fitting showed that these films have a negative inhomogeneity structure with a thin (an optical thickness of less than a quarterwave) sublayer either in contact with the substrate or at film-air interface. It is demonstrated that while the merit function may not be a universal value to differentiate between a structure with linear inhomogeneity and the two-layer structures having a thinner sublayer in contact either with the substrate or with air, a difference can be made using a physical thickness result from profilometry. In the case of Y_2O_3, a thinner sublayer is shown to be in contact with a fused silica substrate.

For ALD deposited layers we meet a different situation. The Al_2O_3 and ZrO_2 films grown using atomic layer deposition had a positive type of inhomogeneity. The ALD grown TiO_2 films were analysed in a wider range of process parameters. The results show that a type of material inhomogeneity can change with changing process conditions (in our case from negative to positive i.e. having the upper sublayer with a lower or higher refractive index compared to the lower one, with rising nitrogen carrier gas flow) and to be dependent on the substrate temperature. The transmission spectra of TiO_2 films with a thickness of less than 160 nm were measured and it is shown that a multiparameter fitting makes it possible to obtain the consistent inhomogeneity results even if the spectra do not contain the extrema for drawing the fringe envelopes. At the lowest ratio of carrier and precursor gas flows where the growth switches over from anatase to rutile, the existence of a thin layer with a lower refractive index was shown at the border with fused silica substrate.

Modelling of the evaporated and ALD grown films with a different thickness also revealed a rise of the absorption index with film the film thickness at the growth conditions used by us, a result we have not met in literature.

In the simplified approach used in this work, the refractive index difference between sublayers is taken as a constant. A physically better based approximation could incorporate the void factor in the material allowing us to take into account the film dispersion. Also, to widen the limits of this approach introducing a scattering in the film formulae could be useful. In our case, the procedure failed if the XRR roughness of the films exceeded a value of 5 nm. Finally, any data on the optical properties of the inhomogeneous thin films are comparable to each other only when the analysis methods to obtain the results are clearly specified. The contradiction between the models used here for transmission spectroscopy and those used in spectral ellipsometry remains yet to be clarified.

APPENDIX I. AN INFLUENCE OF MEASUREMENT ACCURACY

Throughout our work, we have used a transmission spectrum of an uncoated specimen, not tabulated values of a material, to calculate a refractive index of the substrate. A reason for this approach is related to measurement errors, either noise-type or systematic. The random errors may be eliminated using smoothing or higher signal collecting time, but the systematic errors are transferred into calculation results. In Fig. 39 a model case is presented with a substrate index of refraction 1.50 and that for a coated layer, 1.60 – 0i (no absorption).

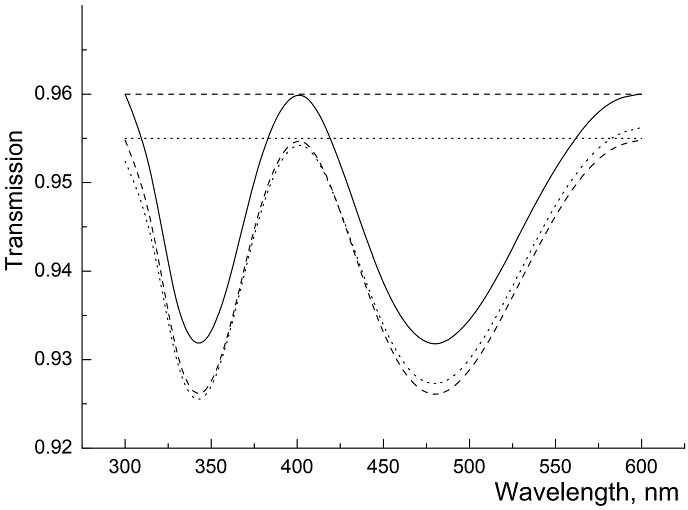

Figure 39. Nonabsorbing film on a semi-infinite substrate. Horizontal lines – substrate with n_0 = 1.50 (upper) or n_0 = 1.54. Upper curve – film with n = 1.60, downward curves – n = 1.60 – 0.0005i and n = 1.64.

A horizontal line and upper curve correspond to the theoretical transmission results for a semi-infinite uncoated substrate and for the same substrate with a film having thickness of 375 nm on it. If we introduce a systematic error –0.5% *T*, the measured transmission values will be accordingly less. They are presented by a downward horizontal line and two curves presenting the cases of an absorbing layer n = 1.60 – 0.0005i on a substrate with n_0 = 1.50 and a nonabsorbing material n = 1.64 on a substrate with n_0 = 1.54. The first case results if the tabulated substrate refractive index values are used without measuring them, the second case, if both the uncoated substrate and the substrate with the film have been measured. In the first case, the transmission errors are transferred into an absorption index; in the second case, the refractive indices of both uncoated substrate and coated specimen will have the values different from the original ones, but their relative position, inhomogeneity, and absorption results are influenced only a little. For inhomogeneity analysis, where we are interested in the refractive index change through a layer and also for optical coatings where the absorption means much, the second approach is preferred.

APPENDIX II. A CONNECTION BETWEEN ONE OSCILLATOR FORMULA AND LORENTZ DISPERSION

Let us define a formula for a damped oscillator like it was done in [32] as

$$\varepsilon = \varepsilon_\infty + \frac{(\varepsilon_s - \varepsilon_\infty)\omega_t^2}{\omega_t^2 - \omega^2 + i\Gamma\omega} ,$$

where ε_∞ – high-frequency dielectric constant, ε_s – oscillator strength, ω_t – oscillator frequency and Γ – its damping constant. Changing to a complex refractive index and wavelength dependence as

$$\varepsilon = (n - ik)^2 , \quad \omega_t = \frac{2\pi \cdot c}{\lambda_0} , \ \omega = \frac{2\pi \cdot c}{\lambda}$$

gives us $$(n^2 - k^2) - 2ink = \varepsilon_\infty + \frac{(\varepsilon_s - \varepsilon_\infty) \cdot 4\pi^2 c^2 \lambda^2}{4\pi^2 c^2 (\lambda^2 - \lambda_0^2) + i\Gamma \cdot 2\pi \cdot c\lambda\lambda_0^2} .$$

Taking the both sides to a common denominator and dividing the result to the real and imaginary parts we obtain

$$\pi \cdot c(\lambda^2 - \lambda_0^2)(n^2 - k^2) - \Gamma nk\lambda\lambda_0^2 = \pi \cdot c\varepsilon_\infty(\lambda^2 - \lambda_0^2) + (\varepsilon_s - \varepsilon_\infty)\pi \cdot c\lambda^2 \quad (7)$$ and
$$\Gamma\lambda\lambda_0^2(n^2 - k^2) - 4\pi \cdot cnk(\lambda^2 - \lambda_0^2) = \varepsilon_\infty\Gamma\lambda\lambda_0^2 \quad (8).$$

Substituting now *nk* from formula (8) into (7) results in

$$c\pi(\lambda^2 - \lambda_0^2)(n^2 - k^2) = c\pi[\varepsilon_\infty(\lambda^2 - \lambda_0^2) + (\varepsilon_s - \varepsilon_\infty)\lambda^2 + \Gamma\lambda\lambda_0^2[\frac{\varepsilon_\infty\Gamma\lambda\lambda_0^2}{4\pi \cdot c(\lambda^2 - \lambda_0^2)} - (n^2 - k^2)\frac{\Gamma\lambda\lambda_0^2}{4\pi \cdot c(\lambda^2 - \lambda_0^2)}]$$

and then $$n^2 - k^2 = \frac{\dfrac{\varepsilon_\infty\Gamma^2\lambda^2\lambda_0^4}{4\pi^2c^2} + (\lambda^2 - \lambda_0^2)(\varepsilon_s\lambda^2 - \varepsilon_\infty\lambda_0^2)}{(\lambda^2 - \lambda_0^2)^2 + \dfrac{\Gamma^2\lambda_0^4}{4\pi^2c^2}\lambda^2} .$$

Separating a part ε_∞ gives us

$$n^2 - k^2 = \varepsilon_\infty + \frac{(\lambda^2 - \lambda_0^2)(\varepsilon_s\lambda^2 - \varepsilon_\infty\lambda_0^2) - \varepsilon_\infty(\lambda^2 - \lambda_0^2)^2}{(\lambda^2 - \lambda_0^2)^2 + \dfrac{\Gamma^2\lambda^2\lambda_0^4}{4\pi^2c^2}} = \varepsilon_\infty + \frac{(\varepsilon_s - \varepsilon_\infty)\lambda^2(\lambda^2 - \lambda_0^2)}{(\lambda^2 - \lambda_0^2)^2 + \dfrac{\Gamma^2\lambda_0^4}{4\pi^2c^2}\lambda^2} .$$

Now, for an imaginary part we get (8)

$$nk = (n^2 - k^2)\frac{\Gamma\lambda\lambda_0^2}{4\pi \cdot c(\lambda^2 - \lambda_0^2)} - \frac{\varepsilon_\infty\Gamma\lambda\lambda_0^2}{4\pi \cdot c(\lambda^2 - \lambda_0^2)}$$ and from here

$$k = \frac{1}{4\pi \cdot cn} \cdot \frac{\Gamma\lambda_0^2\lambda^3(\varepsilon_s - \varepsilon_\infty)}{(\lambda^2 - \lambda_0^2)^2 + \dfrac{\Gamma^2\lambda^2\lambda_0^4}{4\pi^2c^2}} .$$

Introducing the new variables $A = \varepsilon_\infty$, $B = \varepsilon_s - \varepsilon_\infty$, $C = \lambda_0$, $D = \dfrac{\Gamma\lambda_0^2}{2\pi \cdot c}$ results in

$$n^2 = A + k^2 + \frac{B\lambda^2(\lambda^2 - C^2)}{(\lambda^2 - C^2)^2 + D^2\lambda^2} \quad \text{and} \quad k = \frac{1}{2n} \cdot \frac{BD\lambda^3}{(\lambda^2 - C^2)^2 + D^2\lambda^2}$$

like in paper of Dobrowolski et al. [27] up to a variation of a sign of *k*.

SUMMARY IN ESTONIAN

Esitatud töös „Mittehomogeensete õhukeste kilede optiline iseloomustamine” analüüsitakse mittehomogeensete õhukeste kilede optiliste parameetrite määramise võimalusi ja sellele protseduurile kehtivaid piiranguid. Näidatakse, et mitteneelavale alusele sadestatud väheneelava kile optilist struktuuri on võimalik modelleerida, kasutades ainult kilega kaetud ja ekvivalentse katmata aluse läbilaskvusspektreid ning rakendades neile Lorentzi dispersioonvalemit ja kahest alakihist koosnevat struktuuri, milles alakihtide vahel on lainepikkusest sõltumatu murdumisnäitaja hüpe. Selleks on kasutatud mitmeparameetrilist optimiseerimist [27], Nelder-Meadi algoritmi ja laiendatud seda lähenemist mitmest alakihist koosnevale süsteemile. Näidatakse, et optimeerimisprotseduurist saadav struktuur on korratav, kui kilede sadestamine toimub samadel tingimustel. Paremaid tulemusi on võimalik saada, kui tuua sisse sujuv üleminek alakihtide vahel, kuid sel juhul on vaja kasutada rohkem vabu parameetreid ja pole selge, kas lähendi paranemine on tingitud mudeli täpsemast vastavusest kile tegelikule struktuurile või on arvutusliku kõvera parem sobivus müra sisaldavate lähteandmetega saadud ainult tänu sellele, et suurema arvu parameetrite varieerimine lubab paremini lähendada mistahes kujuga kõverat. Vaakum-aurustatud kilede jaoks (MgF_2, LaF_3, Y_2O_3, aga ka muud oksiidid), andis mitmeparameetriline optimeerimine tulemuseks negatiivse (kile kasvu suunas väheneva murdumisnäitajaga) mittehomogeensusega struktuuri, mille korral õhuke (optiline paksus väiksem kui veerand mõõtmisel kasutatud valguse lainepikkust) alakiht paikneb kas kontaktis alusega või kile välispinnaga. Näidatakse, et kuigi hüvefunktsioon pole universaalne näitaja, mis üksinda lubaks teha kindlaks, kas paremini kirjeldab tegelikkust lineaarselt muutuva murdumisnäitajaga mudel või kahekihiline mudel, saab ühte juhtu teisele eelistada, kui kasutada analüüsil lisaks veel profilomeetriast määratud kile füüsilise paksuse väärtust. Y_2O_3 kilede jaoks tehtud analüüs näitab, et nendes on õhuke, ülejäänud kihist erineva murdumisnäitajaga alakiht kontaktis sulatatud kvartsist alusega.

Aatomkihtsadestatud kilede korral on olukord teistsugune. Sellel meetodil kasvatatud Al_2O_3 ja ZrO_2 kilesid kirjeldab hästi kahekiline mudel, milles väiksema murdumisnäitajaga kiht on kontaktis alusega. Aatomkihtsadestatud TiO_2 kilesid on uuritud laiemas protsessiparameetrite diapasoonis ja seal näeme materjali mittehomogeensustüübi sõltuvust protsessi tingimustest. Vähem kui 160 nm paksusega TiO_2 kilede läbilaskvusspektrite mõõtmine näitas, et mittehomogeensuse mitmeparameetrilise optimeerimisega on võimalik kooskõlalisi tulemusi saada isegi juhul, kui spektris ei ole ekstreemumeid mähisjoonte konstrueerimiseks. Näiteks kilede jaoks, mille kasvu algfaasis tekkis anataasi struktuuriga kristalliline faas ja hiljem rutiili srtuktuuriga faas, andis parima kooskõla kahekihiline mudel, milles õhuke väiksema murdumisnäitajaga alakiht paikneb sulatatud kvartsist aluse pinnal. Kriteeriumiks õhukeste kilede mittehomogeensusstruktuuri määramise õigsusele oli saadud murdumisnäitaja profiili korratavus erineva paksusega kilede korral.

Optimeerimise hüvefunktsioon on defineeritud kui mõõdetud ja arvutatud väärtuste vahede ruutude summa. Tähelepanu tuleb pöörata asjaolule, et hüvefunktsiooni paranemine vähem kui 1,5 korda võib olla mitteküllaldane järelduste tegemiseks kile struktuuri kohta. Antud töös kasutatud materjalide korral paraneb hüvefunktsioon keskmiselt 2 kuni 7 korda, kui tuua sisse kahest alakihist koosnev mittehomogeensus.

Kilede keskmistatud neeldumisnäitaja suurenes meil kasutatud sadestustingimustel mitmete ainete korral koos kihi paksuse kasvuga.

Töös kasutatud lihtsustatud lähendustes on alakihtide vaheline murdumisnäitajate erinevus olnud lainepikkusest sõltumatu. Füüsikaliselt põhjendatum, kuid samas täiendavaid varieeritavaid parameetreid sisaldav oleks mudel, mis võtaks arvesse murdumisnäitajate erinevuse võimalikku sõltuvust lainepikkusest. Samuti võiks antud lähenemisele kasuks tulla hajumise sissetoomine kilesid kirjeldavatesse valemitesse. Meie juhul andis protseduur eksitulemuse, kui kilede röntgenpeegeldusega määratud kareduse väärtused ulatusid 6 nm. Lisaks tuleb rõhutada, et kõik andmed mittehomogeensete kilede optiliste parameetrite kohta on omavahel võrreldavad vaid juhul, kui selgelt on määratletud nende saamise protseduur. Täiendavat infot kilede optilise struktuuri kohta annaks kahtlemata ka läbilaskvusspektroskoopiast saadud tulemuste võrdlemine spektroskoopilise ellipsomeetria andmetega.

Käesoleva töö käigus ilmes muuhulgas ka vajadust täpsustada mõningate antud valdkonna jaoks oluliste terminite kasutusvalkonda.

Terminoloogiline selgus on olemas dielektrilise konstandi $\varepsilon = \varepsilon_1 + \varepsilon_2$, kompleksse murdumisnäitaja $\tilde{n}$, kus $\varepsilon = \tilde{n}^2$, ja murdumisnäitaja $n = \mathrm{Re}(\tilde{n})$ osas, kuid senini kaldub eesti keelde üle kalduma inglise keeles *absorption coefficient, extinction coefficient* mitmemõttelisest kasutusest tulenev segadus. Terminit neeldumiskoefitsient kasutatakse tihti nii $k = \mathrm{Im}(\tilde{n})$ kui ka kiles toimuvaid energiakadusid iseloomustava suuruse $\alpha = \frac{4\pi k}{\lambda}$ jaoks. [138] annab *absorption coefficient* vasteks neeldumistegur, neeldetegur, neeldumiskonstant, neeldumiskoefitsient, *extinction coefficient* vasteks neeldumistegur, ekstinktsioonitegur, *extinction index* vasteks neeldumisnäitaja, kompleksse murdumisnäitaja imaginaarosa. [3] kasutas главный показатель поглощения k jaoks, et eristada seda α. Selguse huvides teen ettepaneku kasutada järjekindlalt terminit neeldumiskoefitsient (neeldumistegur jm.) α ja neeldumisnäitajat k tähistamiseks. Ekstinktsioonikoefitsient (tegur) võiks jääda olukorra jaoks, kus hajumine moodustab märkimisväärse osa kadudest.

Positiivne ja negatiivne optiline mittehomogeensus on töös defineeritud kui murdumisnäitaja kasv või langus kile kasvusuunas (aluselt keskkonna poole). Lisaks pakun suuruse tähistamiseks, mis näitab funktsiooni modelleerimisel optimeerimisprotsessi käigus leitud lahendi kaugust algsest, mõõdetud suurusest *(merit function)* terminit hüvefunktsioon nagu juba eespool kasutatud.

LITERATURE

1. O.Stenzel, V.Hopfe and P.Klobes “Determination of optical parameters for amorphous thin film materials on semitransparent substrates from transmission and reflectance measurements”, J.Phys.D:Appl.Phys., **24**, 11 (1991), 2088–2094.
2. G.Honcia und K.Krebs “Eine neue hochbrechende Substanz für dielektrische Ultraviolett-Spiegel”, Z.Physik **156**, 2 (1959), 117–124.1.
3. Б.М.Комраков, Б.А.Шапочкин «Измерение параметров оптических покрытии». М. «Машиностроение», 1986, сс.104–106. B.M.Komrakov, B.A. Shapochkin “Measuring of the Optical Coatings Parameters”, Moscow, 1986.
4. О.С.Хевенс «Измерение оптических констант тонких пленок», в: «Физика тонких пленок, т.II, «Мир», Москва, 1967, сс.136–185. O.S.Heavens “Physics of Thin Films”, ed. G.Hass and R.E.Thun (New York: Academic) 1964, pp.193–304.
5. В.Е.Кондрашов «Оптика фотокатодов». «Наука», Москва 1976. V.E.Kondrashov “Optics of Photocathodes”. “Nauka”, Moscow 1976.
6. П.Г.Кард «Анализ и синтез многослойных интерференционных пленок». «Валгус», Таллин 1971. P.G. Kard “Analysis and Synthesis of the Multilayer Interference Films”. “Valgus”, Tallinn 1971.
7. F.Abelés “Methods for determining optical parameters of thin films”, “Progress in Optics” E.Wolf, ed. (North-Holland, Amsterdam), 1963, Vol.2, pp. 249–288.
8. R.Swanepoel “Determination of the thickness and optical constants of amorphous silicon”, J.Phys.E:Sci.Instrum., **16**, 12 (1983), 1214–1222.
9. R.Swanepoel “Determination of surface roughness and optical constants of inhomogeneous amorphous silicon films”, J.Phys.E:Sci.Instrum., **17**, 10 (1984), 896–903.
10. M.Nowak “Determination of optical constants and average thickness of inhomogeneous-rough thin films using spectral dependence of optical transmittance”, Thin Solid Films, **254**, 1–2 (1995), 200–210.
11. K.Reichelt and X.Jiang “The Preparation of Thin Films by Physical Vapour Deposition Methods”, Thin Solid Films, **191**, 1 (1990), 91–126.
12. R.P.Netterfield and K.H.Müller, D.R.McKenzie, M.J.Googan, P.J.Martin “Growth dynamics of aluminum nitride and aluminum oxide thin films synthesized by ion-assisted deposition”, J.Appl.Phys., **63**, 3 (1988), 760–769.
13. J.-E.Sundgren “Ion-assisted film growth: modification of structure and chemistry”, Vacuum **41**, 4–6 (1990), 1347–1349.
14. B.T.Sullivan, K.L.Byrt “Metal/dielectric transmission interference filters with low reflectance. 2. Experimental results”, Appl. Opt., **34**, 25 (1995), 5684–5694.
15. А.С.Валеев «Определение оптических постоянных тонких слабопоглощающих слоев», Опт. и Спектр. **15**, 4 (1963), 500–511. A.S.Valeev “Determination of the Optical Constants of Weakly Absorbing Thin Films”, Optics and Spectrosc., **15**, 4 (1963) 269–274.
16. A.Vašíček “Tables of Determination of Optical Constants from the Intensities of Reflected Light. Таблицы для определения оптических постоянных по интенсивности отраженного света”. Nakladatelství Československé Akademie Věd, Praha 1964.
17. С.П.Ляшенко и В.К.Милославский «Простой метод определения толщины и оптических постоянных полупроводниковых и диэлектрических слоев»; Опт. и Спектр., **16**, 1, 1964, 151–153. S.P.Lyashenko and V.K.Miloslavskii “A Simple

Method for the Determination of the Thickness and Optical Constants of Semiconducting and Dielectric Layers", Optics and Spectrosc., **16**, 1 (1964), 80–81

18. Г.С.Черемухин, Б.В.Кириленко, Е.К.Гурдин «Расчет оптических характеристик пленки», Опт.-Мех. Промышл., 1976, 6, 13–15. G.S.Cheremukhin, B.V.Kirilenko, E.K.Gurdin "Calculating the optical characteristics of a film", Sov.J.Opt.Technol., **43**, 6 (1976), 344–346.
19. J.C.Manifacier, J.Gasiot and J.P.Fillard "A simple method for the determination of the optical constants *n*, *k* and the thickness of a weakly absorbing thin film", J.Phys.E:Sci.Instrum., **9**, 11 (1976), 1002–1004.
20. M.Kubinyi, N.Benkö, A.Grofcsik, W.Jeremy Jones "Determination of the thickness and optical constants of thin films from transmission spectra", Thin Solid Films, **286,** 1–2 (1996), 164–169. M.Kubinyi, N.Benkö, A.Grofcsik, W.Jeremy Jones "Erratum to "Determination of the thickness and optical constants of thin films from transmission spectra", TSF, **286** (1996) vi", Thin Solid Films, **292**, 1–2 (1996), 333.
21. S.-C.Chiao, B.G.Bovard, and H.A.Macleod "Optical-constant calculation over an extended spectral region: application to titanium dioxide film", Appl.Opt., **34**, 31 (1995), 7355–7360.
22. P.Meredith, G.S.Buller, and A.C.Walker "Improved method for determining the optical constants of thin films and its application to molecular-beam-deposited polycrystalline layers", Appl.Opt., **32**, 28 (1993), 5619–5627.
23. L.Vriens and W.Rippens "Optical constants of absorbing thin films on a substrate", Appl.Opt., **22**, 24 (1983), 4105–4110.
24. V.Panayotov and I.Konstantinov "Determination of thin film optical parameters from photometric measurements: an algebraic solution for the (T, R_f, R_b) method", Appl.Opt., **30**, 19 (1991), 2795–2800.
25. О.П.Коновалова, И.И.Шаганов «Определение оптических констант слабопоглощающих диэлектрических слоев на прозрачной подложке», Опт.-Мех. Пром., 8 (1988), 39–41. O.P.Konovalova, I.I.Shaganov "Determination of optical constants of weakly absorbing dielectric layers on a transparent substrate", Sov.J.Opt.Technol., **55**, 8, (1988), 489–491.
26. D.P.Arndt, R.M.A.Azzam, J.M.Bennett, J.P.Borgogno, C.K.Carniglia, W.E.Case, J.A.Dobrowolski, U.J.Gibson, T.Tuttle Hart, F.C.Ho, V.A.Hodgkin, W.P.Klass, H.A.Macleod, E.Pelletier, M.K.Purvis, D.M.Quinn, D.H.Strome, R.Swenson, P.A.Temple, and T.F.Thonn "Multiple determination of the optical constants of thin-film coating materials", Appl.Opt., **23**, 20 (1984), 3571–3596.
27. J.A.Dobrowolski, F.C.Ho, and A.Waldorf "Determination of optical constants of thin film coating materials based on inverse synthesis", Appl.Opt., **22**, 20 (1983), 3191–3200.
28. "Encyclopedia of Statistical Sciences. Second Edition". Vol.8. Wiley-Interscience. A John Wiley&Sons, Inc., Publication. 2006, 5424–5426.
29. A.R.Forouhi, I.Bloomer "Optical dispersion relations for amorphous semiconductors and amorphous dielectrics", Phys.Rev.B, **34**, 10 (1986), 7018–7026.
30. M.Nenkov and T.Pencheva "Calculation of thin-film optical constants by transmittance-spectra fitting", J.Opt.Soc.Am.A **15**, 7 (1998), 1852–1857.
31. J.I.Cisneros "Optical characterization of dielectric and semiconductor thin films by use of transmission data", Appl.Opt., **37**, 22 (1998), 5262–5270.
32. Md.Mosaddeq-ur-Rahman, G.Yu, K.M.Krishna, T.Soga, J.Watanabe, T.Jimbo, and M.Umeno "Determination of optical constants of solgel-derived inhomo-

geneous TiO_2 thin films by spectroscopic ellipsometry and transmission spectroscopy", Appl.Opt., **37**, 4 (1998), 691–697.

33. J.Rodríguez, M.Gómez, J.Ederth, G.A.Niklasson, C.G.Granqvist "Thickness dependence of the optical properties of sputter deposited Ti oxide films", Thin Solid Films, **365**, 1 (2000), 119–125.
34. G.E.Jellison, Jr. and F.A.Modine "Parametrization of the optical functions of amorphous materials in the interband region", Appl.Phys.Lett., **69**, 3 (1996), 371–373; G.E.Jellison, Jr. and F.A.Modine "Parametrization of the optical functions of amorphous materials in the interband region (erratum)", Appl.Phys.Lett., **69**, 14 (1996), 2137.
35. J.Tauc, R.Grigorovici, and A.Vancu "Optical Properties and Electronic Structure of Amorphous Germanium", phys. status sol. **15**, 2 (1966), 627–637.
36. Y.J.Cho, N.V.Nguyen, C.A.Richter, and J.R.Ehrstein, B.H.Lee and J.C.Lee "Spectroscopic ellipsometry characterization of high-*k* dielectric HfO_2 thin films and the high-temperature annealing effects on their optical properties", Appl.Phys.Lett., **80**, 1 (2002), 1249–1251.
37. L.-J. Meng, R.A.Silva, H.-N.Cui, V.Teixeira, M.P. dos Santos, Z.Xu "Optical and structural properties of vanadium pentoxide films prepared by d.c. reactive magnetron sputtering", Thin Solid Films **515**, 1 (2006), 195–200.
38. I.Chambouleyron, J.M.Martinez, A.C.Moretti, and M.Mulato "Retrieval of optical constants and thickness of thin films from transmission spectra", Appl.Opt., **36**, 31 (1997), 8238–8247.
39. A.K.S.Aqili and A.Maqsood "Determination of thickness, refractive index, and thickness irregularity for semiconductor thin films from transmission spectra", Appl.Opt., **41**, 1 (2002), 218–224.
40. R.Swanepoel "Determining refractive index and thickness of thin films from wavelength measurements only", J.Opt.Soc.Am.A, **2**, 8 (1985), 1339–1343.
41. H.-Y.Joo and H.J.Kim, S.J.Kim and S.Y.Kim "Spectrophotometric analysis of aluminum nitride thin films", J.Vac.Sci.Technol.A **17**, 3 (1999), 862–870.
42. S.Lee and J.Hong "Comparison of Various Parametrization Models for Optical Functions of Amorphous Materials: Application for Sputtered Titanium Dioxide Thin Films", Jpn.J.Appl.Phys. Part1, **39**, 1 (2000), 241–244.
43. D.Davazoglou "Optical properties of SnO_2 thin films grown by atmospheric pressure chemical vapour deposition oxidizing $SnCl_4$", Thin Solid Films, **302**, 1–2 (1997), 204–213.
44. M.Reichling, J.Siegel, E.Matthias, H.Lauth, E.Hacker "Photoacoustic studies of laser damage in oxide thin films", Thin Solid Films, **253**, 1–2 (1994), 333–338.
45. O.R Wood II, H.G.Craighead, J.E.Sweeney, and P.J.Maloney "Vacuum ultraviolet loss in magnesium fluoride films", Appl.Opt., **23**, 20 (1984), 3644–3649.
46. Md.Mosaddeq-ur-Rahman, G.Yu, T.Soga, T.Jimbo, H.Ebisu and M.Umeno "Refractive index and degree of inhomogeneity of nanocrystalline TiO_2 thin films: Effects of substrate and annealing temperature", J.Appl.Phys., **88**, 8 (2000), 4634–4641.
47. A.Roos and D.Rönnow "Diffuse reflectance and transmittance spectra of an interference layer: 1. Model formulation and properties", Appl.Opt., **33**, 34 (1994), 7908–7917.
48. A.Duparré, R.Dohle and H.Müller "Relation between light scattering and morphology of columnar structured optical thin films", J.Mod.Optics, **37**, 8 (1990), 1383–1390.

49. M Ylilammi and T.Ranta-aho "Optical determination of the film thicknesses in multilayer thin film structures", Thin Solid Films, **232**, 1 (1990), 56–62.
50. G.Hass and W.R.Hunter "Laboratory Experiments to Study Surface Contamination and Degradation of Optical Coatings and Materials in Simulated Space Environments", Appl.Opt., **9**, 9 (1970), 2101–2110.
51. A.Roos, M.Bergkvist, and C.G.Ribbing "Determination of the SiO_2/Si interface roughness by diffuse reflectance measurements", Appl.Opt., **27**, 20 (1988), 4314–4317.
52. D.Rönnow and A.Roos "Diffuse reflectance and transmittance spectra of an interference layer. 2. Evaluation of tin oxide-coating glass", Appl.Opt., **33**, 34 (1994), 7918–7927.
53. J.-P.Borgogno and E.Pelletier "Determination of the extinction coefficient of dielectric thin films from spectrophotometric measurements", Appl.Opt., **28**, 14 (1989), 2895–2901.
54. C.Amra "Light scattering from multilayer optics. II. Application to experiment", J.Opt.Soc.Am.A **11**, 1 (1994), 211–226.
55. J.R.McNeil, L.J.Wei, G.A.Al-Jumaily, S.Shakir, and J.K.McIver "Surface smoothing effects of thin film deposition?", Appl.Opt., **24**, 4 (1985), 480–485.
56. E.Schmidt, H.Müller, P.Pertsch and D.Gäbler "Scattering of Light in TiO_2 Layers of Broad Band Mirrors", Thin Solid Films, **176**, 1 (1989), 25–32.
57. K.Zakrzewska "Mixed oxides as gas sensors", Thin Solid Films, **391**, 2 (2001), 229–238.
58. A.A.J.Al-Douri, O.S.Heavens "The effects of deposition parameters on the optical performance of thin dielectric films", Vacuum, **36**, 4 (1986), 207–212.
59. J.P.Borgogno, B.Lazarides, and E.Pelletier "Automatic Determination of the Optical Constants of Inhomogeneous Thin Films", Appl.Opt., **21**, 22 (1982), 4020–4029.
60. Л.Сосси, П.Кард «К теории отражения и пропускания света тонким неоднородным диэлектрическим слоем», Eesti NSV Tead.Akad.Toim.Füüs.Matem., **17**, 1 (1968), 41–48. L.Sossi, P.Kard "On the theory of the reflection and transmission of light by a thin inhomogeneous dielectric film".
61. Р.Якобсон «Неоднородные и совместно напыленные однородные пленки для оптических применений». В: «Физика тонких пленок. Современное состояние исследований и технические применения». Том VIII. Издательство «Мир». Москва. 1978, сс.61–105. R.Jacobsson "Inhomogeneous and coevaporated homogeneous films for optical applications", in "Physics of Thin Films", G.Hass, M.H.Francombe, and R.W.Hoffman, eds. (Academic, New York, 1975), Vol. 8, pp. 51–98.
62. П.Кард, Х.Ихер, Ю.Лембра «Новый приближенный метод анализа неоднородного оптического слоя», Eesti NSV Tead.Akad.Toim.Füüs.Matem., **25**, 1 (1976), 29–37. P.Kard, H.Iher, J.Lembra "A new approximate method for analysis of an inhomogeneous optical film".
63. B.Bovard, F.J.V.Milligen, M.J.Messerly, S.G.Saxe, and H.A.Macleod "Optical constants derivation for an inhomogeneous thin film from *in situ* transmission measurements", Appl.Opt., **24**, 12 (1985), 1803–1807.
64. F.J.Van Milligan, B.Bovard, M.R.Jacobson, J.Mueller, R.Potoff, R.L.Shoemaker, and H.A.Macleod "Development of an automated scanning monochromator for monitoring thin films", Appl.Opt., **24**, 12 (1985), 1799–1802.

65. Y.-Y.Liou, C.-C.Lee, C.-C.Jaing, C.-W.Chu "Determination of the Optical Constant Profiles of Thin Weakly Absorbing Inhomogeneous Films", Jap.J.Appl.Phys. Part1, **34**, 4A (1995), 1952–1957.
66. J.P.Borgogno, F.Flory, P.Roche, B.Schmitt, G.Albrand, E.Pelletier, and H.A.Macleod "Refractive index and inhomogeneity of thin films", Appl.Opt., **23**, 20 (1984), 3567–3570.
67. G.Koppelmann und K.Krebs „Die optischen Eigenschaften dielektrischer Schichten mit kleinen Homogenitätsstörungen", Z. für Physik **163**, 5 (1961), 539–556.
68. G.Koppelmann, K.Krebs und H.Leyendecker „Optische Untersuchungen des Aufbaus von Kryolith-Aufdampfschichten", Z. für Physik, **163**, 5 (1961), 557–570.
69. C.K. Carniglia "Ellipsometric calculations for nonabsorbing thin films with linear refractive-index gradients", J.Opt.Soc.Am. A **7**, 5 (1990), 848–856.
70. A.V.Tikhonravov, M.K.Trubetskov, and A.V.Krasilnikova "Spectroscopic ellipsometry of slightly inhomogeneous nonabsorbing thin films with arbitrary refractive-index profiles: theoretical study", Appl.Opt., **37**, 25 (1998), 5902–5911.
71. L.A.A.Pettersson, L.Hultman, and H.Arwin "Porosity depth profiling of thin porous silicon layers by use of variable-angle spectroscopic ellipsometry: a porosity graded-layer model", Appl.Opt., **37**, 19 (1998), 4130–4136.
72. X.Ying, A.Feldman, and E.N.Farabaugh "Fitting of transmission data for determining the optical constants and thicknesses of optical films", J.Appl.Phys., **67**, 4 (1990), 2056–2059.
73. A.Piegari and G.Emiliani "Analysis of inhomogeneous thin films by spectrophotometric measurements", Thin Solid Films, **179** (1989), 243–250.
74. B.Akaoğlu, İ.Atılgan, and B.Katırcıoğlu "Correlation between optical path modulations and transmittance spectra of *a*-Si:H thin films", Appl.Opt., **39**, 10 (2000), 1611–1616.
75. M.Montecchi, R.M.Montereali, E.Nichelatti "Reflectance and transmittance of a slightly inhomogeneous thin film bounded by rough, unparallel interfaces", Thin Solid Films, **396**, 1–2 (2001), 262–273.
76. P.Chindaudom and K.Vedam "Determination of the optical constants of an inhomogeneous transparent LaF_3 thin film on a transparent substrate by spectroscopic ellipsometry", Opt.Letters, **17**, 7 (1992), 538–540.
77. H.Kumagai, M.Matsumoto, K.Toyoda, M.Obara, and M.Suzuki "Fabrication of titanium oxide thin films by controlled growth with sequential surface chemical reactions", Thin Solid Films, **263**, 1 (1995), 47–53.
78. J.M.M.De Nijs and A.Van Silfhout "A novel derivative ellipsometric method for the study of the growth of thin films: titanium", Thin Solid Films, **173**, 1 (1990), 1–12.
79. D.Franta and I.Ohlídal "Optical characterization of inhomogeneous thin films of ZrO_2 by spectroscopic ellipsometry and spectroscopic reflectometry", Surf.Interface Anal., **30** (2000), 574–579.
80. L.Q.Zhu, Q.Fang, G.He, M.Liu, X.X.Xu, L.D.Zhang "Spectroscopic ellipsometry characterization of ZrO_2 thin films by nitrogen-assisted reactive magnetron sputtering", Materials Science in Semiconductor Processing **9**, 6 (2006), 1025–1030.
81. A.H.Jayatissa, T.Yamaguchi, K.Sawada, M.Aoyama and F.Sato "Characterization of Interface Layer of Silicon on Sapphire Using Spectroscopic Ellipsometry", Jpn.J.Appl.Phys. Part1, **36**, 12A (1997), 7152–7155.

82. A.F.Hebard, A.T.Fiory, S.Nakahara, and R.H.Eick “Oxygen-rich polycrystalline magnesium oxide - A high quality thin-film dielectric”, Appl.Phys.Lett., **48**, 8 (1986), 520–522.
83. C.Y.Ma, F.Lapostolle, P.Briois, Q.Y.Zhang “Effect of O_2 gas partial pressure on structures and dielectric characteristics of rf sputtered ZrO_2 thin films”, Appl.Surf. Sci. **253,** 21 (2007), 8718–8724.
84. F.Lai, Y.Wang, M.Li, H.Wang, Y.Song, Y.Jiang “Determination of optical constants and inhomogeneity of optical films by two-step film envelope method”, Thin Solid Films, **515**, 11 (2007), 4763–4767.
85. H.K.Pulker “Characterization of optical thin films”, Appl.Opt., **18**, 12 (1979), 1969–1977.
86. C.Ben Amor, G.Baud, J.P.Besse, M.Jacquet “Elaboration and characterization of titania coatings”, Thin Solid Films, **293**, 1–2 (1997), 163–169.
87. N.E.Stankova, I.G.Dimitrov, T.R.Stoyanchev, P.A.Atanasov and D.Kovacheva “Structure and optical anisotropy of pulsed-layer deposited TiO_2 films for optical applications”, Appl.Surf.Sc. **255**, 10 (2009), 5275–5279.
88. Y.Leprince-Wang, K.Yu-Zhang, V.Nguyen Dan, D.Souche, J.Rivory “Correlation between microstructure and the optical properties of TiO_2 thin films prepared on different substrates”, Thin Solid Films, **307**, 1–2 (1997), 38–42.
89. N.Sonnenberg, A.S.Longo, M.J.Cima, B.P.Chang, K.G.Ressler, P.C.McIntyre, and Y.P.Liu “Preparation of biaxially aligned cubic zirconia films on pyrex glass substrates using ion-beam assisted deposition”, J.Appl.Phys., **74**, 2 (1993), 1027–1034.
90. R.-C.Lin, Y.-C.Chen, K.-S.Kao “Two-step sputtered ZnO piezoelectric films for film bulk acoustic resonators”, Appl.Phys.A**89**, 2 (2007), 475–479.
91. E.Hacker, R.Th.Kersten, P.Weißbrodt “Structure-Properties Relationships in Optical Coatings”, Phys.Scripta **T49B** (1993), 525–538.
92. U.Kaiser, M.Adamik, G.Sáfrán, P.B.Barna, S.Laux, W.Richter “Growth structure investigation of MgF_2 and NdF_3 films grown by molecular beam deposition on CaF_2 (111) substrate”, Thin Solid Films, **280**, 1–2 (1996), 5–15.
93. D.S.Rickerby and P.J.Burnett “Correlation of Process and System Parameters with Structure and Properties of Physically Vapour-Deposited Hard Coatings”, Thin Solid Films, **157**, 2 (1988), 195–222.
94. D.Bhattacharyya, N.K.Sahoo, S.Thakur, N.C.Das “Spectroscopic ellipsometry of TiO_2 layers prepared by ion-assisted electron-beam evaporation”, Thin Solid Films, **360**, 1–2 (2000), 96–102.
95. H.Selhofer, E.Ritter, and R.Linsbod “Properties of titanium dioxide films prepared by reactive electron-beam evaporation from various starting materials”, Appl.Opt., **41**, 4 (2002), 756–762.
96. B.Schmitt, J.P.Borgogno, G.Albrand, and E.Pelletier “*In situ* and air measurements: influence of the deposition parameters on the shift of TiO_2/SiO_2 Fabry-Perot filters”, Appl.Opt., **25**, 12 (1986), 3909–3915.
97. J.-S.Chen, S.Chao, J.-S.Kao, H.Niu, and C.-H.Chen “Mixed films of TiO_2-SiO_2 deposited by double electron-beam coevaporation”, Appl.Opt., **35**, 1 (1996), 90–96.
98. Y.Leprince-Wang, D.Souche, K.Yu-Zhang, S.Fisson, G.Vuye, J.Rivory “Relations between the optical properties and the microstructure of TiO_2 thin films prepared by ion-assisted deposition”, Thin Solid Films, **359**, 2 (2000), 171–176.
99. K.Narasimha Rao, M.A.Murthy and S.Mohan “Optical Properties of Electron-Beam-Evaporated TiO_2 Films”, Thin Solid Films **176**, 2 (1989), 181–186.

100. R.P.Netterfield, R.C.Schaeffer, and W.G.Sainty “Coating Fabry-Perot interferometer plates with broadband multilayer dielectric mirrors”, Appl.Opt., **19**, 11 (1980), 3010–3017.
101. W.R.Oliver “Refractive Index of Inhomogeneous Films”, Phil.Mag., **21**, 174 (1970), 1229–1235.
102. J.Isidorsson, C.G.Granqvist, K.v.Rottkay, and M.Rubin “Ellipsometry on sputter-deposited tin oxide films: optical constants versus stoichiometry, hydrogen content, and amount of electrochemically intercalated lithium”, Appl.Opt., **37**, 31 (1998), 7334–7341.
103. E.E.Khawaja and S.G.Tomlin “The optical properties of thin films of tantalum pentoxide and zirconium dioxide”, Thin Solid Films **30**, 2 (1975), 361–369.
104. J.F.Tang, P.F.Gu, and Q.H.Wu “Some aspects of optical coatings in China: a brief description of research work in Zhejiang University”, Appl. Opt., **23**, 20 (1984), 3602–3607.
105. M.Oikkonen and T.Tuomi, M.Luomajärvi “Density of ZnS thin films grown by atomic layer epitaxy”, J.Appl.Phys. **63**, 4 (1988), 1070–1074.
106. P.Baumeister and O.Arnon “Use of hafnium dioxide in multilayer dielectric reflectors for the near uv”, Appl.Opt., **16**, 2 (1977), 439–444.
107. D.Reicher, P,Black, and K.Jungling “Defect formation in hafnium dioxide thin films”, Appl.Opt., **39**, 10 (2000), 1589–1599.
108. M.Fadel, O.A.Azim M., O.A.Omer, R.R.Basily “A study of some optical properties of hafnium dioxide (HfO_2) thin films and their applications”, Appl. Phys.A, **66**, 3 (1998), 335–343.
109. M.F.Al-Kuhaili, S.M.A.Durrani and E.E.Khawaja “Characterization of hafnium oxide thin films prepared by electron beam evaporation”, J.Phys.D:Appl.Phys., **37**, 8 (2004), 1254–1261.
110. D.Franta, I.Ohlídal, P.Klapetek, P.Pokorný and M.Ohlídal “Analysis of inhomogeneous thin films of ZrO_2 by the combined optical method and atomic force microscopy”, Surf.Interface Anal., **32**, 1 (2001), 91–94.
111. P.Klapetek, I.Ohlídal, D.Franta and P.Pokorný “Analysis of the boundaries of ZrO_2 and HfO_2 thin films by atomic force microscopy and the combined optical method”, Surf.Interface Anal., **33**, 7 (2002), 559–564.
112. E.E.Khawaja, S.M.A.Durrani and M.A.Daous “Depth profiling of inhomogeneous zirconia films by optical and Rutherford backscattering spectrometric techniques”, J.Phys.D:Appl.Phys., **32**, 4 (1999), 388–394.
113. H.H.Zhang, C.Y.Min and Q.Y.Zhang “Scaling behavior and structure transition of ZrO_2 films deposited by RF magnetron sputtering”, Vacuum **83**, 11 (2009), 1311–1316.
114. R.E.Klinger and C.K.Carniglia “Optical and crystalline inhomogeneity in evaporated zirconia films”, Appl.Opt., **24**, 19 (1985), 3184–3187.
115. A.Duparré, E.Welsch and H.-G.Walther, N.Kaiser and H.Müller, E.Hacker, H.Lauth, J.Meyer and P.Weissbrodt “Structure-related bulk losses in ZrO_2 optical thin films”, Thin Solid Films **187**, 2 (1990), 275–288.
116. M.Bellotto, A.Caridi, E.Cereda, G.Gabetta, and M.Scagliotti, G.M.Braga Marcazzan “Influence of the oxygen stoichiometry on the structural and optical properties of reactively evaporated ZrO_x films”, Appl.Phys.Lett., **63**, 15 (1993), 2056–2058.
117. S.Zhao, F.Ma, Z.Song, K.Xu “Thickness-dependent structural and optical properties of sputter deposited ZrO_2 films”, Opt.Mat. **30**, 6, (2008), 910–915.

118. W.Heitmann “Reaktiv aufgedampfte Seltenerde-Schichten. Reactively Evaporated Films of Rare Earth Oxides”, Vakuum-Technik **22**, 2 (1973), 49–55.
119. J.Aarik, A.Aidla, H.Mändar, T.Uustare, V.Sammelselg “Growth kinetics and structure formation of ZrO_2 thin films in chloride-based atomic layer deposition process”, Thin Solid Films, **408**, 1–2 (2002), 97–103.
120. S.N.Tkachev, M.H.Manghnani, A.Niilisk, J.Aarik, H.Mändar “Raman and Brillouin scattering spectroscopy studies of atomic layer-deposited ZrO_2 and HfO_2 thin films”, Spectrochim.Acta A**61**, 10 (2005), 2434–2438.
121. S.N.Tkachev, M.H.Manghnani, A.Niilisk, J.Aarik, H.Mändar “Micro-Raman spectroscopy and X-ray diffraction studies of atomic-layer deposited ZrO_2 and HfO_2 thin films”, J. of Mat.Sc., **40**, 16 (2005), 4293–4298.
122. J.Aarik, A.Aidla, A.-A.Kiisler, T.Uustare, V.Sammelselg “Influence of substrate temperature on atomic layer growth and properties of HfO_2 thin films”, Thin Solid Films, **340**, 1–2 (1990), 110–116.
123. J.Aarik, A.Aidla, H.Mändar, V.Sammelselg, T.Uustare “Texture development in nanocrystalline hafnium dioxide thin films grown by atomic layer deposition”, J. of Crystal Growth, **220**, 1–2 (2000), 105–113.
124. J.Aarik, A.Aidla, T.Uustare, V.Sammelselg “Morphology and structure of TiO_2 thin films grown by atomic layer deposition”, J.Cryst.Growth **148**, 3 (1995), 268–275.
125. J.Aarik, A.Aidla, V.Sammelselg, T.Uustare “Effect of growth conditions on formation of TiO_2-II thin films in atomic layer deposition process”, J.Cryst. Growth, **181**, 3 (1997), 259–264.
126. G.Hass “Reflectance and preparation of front-surface mirrors for use at various angles of incidence from the ultraviolet to the far infrared”, J.Opt.Soc.Am., **72**, 1 (1982), 27–39.
127. K.Nagata “Inhomogeneity in Refractive Index of Evaporated MgF_2 Film”, Jap.J.Appl.Phys., **7**, 10 (1968), 1181–1186.
128. E.Ritter and R.Hoffmann “Influence of Substrate Temperature on the Condensation of Vacuum Evaporated Films of MgF_2 and ZnS”, J.Vac.Sci. Techn., **6**, 4 (1969), 733–736.
129. D.H.Gill “Damage resistance of uv coatings”, Laser Focus, September 1979, 76–79.
130. P.Chindaudom and K.Vedam “Characterization of inhomogeneous transparent thin films on transparent substrates by spectroscopic ellipsometry: refractive indices $n(\lambda)$ of some fluoride coating materials”, Appl.Opt., **33**, 13 (1994), 2664–2671.
131. Y.Taki “Film structure and optical constants of magnetron-sputtered fluoride films for deep ultraviolet lithography”, Vacuum, **74**, 3–4 (2004), 431–435.
132. G.Atanassov, R.Thielsch and D.Popov “Optical properties of TiO_2, Y_2O_3 and CeO_2 thin films deposited by electron beam evaporation”, Thin Solid Films, **223**, 2 (1993), 288–292.
133. W.Heitmann “Reactively Evaporated Films of Scandia and Yttria”, Appl.Opt., **12**, 2 (1973), 394–397.
134. J.Aarik, A.Aidla, H.Mändar, and T.Uustare “Atomic layer deposition of titanium dioxide from $TiCl_4$ and H_2O: investigation of growth mechanism”, Appl.Surf. Sc., **172**, 1–2 (2001), 148–158.

135. R. G. Mitchell, A. Aidla, J. Aarik “Transmission electron microscopy studies of HfO_2 thin films grown by chloride-based atomic layer deposition”, Thin Solid Films, **253**, (2006), 606–617.
136. T.Arroval „Titaanoksiidkilede röntgenanalüüs”. Bac.Th. Tartu University, 2008. T.Arroval “XRR analysis of the titania films”.
137. Z.L.Wu and K.Bange “Comparative photothermal study of reactive low-voltage ion-plated and electron-beam-evaporated TiO_2 thin films”, Appl.Opt., **33**, 34 (1994) 7901–7907.
138. „Inglise-eesti füüsikasõnaraamat. English-Estonian Dictionary of Physics”, Viktor Korrovits, Henn Käämbre. TEA, Tallinn 2002.

ACKNOWLEDGEMENTS

I would like to thank Mr. Tõnu Jõesaar whom the idea about the applicability of a two-layer optical inhomogeneity model belongs, and Dr. Anatoli Kuznetsov who wrote the main program used for film parameters optimisation, Dr. Lembit Sossi who wrote a program for thin film analysis and helped us to understand the problems on multilayer thin film optics. Dr. Leonard Matisen worked with me on the electron beam evaporation of films. I am also thankful to Mr. Taivo Kotsar for his help for performing spectrophotometric measurements.

I would like to extend my thanks to the people of Film Technology Lab, Institute of Physics, who introduced me to the problems of atomic layer deposited films, especially Prof. Jaan Aarik, Dr. Arnold Rosental, Mr. Aivar Tarre and Prof. Väino Sammelselg. Dr. Ilmo Sildos kindly offered help in solving the organizational problems.

Orders from “Estla, Ltd.” (Dr. Yevgeni Berik and Mr. Vladimir Biryukov) provided the main financial basis for the work, a by-product of which is this dissertation.

PUBLICATIONS

CURRICULUM VITAE

Name: Aarne Kasikov
Date and place of birth: April 22, 1957, Jõhvi, Estonian SSR
Citizenship: Estonian
Current employment: Institute of Physics, University of Tartu, researcher
Address: Institute of Physics, University of Tartu, Riia 142,
51014 Tartu, Estonia
Telephone: +372 737 4651
E-mail: aarne@fi.tartu.ee

Education:

1971	Kohtla-Järve X 8-grade School
1974	Nõo Secondary School
1979	Tartu State University, physicist, physicist-pedagogue,
1995	University of Tartu, MSc,

Research and professional experience:

1979–1980	Institute of Physics, Academy of Sciences of Estonian SSR (engineer)
1983–1997	Institute of Physics, Academy of Sciences of Estonian SSR (senior engineer, junior researcher, section head)
1997–	present Institute of Physics, University of Tartu (section head, researcher)

Main research areas: vacuum evaporation, thin film optics

Publications: 27 scientific papers

ELULOOKIRJELDUS

Nimi: Aarne Kasikov
Sünniaeg ja koht: 22. aprill 1957, Jõhvi linn
Kodakondsus: Eesti
Töökoht: Tartu Ülikooli Füüsika Instituut, teadur
Aadress: Tartu Ülikool Füüsika Instituut, Riia 142, Tartu, Eesti
Telefon: 737 4651
E-mail: aarne@fi.tartu.ee

Haridus:

1971	Kohtla-Järve X 8-kl. kool
1974	Nõo Keskkool
1979	Tartu Riiklik Ülikool, füüsik, füüsik-pedagoog
1995	Tartu Ülikool, M.Sc.

Kutsealane kogemus:

1979–1980	ENSV Teaduste Akadeemia Füüsika Instituut, insener
1983–1997	ENSV TA Füüsika Instituut, vaneminsener, nooremteadur, sektorijuhataja
1997–	Tartu Ülikooli Füüsika Instituut, sektorijuhataja, teadur

Peamised uurimisalad: vaakumaurustamine, õhukeste kilede optika

Publikatsioonid: 27 teaduslikku artiklit

DISSERTATIONES PHYSICAE UNIVERSITATIS TARTUENSIS

1. **Andrus Ausmees.** XUV-induced electron emission and electron-phonon interaction in alkali halides. Tartu, 1991.
2. **Heiki Sõnajalg.** Shaping and recalling of light pulses by optical elements based on spectral hole burning. Tartu, 1991.
3. **Sergei Savihhin.** Ultrafast dynamics of F-centers and bound excitons from picosecond spectroscopy data. Tartu, 1991.
4. **Ergo Nõmmiste.** Leelishalogeniidide röntgenelektronemissioon kiiritamisel footonitega energiaga 70–140 eV. Tartu, 1991.
5. **Margus Rätsep.** Spectral gratings and their relaxation in some low-temperature impurity-doped glasses and chrystals. Tartu, 1991.
6. **Tõnu Pullerits.** Primary energy transfer in photosynthesis. Model calculations. Tartu, 1991.
7. **Olev Saks.** Attoampri diapasoonis voolude mõõtmise füüsikalised alused. Tartu, 1991.
8. **Andres Virro.** AlGaAsSb/GaSb heterostructure injection lasers. Tartu, 1991.
9. **Hans Korge.** Investigation of negative point discharge in pure nitrogen at atmospheric pressure. Tartu, 1992.
10. **Jüri Maksimov.** Nonlinear generation of laser VUV radiation for high-resolution spectroscopy. Tartu, 1992.
11. **Mark Aizengendler.** Photostimulated transformation of aggregate defects and spectral hole burning in a neutron-irradiated sapphire. Tartu, 1992.
12. **Hele Siimon.** Atomic layer molecular beam epitaxy of A^2B^6 compounds described on the basis of kinetic equations model. Tartu, 1992.
13. **Tõnu Reinot.** The kinetics of polariton luminescence, energy transfer and relaxation in anthracene. Tartu, 1992.
14. **Toomas Rõõm.** Paramagnetic H^{2-} and F^+ centers in CaO crystals: spectra, relaxation and recombination luminescence. Tallinn, 1993.
15. **Erko Jalviste.** Laser spectroscopy of some jet-cooled organic molecules. Tartu, 1993.
16. **Alvo Aabloo.** Studies of crystalline celluloses using potential energy calculations. Tartu, 1994.
17. **Peeter Paris.** Initiation of corona pulses. Tartu, 1994.
18. **Павел Рубин.** Локальные дефектные состояния в CuO_2 плоскостях высокотемпературных сверхпроводников. Тарту, 1994.
19. **Olavi Ollikainen.** Applications of persistent spectral hole burning in ultrafast optical neural networks, time-resolved spectroscopy and holographic interferometry. Tartu, 1996.
20. **Ülo Mets.** Methodological aspects of fluorescence correlation spectroscopy. Tartu, 1996.
21. **Mikhail Danilkin.** Interaction of intrinsic and impurity defects in CaS:Eu luminophors. Tartu, 1997.

22. **Ирина Кудрявцева.** Создание и стабилизация дефектов в кристаллах KBr, KCl, RbCl при облучении ВУФ-радиацией. Тарту, 1997.
23. **Andres Osvet.** Photochromic properties of radiation-induced defects in diamond. Tartu, 1998.
24. **Jüri Örd.** Classical and quantum aspects of geodesic multiplication. Tartu, 1998.
25. **Priit Sarv.** High resolution solid-state NMR studies of zeolites. Tartu, 1998.
26. **Сергей Долгов.** Электронные возбуждения и дефектообразование в некоторых оксидах металлов. Тарту, 1998.
27. **Kaupo Kukli.** Atomic layer deposition of artificially structured dielectric materials. Tartu, 1999.
28. **Ivo Heinmaa.** Nuclear resonance studies of local structure in $RBa_2Cu_3O_{6+x}$ compounds. Tartu, 1999.
29. **Aleksander Shelkan.** Hole states in CuO_2 planes of high temperature superconducting materials. Tartu, 1999.
30. **Dmitri Nevedrov.** Nonlinear effects in quantum lattices. Tartu, 1999.
31. **Rein Ruus.** Collapse of 3d (4f) orbitals in 2p (3d) excited configurations and its effect on the x-ray and electron spectra. Tartu, 1999.
32. **Valter Zazubovich.** Local relaxation in incommensurate and glassy solids studied by Spectral Hole Burning. Tartu, 1999.
33. **Indrek Reimand.** Picosecond dynamics of optical excitations in GaAs and other excitonic systems. Tartu, 2000.
34. **Vladimir Babin.** Spectroscopy of exciton states in some halide macro- and nanocrystals. Tartu, 2001.
35. **Toomas Plank.** Positive corona at combined DC and AC voltage. Tartu, 2001.
36. **Kristjan Leiger.** Pressure-induced effects in inhomogeneous spectra of doped solids. Tartu, 2002.
37. **Helle Kaasik.** Nonperturbative theory of multiphonon vibrational relaxation and nonradiative transitions. Tartu, 2002.
38. **Tõnu Laas.** Propagation of waves in curved spacetimes. Tartu, 2002.
39. **Rünno Lõhmus.** Application of novel hybrid methods in SPM studies of nanostructural materials. Tartu, 2002.
40. **Kaido Reivelt.** Optical implementation of propagation-invariant pulsed free-space wave fields. Tartu, 2003.
41. **Heiki Kasemägi.** The effect of nanoparticle additives on lithium-ion mobility in a polymer electrolyte. Tartu, 2003.
42. **Villu Repän.** Low current mode of negative corona. Tartu, 2004.
43. **Алексей Котлов.** Оксианионные диэлектрические кристаллы: зонная структура и электронные возбуждения. Tartu, 2004.
44. **Jaak Talts.** Continuous non-invasive blood pressure measurement: comparative and methodological studies of the differential servo-oscillometric method. Tartu, 2004.
45. **Margus Saal.** Studies of pre-big bang and braneworld cosmology. Tartu, 2004.

46. **Eduard Gerškevitš.** Dose to bone marrow and leukaemia risk in external beam radiotherapy of prostate cancer. Tartu, 2005.
47. **Sergey Shchemelyov.** Sum-frequency generation and multiphoton ionization in xenon under excitation by conical laser beams. Tartu, 2006.
48. **Valter Kiisk.** Optical investigation of metal-oxide thin films. Tartu, 2006.
49. **Jaan Aarik.** Atomic layer deposition of titanium, zirconium and hafnium dioxides: growth mechanisms and properties of thin films. Tartu, 2007.
50. **Astrid Rekker.** Colored-noise-controlled anomalous transport and phase transitions in complex systems. Tartu, 2007.
51. **Andres Punning.** Electromechanical characterization of ionic polymer-metal composite sensing actuators. Tartu, 2007.
52. **Indrek Jõgi.** Conduction mechanisms in thin atomic layer deposited films containing TiO_2. Tartu, 2007.
53. **Aleksei Krasnikov.** Luminescence and defects creation processes in lead tungstate crystals. Tartu, 2007.
54. **Küllike Rägo.** Superconducting properties of MgB_2 in a scenario with intra- and interband pairing channels. Tartu, 2008.
55. **Els Heinsalu.** Normal and anomalously slow diffusion under external fields. Tartu, 2008.
56. **Kuno Kooser.** Soft x-ray induced radiative and nonradiative core-hole decay processes in thin films and solids. Tartu, 2008.
57. **Vadim Boltrushko.** Theory of vibronic transitions with strong nonlinear vibronic interaction in solids. Tartu, 2008.
58. **Andi Hektor.** Neutrino Physics beyond the Standard Model. Tartu, 2008.
59. **Raavo Josepson.** Photoinduced field-assisted electron emission into gases. Tartu, 2008.
60. **Martti Pärs.** Study of spontaneous and photoinduced processes in molecular solids using high-resolution optical spectroscopy. Tartu, 2008.
61. **Kristjan Kannike.** Implications of neutrino masses. Tartu, 2008.
62. **Vigen Issahhanjan.** Hole and interstitial centres in radiation-resistant MgO single crystals. Tartu, 2008.
63. **Veera Krasnenko.** Computational modeling of fluorescent proteins. Tartu, 2008.
64. **Mait Müntel.** Detection of doubly charged higgs boson in the CMS detector. Tartu, 2008.
65. **Kalle Kepler.** Optimisation of patient doses and image quality in diagnostic radiology. Tartu, 2009.
66. **Jüri Raud.** Study of negative glow and positive column regions of capillary HF discharge. Tartu, 2009.
67. **Sven Lange.** Spectroscopic and phase-stabilisation properties of pure and rare-earth ions activated ZrO_2 and HfO_2. Tartu, 2010.